Development of Regional Economic Supply Curves for Surface Water Resources and Climate Change Assessments: A Case Study of China

David Arthur Wiberg and Kenneth Marc Strzepek

RR-05-001
November 2005

The International Institute for Applied Systems Analysis

is an interdisciplinary, nongovernmental research institution founded in 1972 by leading scientific organizations in 12 countries. Situated near Vienna, in the center of Europe, IIASA has been producing valuable scientific research on economic, technological, and environmental issues for over three decades.

IIASA was one of the first international institutes to systematically study global issues of environment, technology, and development. IIASA's Governing Council states that the Institute's goal is: *to conduct international and interdisciplinary scientific studies to provide timely and relevant information and options, addressing critical issues of global environmental, economic, and social change, for the benefit of the public, the scientific community, and national and international institutions*. Research is organized around three central themes:

– Energy and Technology
– Environment and Natural Resources
– Population and Society

The Institute now has National Member Organizations in the following countries:

Austria
The Austrian Academy of Sciences

China
National Natural Science Foundation of China

Czech Republic
The Academy of Sciences of the Czech Republic

Egypt
Academy of Scientific Research and Technology (ASRT)

Estonia
Estonian Association for Systems Analysis

Finland
The Finnish Committee for IIASA

Germany
The Association for the Advancement of IIASA

Hungary
The Hungarian Committee for Applied Systems Analysis

Japan
The Japan Committee for IIASA

Netherlands
The Netherlands Organization for Scientific Research (NWO)

Norway
The Research Council of Norway

Poland
The Polish Academy of Sciences

Russian Federation
The Russian Academy of Sciences

Sweden
The Swedish Research Council for Environment, Agricultural Sciences and Spatial Planning (FORMAS)

Ukraine
The Ukrainian Academy of Sciences

United States of America
The National Academy of Sciences

Development of Regional Economic Supply Curves for Surface Water Resources and Climate Change Assessments: A Case Study of China

David Arthur Wiberg
Kenneth Marc Strzepek

RR-05-001
November 2005

International Institute for Applied Systems Analysis
Laxenburg, Austria

International Standard Book Number 3-7045-0143-3

Cover design by Anka James.

Printed by **Rema***print*, Vienna.

Contents

Abstract

Recently, a number of reports on global renewable water resources have been produced. These studies generally report the average annual renewable water resources for large regions or countries based on runoff from rivers and streams. These average resource data are then compared with estimated current and future water demand to determine which regions and countries could be facing serious water scarcity problems. Microeconomic analysis, however, suggests that increasing the supply leads to higher costs and could thereby reduce demand. Furthermore, the total renewable water resources are not 100% usable. The global studies to date have not systematically considered the costs of developing and supplying water, the potential water losses due to development, or the relationship between supply and demand. This report aims to improve the analysis of global and regional water resources by developing a methodology for calculating regional supply curves from storage for surface water resources and to apply this methodology to study climate change impacts on the supply of water from storage in large watershed regions of China.

There are four major steps in developing the supply curves from regional reservoir storage. In step one, the Climate- and Human Activities-sensitive Runoff Model (CHARM), a spatially explicit hydrologic model that is sensitive to land-use and climate changes, is developed to use climate databases to produce time series runoff calibrated to the annual averages. In step two, a methodology is developed to calculate evaporation from regional reservoir storage, incorporating hundreds or thousands of reservoirs for areas where little reservoir information is available. In the third step, the storage–yield curve is calculated based on the CHARM results and the evaporation calculated from the area–volume curves developed in step two. Finally, reservoir storage cost curves are developed based on watershed physiography and reservoir size. These cost curves are then combined with the storage–yield curve to produce a curve representing regional water supply from storage.

This regional water supply curve methodology is applied to examine the impacts of climate change on the water supply from storage in nine major watershed regions in China. The general circulation model scenarios used produce results suggesting that China will benefit from increased runoff in regions of water scarcity and high demand. However, the increased evaporation and flow variability will take its toll in some regions, increasing the frequency of floods and droughts and thereby the cost of and need for storage in those regions.

Acknowledgments

As with any body of work, this paper was made possible by the contributions of a number of individuals and organizations. Although this is an incomplete list, I would particularly like to thank Günther Fischer and the Land Use Change Program at IIASA for funding the majority of the work and providing input, data, advice, and administrative support; the United States Environmental Protection Agency for funding part of the research from a project on climate change impacts in the western United States; the Center for Integrated Study of the Human Dimensions of Global Change, created through a cooperative agreement between the National Science Foundation (SBR-9521914) and Carnegie Mellon University, and generously supported by additional grants from the Electric Power Research Institute, the ExxonMobil Foundation, and the American Petroleum Institute, for also funding some of the research; Xiubin Li and Yufeng Chen, of the Chinese Academy of Sciences, Institute of Geographic Sciences and Natural Resources Research, and Laixiang Sun for obtaining critical data, refining Chinese data, and helping me with Chinese translation; Sylvia Prieler, Michael Gluck, and Ian McCallum for assisting me with GIS; Terry Fulp of the United States Bureau of Reclamation for his assistance in gathering reservoir information; and Rajagopalan Balaji, Jim Heaney, and David Yates for their input and assistance. I would also like to thank all those who have assisted in the creation of the global datasets relied upon for this document and all those responsible for making many of the datasets freely available. Science advances happen at a much faster pace when information is made freely available for all to study and analyze. Finally, I would like to thank my wife, Jenn, for her patience and loving support through the entire process.

David A. Wiberg

1
Introduction

> Irrigation is expected to play an increasingly important role in the agriculture of the developing countries. At present, irrigated production is estimated to account for 20% of the arable land and contribute some 40% of total crop production (nearly 60% of cereal production). This share is expected to increase to 47% by 2030. The irrigated area in developing countries is projected to expand by 23% (or 45 million ha, from 197 million ha in 1995/97 to 242 million ha in 2030), and by 34% in terms of harvested area. Expansion in irrigated agriculture would lead to a 12% increase in water withdrawals for agriculture. This latter result depends crucially on the projected increase in irrigation water use efficiency (from 43% to 50% on average) by reducing water losses during transport from source to crop. (FAO, 2000:12)

This quote from a recent report by the Food and Agriculture Organization of the United Nations (FAO) indicates large increases in water demand within a single sector—agriculture. Other sectors currently use less total water than does agriculture, but the demand in some of these sectors is projected to increase by an even greater percentage. In China, for instance, demand for irrigation water is projected to increase only 3.4% between 2000 and 2010. In comparison, industry demand is projected to rise about 63%; urban water supply by 58%; rural water supply by 33%; and forestry, pasture, and fishery supply by 24% over the same time period (UN, 1997).

All of these estimations are based solely on demand-side analysis, however. Microeconomic analysis suggests that increasing supply leads to higher costs and could thereby reduce demand. *Figure 1.1* illustrates this concept. Initially, equilibrium is established at a price of 8 units and a quantity of 5 units. Demand then increases, so that the "Demand 2" line could indicate future demand for water. If the price were to remain the same for water, then 11 units would now be consumed. However, increasing the supply of water comes at some cost, so that the demand function has a positive slope. The new equilibrium with the increased demand would be found at only 9 units at a price of 12 units. By incorporating supply as well as demand into the analysis, *Figure 1.1* shows that the quantity of water used in the future may not increase by the entire estimated increase in demand.

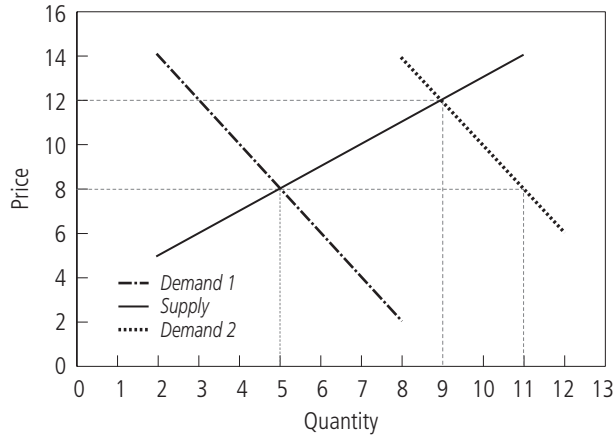

Figure 1.1. Supply and demand curve illustrating how equilibrium price and quantity change as demand is shifted outward.

A comparison of studies performed by the International Water Management Institute (IWMI) and the International Food Policy Research Institute (IFPRI) also illustrates the difference between purely demand-side analysis and supply/demand analysis in the food sector. An analysis of food demand by IWMI suggests a need for 22% more irrigated area by 2025 (Seckler *et al.*, 1998; IWMI, 2000). However, a similar analysis conducted by IFPRI suggests only a 7% increase in irrigated area will be needed by 2025 (Rosegrant and Ringler, 1999). The difference between the IWMI and IFPRI studies is that in the IFPRI study, higher prices will lead to lower demand for food, by the concept illustrated in *Figure 1.1*, but higher prices will also lead to less reduction in hunger. These results from the food sector clearly show that analyzing future water supply requires an economic analysis that incorporates both supply and demand. Because water demand is increasing faster in other sectors than it is in the food sector, water stress could add an additional stress to food production, resulting in an even steeper supply curve for food.

A number of global water assessments have been produced that supply numbers for regional- or national-level water availability (Gleick, 1993, 1998; Shiklomanov, 1997, 1998, 1999; Cosgrove and Rijsberman, 2000). These assessments generally report average annual renewable water resources as a measure of water available to meet water demand, where renewable water resources "represent the water entering a country's river and groundwater systems" (IWMI, 2000, cited in Cosgrove and Rijsberman, 2000). Not all of the available water resources are usable, though. Runoff is often quite variable in time and space. This means that to have the water when and where it is needed, it must be stored and transported. In the process of storing and transporting the water, some will be lost to evaporation. Current

water availability studies generally do not consider how much of the resource can be developed in a region.

This report adds to the existing water resources availability studies by developing a methodology to include one aspect of water supply, namely, the production of cost and supply curves from reservoir storage at the regional level. Producing water cost and supply curves from reservoir storage for a single reservoir is a common practice when planning the reservoir. The parameters of the reservoir, or potential reservoir—such as location, size constraints, the relationship between elevation, surface area, and volume, as well as construction cost estimates—are all known. Much of the information used in such reservoir planning studies is not available for entire regions or countries, however. The regional methodology, then, focuses on approximating relationships among reservoir storage parameters over regions that could contain thousands of reservoirs. The methodology requires the following steps:

1. The first step is to obtain time series runoff data. Water resources availability and runoff data are often provided as annual averages. However, good global databases are available for time series of climatic variables such as precipitation, temperature, wind speed, and cloudiness, among others. A hydrologic rainfall–runoff model, then, can provide the necessary time series values. If the model is to be used for analysis of the impacts of climate change, it should be sensitive to the climate variables. It should also be sensitive to land use and land cover, since they can have sizable impacts on the runoff hydrograph. Furthermore, land use and land cover can influence the local climate, although land-use changes have not been sufficiently studied to include them completely in current general circulation models. In Chapter 2, the Climate- and Human Activities-sensitive Runoff Model (CHARM) is developed and its output is verified on sample basins in China. The model is then applied to produce time series runoff for nine large watershed regions of China based on the annual average runoff values from a report by the United Nations (UN, 1997), and the water resources issues in each of these regions are discussed.
2. The second step is to apply the time series runoff data from step 1 to produce regional storage–yield curves. The yield from reservoirs can be greatly reduced as a result of evaporation, so this loss should be considered when calculating storage–yield curves. To calculate evaporation from the surface of the reservoirs, the surface area of the reservoirs at all time points must be known. Surface area is not constant and varies with volume, so a relationship between total reservoir volume and surface area must be found. In Chapter 3, a relationship is developed between total regional storage volume and surface area: First, a method is developed to approximate the surface area and volume of a single reservoir when data on the relationship between area and volume are not

available. A relationship is then developed between surface area and volume for a combined group of reservoirs. Finally the technique is extended to entire regions. In Chapter 4, the area–volume estimation technique is applied to each of the nine major watershed regions in China to develop the storage–yield curve for each one.

3. Once the storage–yield curve has been developed, the third step is to estimate the average cost per unit of storage for reservoirs in the region. Once a value for cost per unit is found, it can be multiplied by the storage to obtain the total cost of that amount of storage. The storage–yield curve can then be converted directly into a cost versus yield curve, or total cost curve. The derivative of the total cost curve is the marginal cost curve, which is also the economic supply curve for a competitive firm. In Chapter 4, these curves are produced for the nine watershed regions in China.

1.1 China as a Case Study

At 12%, China currently accounts for the largest percentage of the world's population growth (UN, 1999). It is a country that is developing and changing rapidly while trying to be 95% self-sufficient in grain production, with only about 15% of its territory being arable land (World Bank, 1997; Fischer *et al.*, 1998). The combination of the large and still-growing population of about 1.25 billion, increasing incomes, and the nation's agricultural policies puts tremendous pressure on China's water resources. Water is already considered to be scarce in the regions of China with the greatest population density and agricultural activity. The vast majority of the country's large population lives in, and infringes on, the best agricultural land, which lies on the plains in the eastern part of the country. The topographic map of China in *Figure 1.2* clearly shows the most fertile area, known as the North China Plain, surrounding Beijing, Tianjin, Hebei, Shandong, Jaingsu, and parts of a few other provinces. The figure makes clear the reason for the location of the best agricultural land and population density. The population density is shown in *Figure 1.3*.

A recent study by the Food and Agriculture Organization of the United Nations (FAO) and the International Institute for Applied Systems Analysis (IIASA), using the agro-ecological zones (AEZ) methodology to assess food production potential in China, concluded that there is sufficient crop production potential for China to feed its projected population in 2050 and still maintain its goal of 95% self-sufficiency in grain production, although it would be beneficial to lower the goal to 90% (FAO / IIASA, 2000). However, this study assumes that water resources are available when and where they are needed, indicating that a closer

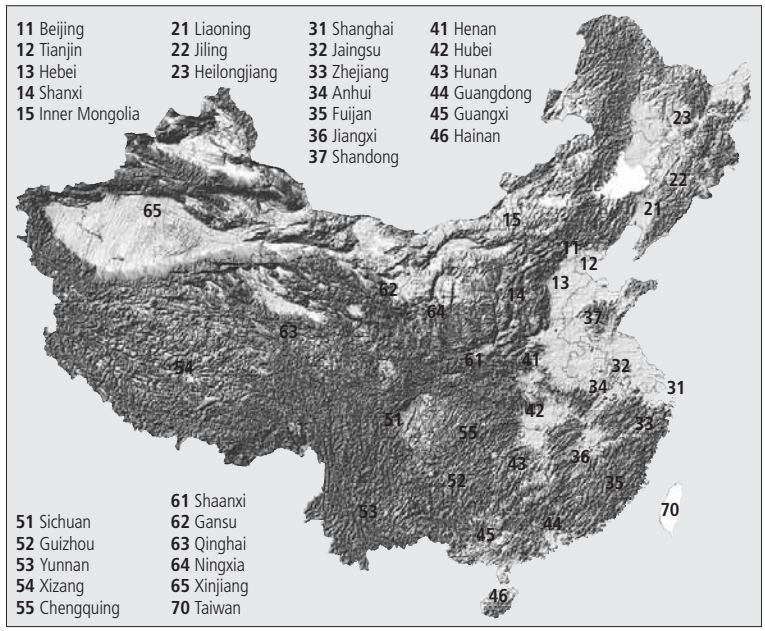

Figure 1.2. China's topography. (Source: Heilig, 1999.)

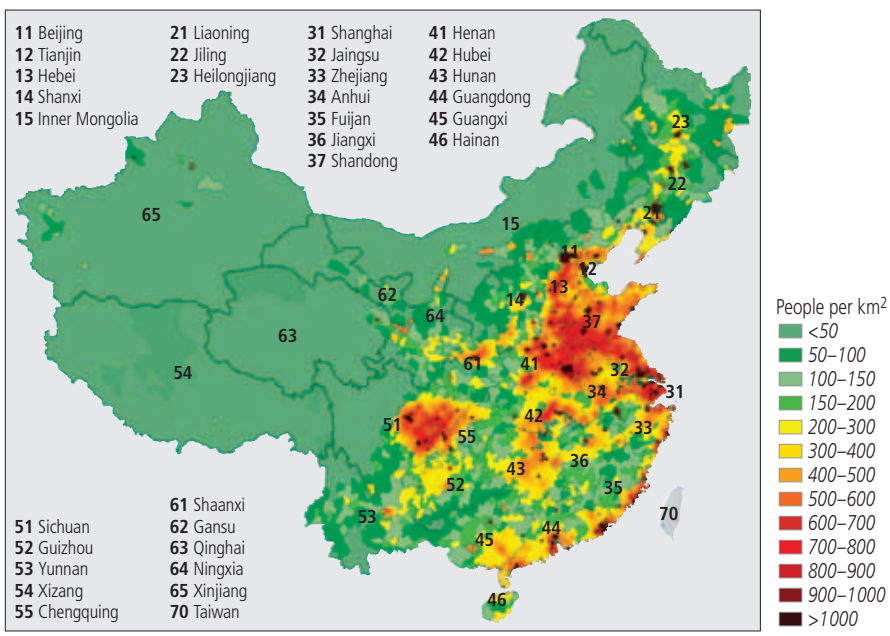

Figure 1.3. China's population density. (Source: Heilig, 1999.)

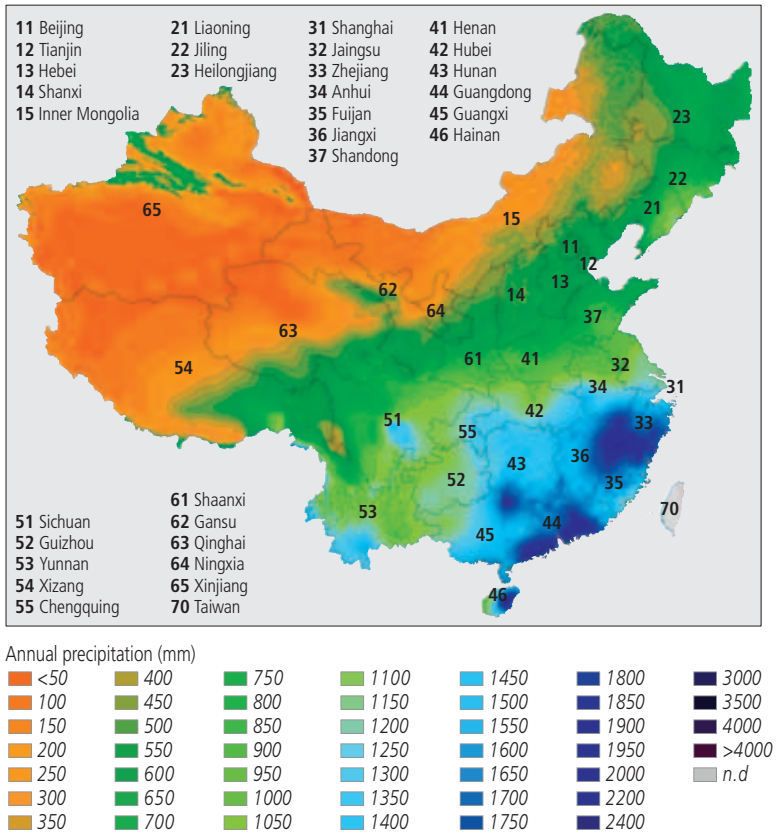

Figure 1.4. Average annual precipitation in China. (Source: Heilig, 1999.)

look at China's water resources is warranted to test the validity of this assumption. China's renewable water resources are now estimated at about 2,200 cubic meters (m^3)/capita/year (UN, 2001). Water scarcity is generally indicated when available water drops below 1,000 m^3/capita/year, while 1,000–2,000 m^3/capita/year is considered a condition of water stress (Postel, 1992). Accordingly, China is not considered to be under water stress. However, a closer look at China's water resources availability reveals significant diversity in water resources challenges, which, combined with the issues mentioned previously, make it a very important study region. *Figure 1.4* and *Tables 1.1* and *1.2* summarize some of the challenges China faces with respect to water resources availability (Nanjing Institute of Hydrology and Water Resources, 1996; UN, 1997). The nine major watershed regions indicated in *Table 1.1* are shown in *Figure 1.5*.

Table 1.1 shows the disparity in surface water resources. Although as a whole, China's per capita water resources are satisfactory, the northern regions of China

Table 1.1. Surface water availability in China by region, 1993.

Watershed region	Water resources (%)	Population (%)	Cultivated land (%)	Per capita water resources (m^3/year)	Water resources per unit of cultivated land (m^3/ha)
Northern China					
1 Northeast	6.9	10.0	19.8	1,479	9,560
2 Hai He–Luan He basin	1.5	10.0	10.9	225	3,760
3 Huai He basin	3.4	16.0	14.9	389	6,310
4 Huang He basin	2.6	8.0	12.7	656	5,730
Subtotal	14.4	44.0	58.3	640	6,180
Southern China					
5 Chang Jiang basin	34.2	34.0	24.0	2,369	39,300
6 South	16.8	12.0	6.8	3,465	67,950
7 Southeast	9.2	6.0	3.2	2,999	73,800
8 Southwest	20.8	2.0	1.7	31,679	327,000
Subtotal	81.0	54.0	35.7		
9 Interior basins	4.6	2.0	5.8	4,832	21,850
China	100.0	100.0	100.0	2,323	28,000

Source: Nanjing Institute of Hydrology and Water Resources, 1996. Cited in UN, 1997, p. 9.

Table 1.2. Comparison of available water resources to demand, in billion cubic meters.

Region	Surface water runoff	Renewable water resources	Demand, 1993	Projected demand, 2000	Projected demand, 2010
1	164.1	192.8	51.93	66.31	87.07
2	27.6	42.1	46.47	50.36	57.29
3	75.7	96.1	73.46	86.83	105.09
4	61.0	74.4	44.95	49.91	63.41
5	938.3	961.3	196.53	224.46	261.45
6	440.7	470.8	77.19	93.13	121.17
7	255.3	259.2	32.09	39.04	47.37
8	587.6	585.3	8.37	10.09	12.39
9	113.1	130.4	62.13	68.26	78.45
China	2,663.4	2,812.4	601.13	688.4	833.7

Note: For watershed regions names, see *Figure 1.5*.
Sources: Ministry of Water Resources and Electric Power, 1997; Nanjing Institute of Hydrology and Water Resources, 1996; and UN, 1997.

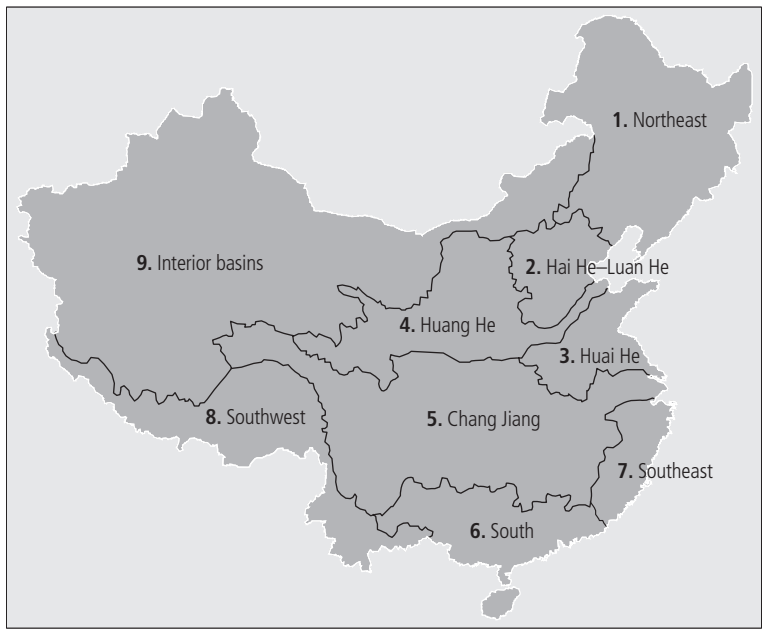

Figure 1.5. Major watershed regions of China.

suffer from a scarcity of water resources, with as little as 225 m^3/capita/year in the Hai He–Luan He basin around Beijing. Furthermore, although water resources are scarce in these northern regions, the majority of the cultivated land is in these areas. Comparing estimated demand to surface water availability and to an estimate of the renewable resources, it is evident that China will have to fully develop its water resources in the North to meet demand. In addition, it will probably have to transfer water from basins in the South to basins in the North.

According to *Table 1.2*, by 2010 water demand in three of the regions will exceed not only the supply, but also the total surface water runoff of those watershed regions. In two of the regions, demand will exceed the entire renewable water resources. Again, this analysis is demand based.

In addition to the discrepancy between water supply and demand in the North, rapid urbanization has resulted in similar discrepancies in urban areas. Construction of new water supply and distribution systems has not been able to keep pace with the phenomenal growth in urban demand throughout China. Variability in water resources is a further problem in China. China's rivers are famous for floods and droughts. China's Huang He, or Yellow River, is named for the amount of sediment it carries. It has also been known as "China's Sorrow," indicating the many disasters it has caused by way of floods and droughts.

Because of the challenges China faces in water resources management, the potential impacts of climate change should be assessed. In the northern parts of China, every drop of water is needed to satisfy demand and large capital expenditures are being planned and undertaken to augment supply. Climate change has the potential to exacerbate the water supply problems. Increasing temperatures result in increasing evaporation and transpiration and can lead to dry areas becoming drier. The changes in water availability due to climate change are important to consider when planning future water supply and may change the parameters of a given water supply project. As an application of the methodology for developing regional water resources cost and supply curves presented in this report, the impacts of climate change on water supply and cost curves in China will be investigated.

The large and growing population, the rapid economic growth, and the spatial and temporal variability of water resources availability create a full range of water resources management issues and make China an ideal case study. Data on water resources are not easy to obtain, except from international databases. The lack of data also makes China a good case study, since the methodology to be developed here is meant to be, and often must be, applied to regions where data are scarce. In this paper, then, China will be the focus for the application of the methodology for developing regional supply curves from storage.

2

CHARM: A Hydrologic Model for Land-Use and Climate Change Studies in China

2.1 Introduction

With China's recent rapid economic and population growth, water supply for industry, agriculture, and the growing population is becoming a critical issue. It is estimated that the total renewable freshwater resources of China are 2,700 cubic kilometers (km^3). Water withdrawals for all uses in 1995 were estimated to be 526 km^3. This results in a ratio of use to availability of just under 0.20 mbox(Shiklomanov, 1999). A national ratio of use to availability of 0.20 indicates that a country is at the low end of the "moderately water stressed" category, indicating that regions of the country are facing water stress.

Which regions are currently facing water stress and which regions will face water stress in the future under scenarios of economic growth, land-use change, and climate change cannot be determined using historical observed stream flow. Stream flow is a function of climate and land surface. With a changing climate due to local and global greenhouse gas and pollutant emissions, a detailed spatial model of runoff driven by climate variables and accounting for land-use change is needed to estimate future runoff, regionally and nationally. The runoff model should be coupled with a reservoir storage model to determine firm water supply. Then, the water supply should be linked with a water demand model to examine future water stress.

In this chapter, the development of the hydrologic model CHARM (Climate- and Human Activities-sensitive Runoff Model) is described as one step in assessing the water availability in China and its variability. Section 2.2 discusses in detail the water balance components that are the physical basis for the model. Section 2.3 describes the larger structure of the model and how these components have been linked to model entire basins and regions. In the fourth section, the model is applied at the basin and national scales. At the basin scale, the model is tested on two hydro-climatologically different subbasins of the Huang He (Yellow River) in China. Analyses of the impacts of climate and land-use changes on the available

water in these basins are performed. In Section 2.6, the model is applied to the nine major watershed regions of China to estimate the natural available water supply. Conclusions are discussed in Section 2.7.

2.2 Model Component Description

2.2.1 Water balance

The impacts of land-use change on climate, the environment, and the economy are becoming increasingly important issues. Any hydrologic model developed to assess the water resources in China should therefore be sensitive to land cover, land use, and management practices. This problem is not a new one, and the fact that runoff can vary considerably in time and volume with different land cover, land use, and management practices is well known. As early as 1972, the Soil Conservation Service (SCS) in the United States published a method for estimating stormflow from rainfall events that addressed the problem for direct runoff (USDA, 1985). The method was the result of decades of research and has been evolving ever since. In 1986, the SCS developed the TR-55 model, which uses the "curve number" method, with the specific goal of assessing the effects of urban development on runoff (USDA, 1986). The curve number method has also been used as the direct runoff component in the HELP (Hydrologic Evaluation of Landfill Performance) model used by the US Environmental Protection Agency (EPA, 1994), the SWAT (Soil Water Assessment Tool) model (USDA, 1994), and many others. Because of its wide acceptance and ability to handle different soil types, land uses, and management practices, the curve number method is also used for the direct runoff component of CHARM. Once direct runoff is abstracted, the remaining water enters the soil moisture zone, where a relatively simple water balance is performed, abstracting water for evapotranspiration and subsurface flow. The overall structure of the water balance used in the hydrologic model is depicted in *Figure 2.1*.

As shown in *Figure 2.1*, the water balance consists of five components: precipitation, stormflow, infiltration, evapotranspiration, and subsurface flow. A water balance equation describing the above figure can be written as

$$S_{\max}\frac{dz}{dt} = P(t) - SF(z,t) - E(Et_0, z, t) - SSF(z,t), \tag{2.1}$$

where S_{max} is the maximum soil storage capacity; z is the relative soil storage ($0 \leq z \leq 1$); P is precipitation; SF is stormflow; E is evapotranspiration; and SSF is subsurface flow.

Each component of this water balance is discussed in the following sections.

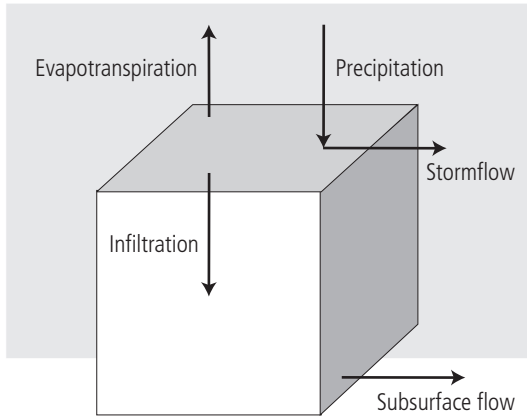

Figure 2.1. Structure of water balance used in CHARM.

2.2.2 Precipitation

Precipitation is given as input to the model and is discussed later with the other model inputs.

2.2.3 Stormflow

As discussed above, stormflow is calculated by CHARM according to the SCS's curve number method. The basic premise of the SCS method is that the ratio of direct runoff to total precipitation, after an initial abstraction, is the same as the ratio of water retained in the soil to the maximum soil retention:

$$\frac{DR}{P - I_a} = \frac{R}{R_{\max}}, \tag{2.2}$$

where I_a is the initial water abstraction before any runoff will occur (mm); R is the water retained in the watershed (mm); R_{max} is the maximum retention in the watershed (mm); and DR is direct runoff, or stormflow (mm). By the continuity principle,

$$R = (P - I_a) - DR\,. \tag{2.3}$$

Substituting Equation (2.3) into Equation (2.2) yields

$$\frac{P - I_a - DR}{R_{\max}} = \frac{DR}{P - I_a}\,. \tag{2.4}$$

The following empirical relationship was developed for the initial abstraction:

$$I_a = 0.2R_{\max}\,. \tag{2.5}$$

Table 2.1. Sample SCS curve number table.

Land use	Hydrologic soil group			
	A	B	C	D
Cultivated land: Without conservation treatment	72	81	88	91
Cultivated land: With conservation treatment	62	71	78	81
Pasture or rangeland: Poor condition	68	79	86	89
Pasture or rangeland: Good condition	39	61	74	80
Wood or forestland: Thin stand, poor cover, no mulch	30	58	71	78
Wood or forestland: Good cover	25	55	70	77
Commercial and business areas (85% impervious)	89	92	94	95
Industrial districts (72% impervious)	81	88	91	93
Residential: 1-acre lot size (20% impervious)	51	68	79	84
Residential: 1/2-acre lot size (25% impervious)	54	70	80	85
Residential: 1/8-acre lot size (65% impervious)	77	85	90	92
Paved parking lots, roofs, driveways, etc.	98	98	98	98

Substituting Equation (2.5) into Equation (2.4) and solving for direct runoff now gives

$$DR = \frac{(P - 0.2R_{\max})^2}{(P + .8R_{\max})} \ . \tag{2.6}$$

Plotting direct runoff over precipitation for many watersheds, the SCS found a family of curves and developed a dimensionless constant, the curve number (*CN*), to describe these curves. The curve number varies from 0 to 100 and depends on land use, management practices, and soil type. The curve number can be used to calculate the maximum retention (in mm) according to the following formula:

$$R_{\max} = 254(\frac{100}{CN} - 1). \tag{2.7}$$

Tables of curve numbers match land use and management practices and soil types to obtain a curve number for those conditions. A small, sample curve number table is shown in *Table 2.1*.

For the China case study, soil types and land-use categories were matched with the SCS land-use tables to obtain curve numbers for China. Since slope data are available, a slope adjustment is also made by CHARM to the curve number according to the following formula (USDA, 1994:13):

$$CN_{2s} = \frac{1}{3}(CN_2 - CN_1)[1 - 2\exp(-13.86SL)] + CN_2 \ , \tag{2.8}$$

where CN_{2s} is the curve number for antecedent moisture condition 2 corrected for slope; CN_2 is the curve number for antecedent moisture condition 2; CN_1 is the curve number for antecedent moisture condition 1; and SL is slope (m/m).

The curve number for antecedent moisture condition 1 can be found from the following equation:

$$CN_1 = CN_2 - \frac{20(100 - CN_2)}{100 - CN_2 + \exp[2.533 - 0.0636(100 - CN_2)]} \,. \tag{2.9}$$

The curve numbers, then, allow for the calculation of stormflow according to Equation (2.6). The remaining rainwater that does not run off directly infiltrates the soil, where it is partitioned into evapotranspiration and subsurface flow as described in the following sections.

2.2.4 Evapotranspiration

To calculate evapotranspiration, CHARM applies a method recommended by the Food and Agriculture Organization of the United Nations (FAO) (Allen *et al.*, 1998) and similar to the method used in the agro-ecological zones (AEZ) methodology (Fischer *et al.*, 2000). Because the estimation of evapotranspiration itself requires a large number of calculations and is discussed in these other sources, the equations are not included here. However, the development of the equations used for evapotranspiration and their implementation in CHARM are discussed in detail in Appendix A.

2.2.5 Subsurface flow

The final component of the water balance in CHARM is subsurface flow (SSF), which accounts for any water that flows beneath the soil surface by percolating down through the soil. This process is also accomplished quite simply in CHARM by use of a calibration coefficient (α) multiplied by a function of the relative storage (z) (Kaczmarek and Krasuski, 1991; Yates, 1996; Bowling and Strzepek, 1997):

$$SSF = \alpha z^2. \tag{2.10}$$

Referring back to *Figure 2.1*, we now see that all the components of the water balance are calculated and Equation (2.1) is solved. With the methods of the individual components established, we can now look at the larger picture of how the model functions.

2.3 Model Structure

The preceding section described the specific details of individual components of the water balance performed by CHARM. This section describes how these components are assembled to model a region or river basin as a whole. The overall structure of the model is depicted in *Figure 2.2*.

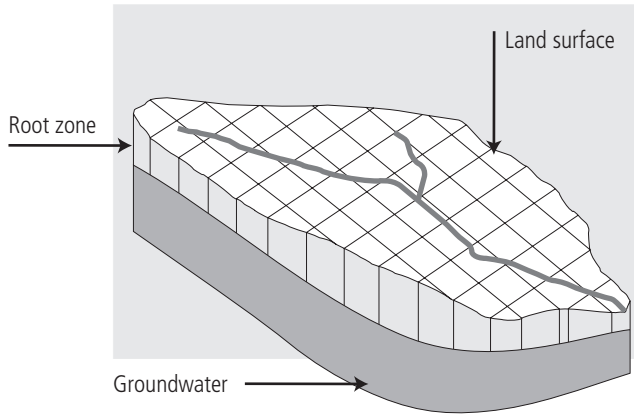

Figure 2.2. Structure of CHARM.

The figure shows a river basin split into grid cells on the surface with a single groundwater cell beneath. This is actually the most detailed modeling option available in CHARM. Here, stormflow, evapotranspiration, and subsurface flow are modeled in each individual cell. However, a single parameter is calibrated for the entire basin, since data are not available for runoff in each cell.

Although the figure shows the river basin split into grid cells, many other configurations are also possible in CHARM. The entire basin can be modeled as a unit using the average curve number and a single station daily rain input. It can also be modeled by creating "virtual" basins where grid cells with similar land uses, management practices, and soil types within the basin are lumped together to form a modeling unit. Both of these methods produce more rapid calculations, but at the expense of information at the individual pixel level. In many cases, however, there is little variation among the different modeling methods (Bowling and Strzepek, 1997). It is important to note that the primary reason for modeling at the grid-cell level is that output from this approach may be aggregated differently later; this is done in the work that involves modeling river basins and reaggregating pixels to economic regions for economic analysis.

2.3.1 Inputs to CHARM

To understand how CHARM functions, knowledge of the inputs and how they are used to produce the output (runoff) is necessary. *Table 2.2* provides a list and brief description of inputs. A more detailed description of how some of the inputs are used is provided in the following sections.

Table 2.2. Inputs to CHARM

Input	Used to calculate	Description
Precipitation	Runoff	Rainfall can be input as average monthly values from a spatial grid, or it can be entered as daily rainfall from individual stations.
Curve number table	Stormflow	Curve number table must include all the combinations of land uses and soil types in the area to be modeled.
Slope	Stormflow	Slope (in m/m) is input at the same scale as the scale of the simulation: grid cell, virtual basin, or basin.
Average temperature	Evapotranspiration	Average temperature is input by grid cell as monthly averages (in $^{\circ}$C) or monthly time series data.
Temperature range	Evapotranspiration	Temperature range is input by grid cell, the same as mean temperature.
Sunshine hours per day	Evapotranspiration	Sunshine hours are also input at the grid-cell scale as average monthly values.
Latitude	Evapotranspiration	Latitude (in decimal degrees) is used in the calculations as well as to keep track of the location of the grid cells.
Longitude	Evapotranspiration	Longitude (in decimal degrees) is used in the same way as latitude.
Altitude	Evapotranspiration	Altitude (in m) is also used like latitude.
Land use	Stormflow	Land use is input at the grid-cell scale and corresponds to the curve number table in the SCS method.
Soil texture	Stormflow	Soil texture is input at the grid-cell scale and corresponds to the curve number table in the SCS method.
Available water content	Water balance and subsurface flow	The available water content (in mm/m) of the soil is the maximum soil storage minus the wilting point storage per meter of soil.
Soil depth	Water balance and subsurface flow	Soil depth (in cm), when multiplied by the available water content, gives the total amount of water that can be used in the soil. This is the figure used for the maximum soil storage.
α*	Subsurface flow	α can be input to the model or can be calibrated within the model.
α bounds*	Subsurface flow/calibration	The α bounds are used to set bounds on, or to bracket, α in the bisection method that is used when calibrating.
α tolerance*	Subsurface flow/calibration	The bisection method calibrates to the maximum error specified by the α tolerance.
Maximum iterations*	Subsurface flow/calibration	Once the calibration loop has gone through the maximum iterations, it will end and the best value of α will be used.
Region/year	Runoff	A region identification and the year to be simulated must be input and be consistent throughout files.
Precipitation station*	Runoff	If not using grid-cell rainfall data or the nearest rain gauge, the user can input a single rain gauge to use for the calculations.
Actual runoff*	Calibration	To calibrate the model, actual annual runoff must be given corresponding to the year of precipitation data used.
Starting soil moisture*	Runoff	In the first time period, the soil moisture is zero, unless set by the modeler here.
Crop coefficient	Evapotranspiration	The user may input an annual average crop coefficient to use in calculating evapotranspiration.
Multipliers	Runoff and climate change	Many components of the model may be increased or decreased for sensitivity studies, improved calibration, or climate change studies using multipliers. Multipliers are available for the curve number, maximum soil storage, average temperature, maximum and minimum temperature, and precipitation.
Modeling options	Runoff	Several modeling options can be input to control the model and its components.

*Optional.

Precipitation

Precipitation is input to CHARM as either monthly values at the grid-cell scale or as daily values from individual stations. If monthly grid-cell values are used and a series of daily values is available at some scale, daily precipitation is calculated by finding the ratio of the daily value to the monthly average value and using this ratio to find the daily precipitation values for other years. Otherwise, spline interpolation (Press *et al.*, 1992) is used to calculate daily values from monthly values.

Actual daily values, however, are strongly preferred. To illustrate why, consider a storm that occurs on a single day of the month and delivers 400 mm of rain, the only rain that falls that month. If the soil can only store 100 mm of water, at least 300 mm of this rainfall must run off. The runoff will even be higher if the storm intensity is greater and the water cannot infiltrate the soil fast enough to be stored there. In contrast, if 400 mm of rain falls over the entire month, spread throughout the month, then only about 13 mm falls per day. Because of interception, evapotranspiration, and percolation, the soil layer may never become saturated, and runoff will be greatly reduced, possibly not occurring at all. For this reason, daily time series precipitation data produce more accurate results that also are more sensitive to land use and management practices.

In the current implementation of CHARM, daily precipitation at individual stations is used and the Thiessen method is applied to generate daily time series values for precipitation at the grid-cell level. The Thiessen method assumes that the precipitation at any point is the same as that at the nearest gauge (Chow *et al.*, 1988). It is also possible in CHARM to select a particular station to use when modeling a basin. However, this is only included for flexibility and can be most useful when a few years of precipitation data at one of the stations in the basin are missing.

Other Climatic and Physical Data

The application of other climatic and physical data is relatively straightforward, as described in *Table 2.2*. Again, daily time series of all the climatic data would be ideal. However, temperature and sunshine hours do not vary as widely on a day-to-day basis as precipitation does and are not as influential as precipitation in calculating monthly runoff. Therefore, average monthly temperature and sunshine values are converted to pseudo-daily values using a spline interpolation.

2.3.2 Calibration

Several of the input coefficients in *Table 2.2* are used only for assisting the process of calibrating model parameters. These parameters are optional, since the model may be used to calibrate the coefficient (Equation [2.10]) or may be applied with a given value. When the model is used to calibrate the coefficient, it does so using

Figure 2.3. Map of China showing the provinces, major rivers, and case study basins.

a bisection method (Press *et al.*, 1992:353). This method of finding roots requires that the root be bracketed so that an upper and lower bound for α must be input. Also, a tolerance must be input to specify the accuracy of the iterative numerical procedure desired by the modeler. Finally, the maximum number of iterations input stops the calibration loop in case a root is not found. In this case, the best value of α obtained during any of the completed iterations is used.

2.4 Case Studies

To test and verify output from CHARM, runoff data were obtained from stations on tributaries of the Huang He. Each station is located on the tributary, but near the confluence of the tributary with the Huang He. Basins were chosen that were between 20,000 and 50,000 km^2 so that the water could easily travel from one end of the watershed to another within a month and routing techniques would not be necessary. These test basins provide good examples of how the model can be used and the results produced. Two of these basins, the Tao He and the Yilou He, are described here in detail along with the results of modeling them with CHARM. Their locations within China are shown in *Figure 2.3*.

2.4.1 Tao He

The Tao He flows through the southwestern part of Gansu province where it borders on Qinghai province (see *Figure 2.3*). Starting at an elevation of 4,000 meters at $34°4'$ north latitude and $101°6'$ east longitude, the elevation of the watershed drops 2,000 m over a distance of 470 km. It ends in the upper reach of the Huang He at Lanzhou, the capital of Gansu province, at an elevation of 2,000 m, draining an area of about 25,000 km^2. The watershed consists primarily of grassland but also includes some bare land, bush, timber forest, and both irrigated and nonirrigated farmland. The region is cold and mountainous and receives an average annual rainfall of 600 mm.

Calibration

To calibrate and test CHARM on the Tao He, rainfall and runoff data must be available for the same time period. Daily rainfall data are available for 1951 to 1982 at certain rain gauges in and around the watershed from the Institute of Geographic Sciences and Natural Resources Research (Kaiser *et al.*, 1996), but only a few years of runoff data (from 1951, 1980–1985, 1987, and 1988) were gathered for this study by the Institute of Geography in the Chinese Academy of Sciences. The runoff data are supplied as monthly average stream flows from a stream gauge at Minhe near the confluence of the Tao He and the Huang He. The raw data are unadjusted for reservoir operations; that is, they do not represent the natural, unmanaged flow. Because the data are unadjusted, the best time period for testing the rainfall–runoff relationship is before dams were built in the area. Although a few small dams may have existed, almost all large dams in China were constructed after 1950 (ICOLD, 1984). Therefore, 1951 is an appropriate year for calibrating the model with available data.

In addition to rainfall and runoff data, CHARM requires soil data, geographic data, and additional climatic data, as shown in *Table 2.2*. The required temperature, land-use, soil, elevation, and slope data were obtained from the IIASA-LUC GIS Database (IIASA, 2001) for 5 km x 5 km grid cells. The Climate Research Unit, University of East Anglia provided wind speed and cloudiness information on a half-degree scale (New *et al.*, 1999).

CHARM was calibrated using the 1951 rainfall and runoff data and a grid resolution of 5 km x 5 km. An initial soil moisture of 55 mm was used, based on average December conditions. The objective of the calibration was to match the runoff volume for the entire year as a measure of the available water resources in the region. The model is calibrated to this yearly value with a tolerance of 5%. *Figure 2.4* shows the model results.

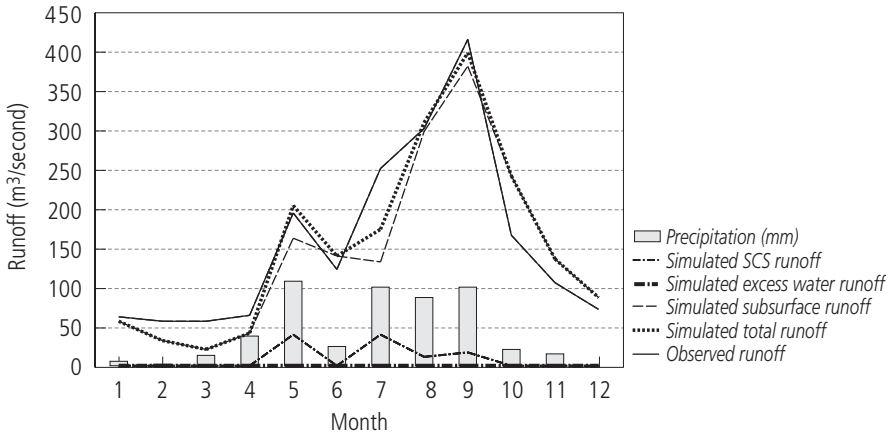

Figure 2.4. Comparison of actual with simulated 1951 total runoff and its components on the Tao He.

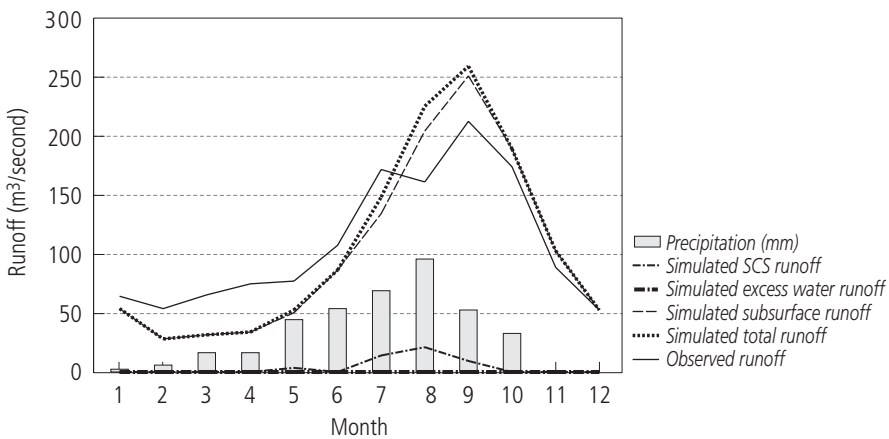

Figure 2.5. Comparison of actual with simulated 1980 total runoff and its components on the Tao He.

For the Tao He, the coefficient for subsurface flow, α, calibrated to 3.125. This produced a difference between the actual and simulated yearly runoff of 1%. *Figure 2.4* shows that although the model was calibrated for yearly runoff, simulated monthly runoff also correlates well with the actual monthly runoff, showing that the dynamics of the system are well modeled. Simulating another year for the same basin produces similar results, as shown by *Figure 2.5*.

When the model is calibrated based on 1980 data, α again calibrates to 3.125, this time with a yearly runoff error of 4%. If the calibration tolerance were set finer than 5%, α would be slightly different between the two years. However,

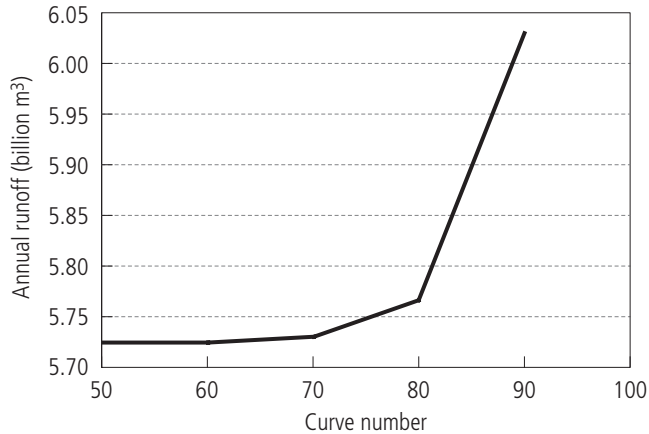

Figure 2.6. Sensitivity of annual runoff in the Tao He to changes in the curve number.

the fact that α remains very close between the two years indicates that the model is effective and verifies one of the major assumptions in the model methodology, namely, that α is a single subsurface flow parameter that describes subsurface flow for the basin. Although the simulated monthly runoff in this case does not correlate to actual monthly runoff as well as it did for 1951, the features of the simulated and actual curves remain similar. An unknown factor that may influence the actual runoff curve and account for the difference is the number of small dams built on the river between 1951 and 1980. At Lanzhou, where the Tao He flows into the Huang He, for example, the Liujiaxia Dam was completed in 1962. Many other dams were built within this time frame, but no data were available for dams on the Tao He.

Sensitivity of the Tao He to Land-Use Change

With CHARM calibrated for the Tao He, we tested the sensitivity of runoff to land-use/cover change in the watershed. This was achieved by quantifying the relationship between monthly runoff in the Tao He basin and a broad range of SCS curve numbers (see *Table 2.1* for the relationship between curve numbers and land uses). The effects of potential land-use change on the Tao He can be seen in *Figures 2.6* and *2.7*.

The figures show that land-use change does not have a large impact on annual flows for the Tao He, with only a 5% difference between a curve number of 50 and one of 90. This result is not unexpected, however, since the time period of one year is very long. Land-use changes produce a greater effect on the timing and variability of flows throughout the year than on annual runoff. Furthermore, only a small

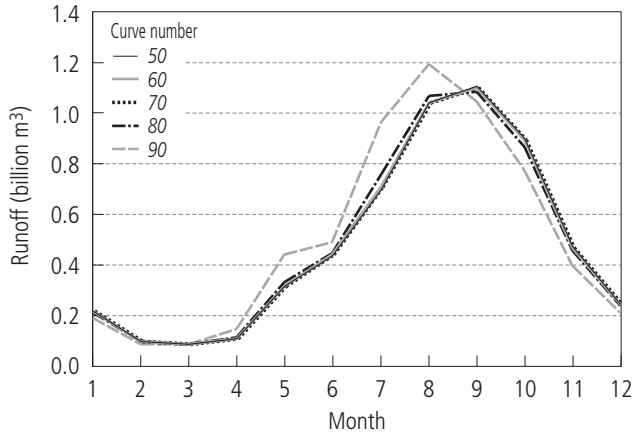

Figure 2.7. Sensitivity of monthly runoff in the Tao He to changes in the curve number.

portion of the total flow in these cases is from stormflow, which is most susceptible to changes in land use. *Figure 2.7* also shows that under increasingly impermeable conditions—that is, with an increasing SCS curve number—the runoff shifts earlier in the year. This is also expected, as runoff flows more quickly from impermeable land.

Sensitivity of the Tao He to Climate Change

To test the sensitivity of the Tao He watershed to climate change, CHARM is first run with rainfall data from 1960–1980 as a baseline scenario and then for average temperature increases of 1°C , 2°C, and 3°C, and for precipitation changes of –30%, –15%, +15%, and +30%. The results of the sensitivity analysis are displayed in *Figure 2.8*.

The figure shows that the sensitivity of annual runoff to temperature in the Tao He is small. Increased evapotranspiration decreases runoff by an average of 2.4% per 1°C increase in temperature. Changes in precipitation naturally have a much larger effect. Increasing precipitation by 30% increases runoff by more than 50%, nearly twice as much.

Impacts of Climate Change on the Tao He

Figure 2.8 shows the results of simulating the Tao He with CHARM under six climate change scenarios from three general circulation models (GCMs) used by Working Group II in the Intergovernmental Panel on Climate Change's Second Assessment Report. The scenarios are transient, coupled ocean–atmosphere scenarios

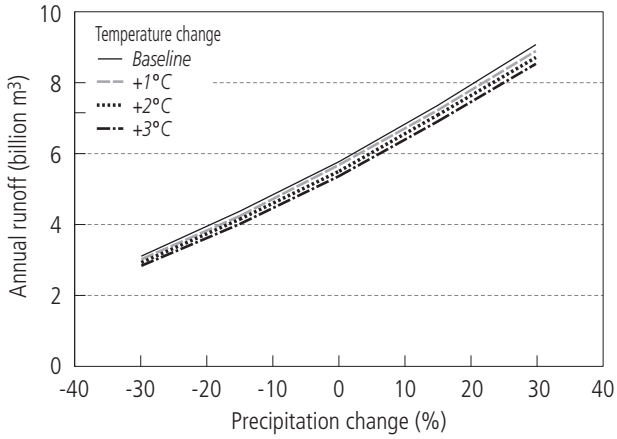

Figure 2.8. Climate sensitivity analysis in the Tao He.

Table 2.3. GCM scenario output for annual temperature and precipitation change for the Tao He basin.

	Scenario					
	GFTR2	GFTR3	MPTR2	MPTR3	HCTR2	HCTR3
Temperature change (°C)	2.27	3.03	1.81	2.88	1.27	2.79
Precipitation change (%)	11.3	18.0	–2.0	–0.2	18.3	18.7

Note: GF refers to the Geophysical Fluid Dynamics Laboratory's model scenarios; MP refers to the Max Planck Institute's model scenarios; HC refers to the Hadley Centre's model scenarios; TR refers to the fact that they are transient models; and 2 and 3 indicate the decades modeled.

from the Geophysical Fluid Dynamics Laboratory's GFDL89 model (Manabe *et al.*, 1991, 1992), the Max Planck Institute's ECHAM1-A model (Cubasch *et al.*, 1992), and the Hadley Centre's UKTR model (Murphy 1995a, 1995b; Murphy and Mitchell, 1995). The scenarios provide monthly temperature and precipitation values under different emissions scenarios designed to represent the current and future situations. In this case, two time periods are used, with decade two representing the years around 2020 and decade three representing the years around 2050. Results of the climate change scenarios are then compared with a baseline climate developed from 30 years of historical data to produce monthly temperature differences and precipitation ratios between the baseline and changed-climate scenarios (Viner *et al.*, 1995). *Table 2.3* shows an overview of the annual temperature and precipitation changes predicted by the GCM scenarios for the Tao He basin.

In all scenarios, temperature increases between 1°C and 4°C. Precipitation, however, decreases in the Tao He under the ECHAM1-A scenarios, while it

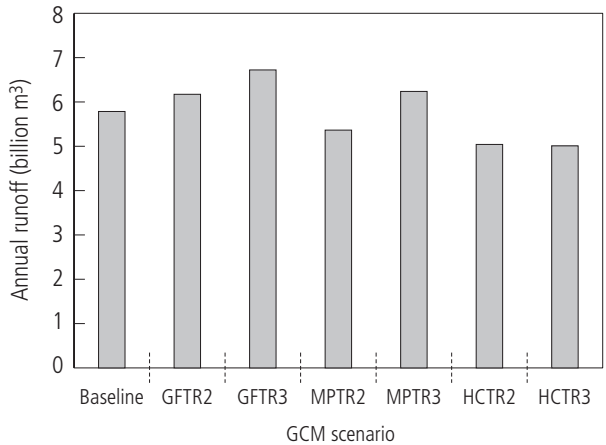

Figure 2.9. Results of climate change scenarios of annual runoff of the Tao He from three GCMs.

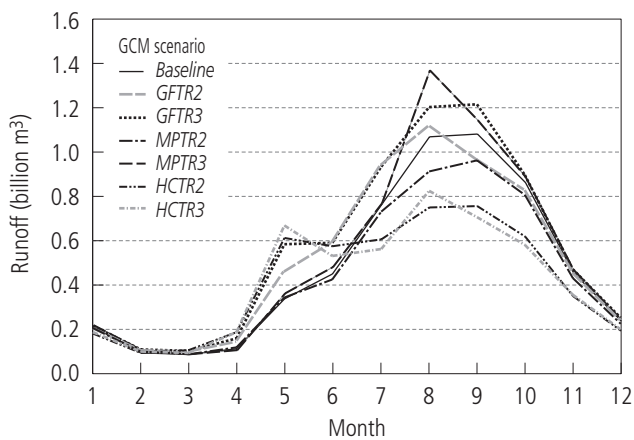

Figure 2.10. Results of climate change scenarios of monthly runoff of the Tao He from three GCMs.

increases in all the other scenarios. The GCM scenarios differ in how they distribute precipitation changes throughout the year, which is apparent in the CHARM simulation results.

The monthly temperature differences and precipitation ratios serve as input to CHARM to simulate runoff under the new climatic conditions. The results of these simulations are shown in *Figures 2.9* and *2.10*.

The GCMs do not agree as to how precipitation will change in the Tao He area and hence differ on how runoff will be affected by climate change. The GFTR

scenario for 2050 (GFTR3) predicts a 16% increase in runoff, while the HCTR scenario for the same decade produces a 13% decrease. These GCMs, however, do not model precipitation variables (as well as other climate variables) well at local scales such as a river basin (Viner *et al.*, 1995; Howe and Henderson-Sellers, 1997). An interesting result is that the changes in annual runoff are, in some cases, in the opposite direction of changes in annual precipitation, owing to changes in the timing of precipitation during the year. The Hadley scenarios, for example, spread precipitation more evenly throughout the year, so that peak flows are not as high and more rain falls during dry periods, when the soil can absorb and evaporate the additional moisture. The end result is less total runoff for the year, even though more precipitation actually fell. *Figure 2.10* illustrates that not only the quantity of flow but also the timing of flows could change in the basin. In three scenarios, the peak is actually shifted earlier in the year. The growing season for agriculture in the area could change as a result, or storage would have to be increased to maintain the original hydrograph in the basin.

2.4.2 Yilou He

As another example of the testing and verification of output from CHARM, the results of calibrating and modeling the Yilou He are discussed here. The Yilou He is actually formed from two rivers, the Yi He and the Lou He, which originate in Shanxi province. For the purpose of this example, the rivers will be grouped into one watershed and called the Yilou watershed. The watershed is about 400 km long and covers an area of approximately 20,000 km^2. Located primarily in Henan province, it varies from an elevation of about 1,700 m at its highest to an altitude of about 100 m at the confluence with the Huang He. It consists primarily of farmland, both irrigated and nonirrigated, but also has a substantial amount of timber forest and patches of hilly grassland and bush.

Calibration

Runoff data are available for the Yilou He for 1951, which is the best year to calibrate the model for the same reason as in the Tao He case study. The results of the calibration simulation for 1951 are shown in *Figure 2.11*.

In the case of the Yilou He for 1951, α calibrated to 3.9 and the difference between the actual and simulated annual runoff was about 4%. *Figure 2.11* shows that the model matched the peak flow well, but the simulated flow declined at a slower rate than the actual runoff, suggesting that the model calculates more water retention in the soil and less stormflow than is actually the case. The model also missed the first peak. However, there are many additional sources of error in modeling this basin as compared to modeling the Tao He. Like the Tao He, one major source of

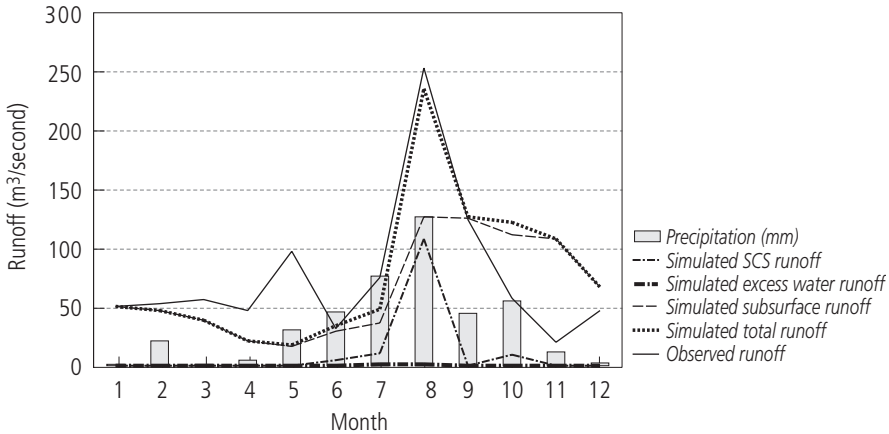

Figure 2.11. Comparison of actual with simulated 1951 total runoff and its components on the Yilou He.

error is that daily rainfall data were only available at one rain gauge in the basin for 1951. Therefore the first peak could have resulted from a local storm that was not recorded at the rain gauge used for the simulation. Overall, the greatest source of error in modeling this basin is the development of irrigation and reservoirs. By 1960, seven completed reservoirs had a combined capacity of 1.24 billion m^3 of storage, about 21% of the average annual flow, and many more reservoirs may have existed. The construction of these reservoirs combined with diversions for agriculture that started long before 1951 had a significant impact on the hydrograph downstream. The results of the modeling can only be viewed as the natural runoff that would occur if the rain gauge used were indicative of the rainfall over the entire basin.

After 1951, the next year of runoff data available for this study was 1971. By then, at least 15 dams had been completed in the watershed. Three of them had just been completed and were filling while others were still under construction. By 1978, almost the entire average annual flow of the basin could be stored. Currently, close to three times the average annual flow can be stored. Trying to calibrate a rainfall–runoff model using raw stream flow measurements becomes futile without knowing more about the operational policy and releases from these reservoirs. The raw flow data now simply measure the releases from the reservoir upstream, which has many more reservoirs upstream of it. The stream flow data no longer necessarily have a simple and direct relationship to rainfall, because water management determines stream flow.

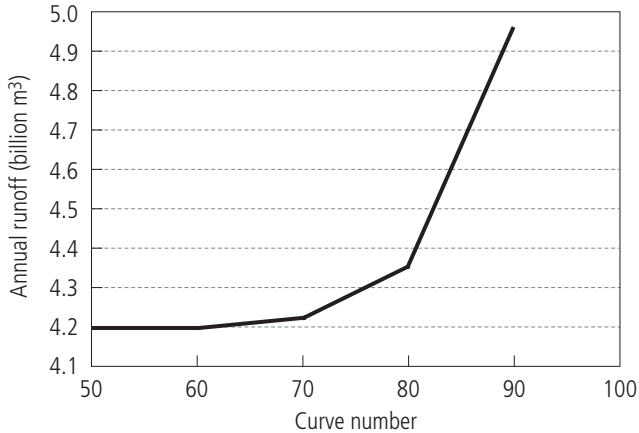

Figure 2.12. Sensitivity of annual runoff in the Yilou He to changes in the curve number.

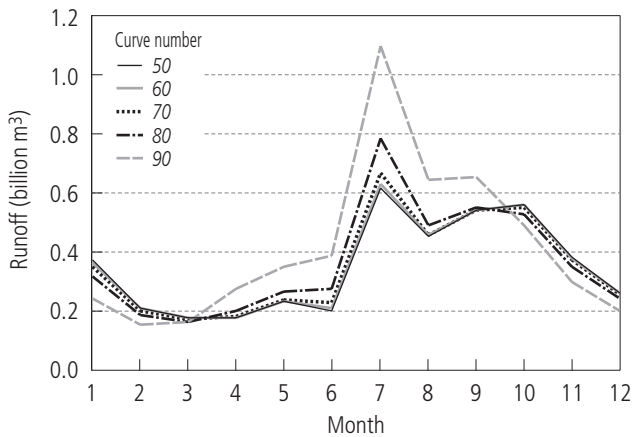

Figure 2.13. Sensitivity of monthly runoff in the Yilou He to changes in the curve number.

Sensitivity of the Yilou He to Land-Use and Climate Change

Figures 2.12 and *2.13* illustrate the impacts of land-use change in the Yilou He, as measured by changing the SCS curve number. The impact of land-use change on runoff is more pronounced in the Yilou He than in the Tao He, primarily because of the sharp peak runoff in July. Impermeable conditions cause even more of the intense rainfall during June through September to run directly off the land. In the Tao He, where the monthly hydrograph is smoother, annual runoff increased only 5% between the curve numbers of 50 and 90, but in the Yilou He, the modeled increase is close to 20%. Flow in the peak month increased by an astounding 78%.

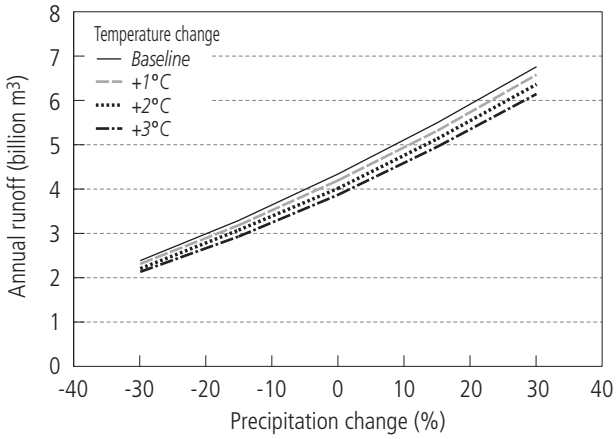

Figure 2.14. Climate sensitivity analysis in the Yilou He.

Table 2.4. GCM scenario output for annual temperature and precipitation change for the Yilou He basin.

	Scenario					
	GFTR2	GFTR3	MPTR2	MPTR3	HCTR2	HCTR3
Temperature change (°C)	2.88	3.79	2.06	2.99	1.21	2.45
Precipitation change (%)	3.7	12.1	4.8	9.0	5.9	11.8

Note: GF refers to the Geophysical Fluid Dynamics Laboratory's model scenarios; MP refers to the Max Planck Institute's model scenarios; HC refers to the Hadley Centre's model scenarios; TR refers to the fact that they are transient models; and 2 and 3 indicate the decades modeled.

Sensitivity to temperature and precipitation change in the Yilou He, shown in *Figure 2.14*, is comparable to that in the Tao He. The sensitivity to precipitation changes is about the same as in the Tao He, whereas the temperature sensitivity is slightly higher at 3.4% per 1°C.

Table 2.4 shows the annual temperature and precipitation changes predicted by the GCM scenarios for the Yilou He basin. In the Yilou He basin, all scenarios predict an increase in both temperature and precipitation.

Figures 2.15 and *2.16* show the changes in annual and monthly runoff, respectively, under the GCM scenarios. Once again, the changes predicted by different GCM scenarios differ in both magnitude and direction. The changes, though, are substantial. At the extremes, the HCTR for the third decade (HCTR3) indicates an increase in runoff of over 30%, whereas the GFTR scenario for the second decade (GFTR2) shows a decrease of close to 25%. In HCTR3, the peak monthly flow increases by more than 75%.

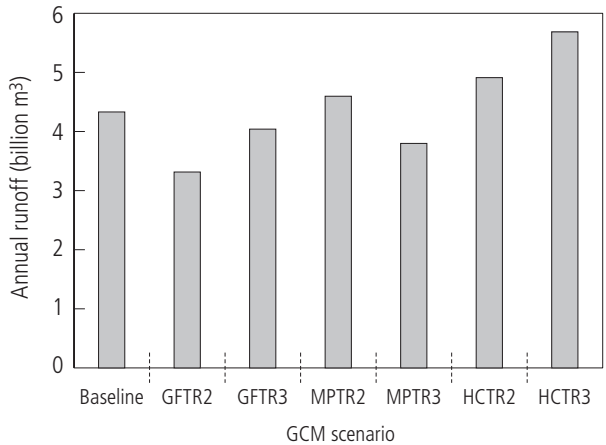

Figure 2.15. Results of climate change scenarios of annual runoff of the Yilou He from three GCMs.

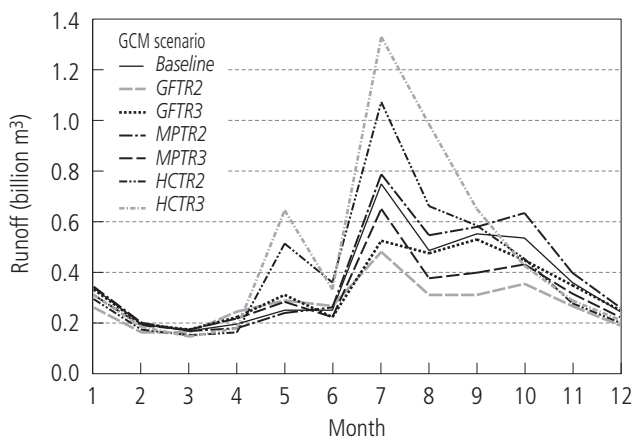

Figure 2.16. Results of climate change scenarios of monthly runoff of the Yilou He from three GCMs.

2.4.3 Analysis of land-use and climate change on the Tao He and Yilou He

The land-use change figures for the Tao He and Yilou He basins produce several important results. First, they show that different basins can respond quite differently to changes in land use, because of different geologic, geomorphometric, and climatic conditions. Second, the figures show that land-use changes have a much smaller impact annually than they do intra-annually. Land-use changes have the effect of changing the timing of flows within the year, rather than making large changes in

annual runoff, although significant changes can also be made in annual flows. The runoff changes within a year usually produce more extreme events, greater peaks, and longer dry spells. Third, the more impermeable the land is made, the greater the impact of further land-use changes. Each of these results has repercussions for water management.

Figure 2.8 shows that the sensitivity of runoff to changes in average temperature in the Tao He is only about 2.4% per 1°C increase and that runoff changes by an average of 1.72% per 1% change in precipitation. Results were similar for the Yilou He, where the sensitivity to average temperature was a little greater at 3.4% per 1°C increase and runoff again changed 1.69% per 1% change in precipitation. These results between the basins illustrate that different basins may react to climate change in different ways, depending on the climatic and physical conditions of the basins. *Figure 2.7* also shows that with increasing curve numbers, the peak flow of the Tao He occurs earlier in the year, changing the hydrograph and perhaps presenting further challenges and expenses to water management in the watershed if the new hydrograph shape is less ideal. In the Yilou He the peak monthly flow remained in the same month.

Although the GCM scenarios show significant changes in the annual runoff for both the Tao He and the Yilou He, the different GCMs do not agree with one another on the magnitude or direction of these changes. In the Tao He, changes in precipitation in the second decade range from a 6.8% increase for the GFTR scenario to a 12.8% decrease for the HCTR scenario. In the third decade, the GFTR scenario predicts a 16.2% increase while the HCTR scenario predicts a 13.1% decrease in runoff. Ranges in the Yilou He are similar, but the directions are reversed. The GFTR scenario predicts a 23.5% decrease in runoff for the first decade, while the HCTR scenario predicts a 13.3% increase. In the third decade, the MPTR scenario predicts the biggest decrease at 12.2%, while the HCTR scenario predicts a 31.4% rise. Each of the GCM scenarios predicts a substantial change in runoff, with the smallest changes being more than 6%. However, no further conclusions can be drawn from these climate scenarios.

2.5 Discussion of the Verification of CHARM and Data Limitations

The examples of calibration and use of CHARM on the Tao He and Yilou He show that the model, which is calibrated to a yearly runoff value, also simulates monthly flows quite well. Because of heavy development in the Yilou He and in later years in the Tao He, the monthly runoff hydrograph has been significantly altered from the natural state calculated by CHARM. Smaller amounts of storage, as seen in 1951, can affect the timing of flows significantly, but should not affect the total annual

runoff much; thus CHARM could still be calibrated to annual runoff at these basins in earlier years. Validating the model with monthly flows, though, is difficult, since both these watersheds were at least partially developed in the years that they could be modeled. The Tao He in 1951 was the least developed and so provides the best opportunity for model testing and verification.

The simulation for the Tao He basin matched the shape of the observed hydrograph reasonably well, but more and better-quality data would result in more reliable parameterization of the model and improved simulations. Only one rain gauge measured daily rainfall for the basin in 1951. The one flow gauge at the end of the basin provided only monthly average flows measured at the gauge, and other climatic data come as monthly averages and not daily values. The benefits of more and better-distributed rainfall data and data from more flow gauges in the basin are obvious. More rain gauges provide more accurate precipitation data and a better accounting of how much water is entering the basin. More flow gauges with more frequent data would provide for better verification of the model and would enable routing components to be added to it.

Slightly less obvious is how much help hydraulic soil parameters, which are not available, could be. As shown in *Figures 2.4*, *2.5*, and *2.11*, very little of the total simulated runoff is explained by the SCS curve number method for direct runoff. The majority of the runoff is from what the model describes as subsurface flow, which places a substantial burden on the calibration coefficient. Furthermore, in the model, land-use change affects only the stormflow component. While in reality, land-use change may indeed have the greatest effect on the stormflow, the subsurface component could still be affected by increased or decreased hydraulic conductivity. This suggests that the coefficient could also change slightly with land-use change, but the magnitude of this change is unknown. Two potential solutions to this problem are as follows:

1. Detailed groundwater modeling may give more accurate results in the case of land-use change, but it would also introduce many more parameters and unknowns into the system and require many more data.
2. Similar to what is done with the curve numbers for stormflow, coefficients could be applied for subsurface flow that correspond to different land uses, management practices, and soil types. To estimate such a set of land-use-specific coefficients, however, homogenous watersheds would need to be found that contain only one land use and soil type each. Estimations would need to be made for each land-use class, and data would need to be available accordingly.

Both of these solutions would add greater complexity to the model and require additional data. In the process, they may only result in small improvements to the simulations and are probably not justified for the primary use of the model.

Some fine-tuning could be done to CHARM itself, such as adding a simple routing scheme and improving the modeling of transpiration changes throughout the year. These changes could be made without more input data, but additional flow data would be required to verify the model's performance.

Ultimately, however, CHARM was designed to provide water availability estimates over large areas where detailed data are not always available. While the limitations of a model should be carefully considered when modeling and interpreting results, CHARM demonstrates that it is quite capable of approximating a complex system with limited data. Monthly flows in the less developed Tao He are well simulated. The calibration coefficient remains stable when calibrating the model for different years in the same basin, but varies slightly from basin to basin. This shows, as should be expected, that the calibration coefficient is a function of the physical features of the basin, such as the land use and soil type. Finally, as shown in the previous section, CHARM is well suited to assessing the impacts of climate and land-use change on available surface water resources.

2.6 Assessing China's Water Supply and Demand Balance

Now that CHARM has been developed, tested, and verified, it is ready to be used to assess the surface water resources in China as a whole and the variability in the surface water supply. Knowledge of the surface water resources and their variability is essential for calculating how much water can be reliably supplied to satisfy different demands and how much investment is needed to use the available water efficiently and effectively.

A series of indices, termed factors 1 to 5, is used to define and compare the water stress and security in major watershed regions in China. The first index is a per capita water resources scarcity index. It defines a condition of *water scarcity* when annual water supply is less than 1,000 m^3 per capita. *Water stress* is defined as between 1,000 m^3 and 2,000 m^3 per capita per annum. A second water stress index is related to water use and defines *water stress* as a condition when the use-to-supply ratio is greater than 0.4. *Water surplus* is indicated by a use-to-supply ratio of less than 0.1. The third index is a measure of hydrologic variability. Higher variability results in higher risk. Here, an interannual coefficient of variation of more than 0.3 is considered highly variable. Factor 4 is a risk reduction factor to indicate the extent to which current development has already reduced the risk from variability. If the ratio of storage to annual flow is greater than 1, the supply risk from runoff variability is highly reduced. Combining the variability factor and the risk reduction factor produces a water resources security factor, factor 5. By assigning each category of each factor a number, a total water resources availability rating (factor 6) can be derived. Since factors 3 and 4 are already combined to

create factor 5, only category values for factors 1, 2, and 5 are added to create this comprehensive water resources stress index. *Table 2.5* summarizes the class ranges of these indices; *Table 2.6* gives factor 5 values resulting from combinations of factors 3 and 4.

To calculate the surface water resources of China and the variability in the resource, the country was split into nine major watershed regions for calibration with data from China's Ministry of Water Resources and Electric Power (UN, 1997). CHARM was then calibrated for each region to the average annual runoff of the region. The inputs to the model are the same datasets used in the case studies described in the previous sections. The results of simulating stream flow from 1965 to 1980 are listed in *Table 2.7* and displayed in *Figure 2.17*. For the sake of comparison, *Figure 2.18* shows the average monthly precipitation and its variability, as calculated by applying the Thiessen polygon method to assign the precipitation from the nearest gauge to each pixel.

Using the information garnered from CHARM, basin-specific stress indices were calculated and are displayed in *Table 2.7*. *Table 2.8* contains a summary of the data necessary to calculate the index values. The following sections discuss the regions and results in greater detail.

2.6.1 General water resource issues in China

Table 2.9 and *Figure 2.17* show that runoff varies considerably among the different regions and years. Modeled runoff is within 2% of observed runoff for the entire country. The Interior basins, by far the driest, produce only 34 mm of runoff throughout the area, whereas the Southeast produces nearly 40 times as much. Three of the nine basins do not have the surface water resources to meet projected demand in 2010. If demand grows at the projected rate, water will have to be transferred from southern basins in order to meet demand in the northern part of the densely populated North China Plain.

The interannual variation is also significant. On average, the minimum annual flow for these 16 years is 40% below the average runoff. In regions that have water shortages, enough storage must be built to hold more than an entire year's runoff in order to reliably supply water over many years.

Since the variation within the year is not shown in *Table 2.9*, it is illustrated separately in *Figure 2.17*. *Figure 2.17* clearly shows that in almost all of the watersheds, 60% of the runoff occurs during only three months of the year, with the remaining months being quite dry. This high variability in both seasonal and annual flows is what led to the construction of more than 83,000 dams in China by 1990 (UN, 1997). In the following subsections, the key features of each of the nine watershed regions are summarized and the simulation results presented in *Table 2.9* are discussed.

Table 2.5. Indices of water resources stress.

Factor	Category	Value	Description
Factor 1: Per capita water scarcity index[a] (total annual renewable water resources/population)	0	>2,000 m^3/capita	Sufficient water
	1	1,000–2,000 m^3/capita	Water stress
	2	<1,000 m^3/capita	Water scarcity
Factor 2: Water use stress index[b] (use/supply)	0	<0.1	Water surplus
	1	0.1–0.2	Sufficient water
	2	0.2–0.4	Moderate water stress
	3	>0.4	Water stress
Factor 3: Hydrologic variability (coefficient of variation in annual runoff series)	0	<0.1	Low variability
	1	0.1–0.2	Mild variability
	2	0.2–0.3	Variable
	3	>0.3	High variability
Factor 4: Water supply risk reduction (storage/annual flow)	3	<0.3	Limited reduction
	2	0.3–0.6	Mild reduction
	1	0.6–1.0	Reduction
	0	>1.0	High reduction
Factor 5: Water resources security (factor 3 category number + factor 4 category number)[c]		0–6	Value of 0 indicates most secure, value of 6, least secure
Factor 6: Combined water resources availability (factor 1 + factor 2 + factor 5)		0–3	Very low stress
		4–5	Moderate stress
		5–7	High stress
		8–9	Very high stress
		10–11	Extremely high stress

[a] Postel (1992) uses this as a scarcity index, pointing to Falkenmark (1991). Shiklomanov (1993, 2000) arrives at a similar scarcity index by subtracting unrecoverable water consumption from total runoff and dividing by population. In Shiklomanov's grouping, <1,000 m^3 per capita per year is considered catastrophically low, 1,100–2,000 is very low, 2,100–5,000 is low, 5,100–10,000 is average, 10,100–20,000 is high, and >20,000 is very high.

[b] Falkenmark and Lindh (1993) state that "Many countries, therefore, consider 30%–60% of theoretically available water resources to be the practical limit of what they can mobilize." They go on to say that 20% may be a better estimate in the short to medium term for developing countries, since costs of water development have become "increasingly dominant in national economies" in the developed countries that have gone above this point. Raskin *et al.* (1997) use and explain the values used here.

[c] See matrix in *Table 2.6*, which shows the trade-off more clearly.

Table 2.6. Factor 5 values resulting from combinations of factors 3 and 4.

Factor 4: Water supply risk reduction	Factor 3: Hydrologic variability			
	0 – Low	1 – Mild	2 – Variable	3 – High
3 – Limited	3 – Secure	4 – Mildly	5 – Mild	6 – Low
2 – Mild	2 – Highly	3 – Secure	4 – Mild	5 – Mild
1 – Reduction	1 – Highly	2 – Highly	3 – Secure	4 – Secure
0 – High	0 – Highly	1 – Highly	2 – Highly	3 – Secure

Table 2.7. Statistical results of calibrating and simulating CHARM for the nine watershed regions, 1965–1980.

Watershed region[a]	Observed average annual runoff[b]	Area[c]	Modeled results: Average annual runoff[b]	Standard deviation[b]	Minimum[b]	Maximum[b]	Range[b]	Average annual depth[d]
1	165.3	1,242,375	164.1	32.3	114.6	230.6	116.0	132.1
2	28.8	297,625	27.6	12.0	9.3	47.6	38.2	92.9
3	74.1	312,050	75.7	24.7	44.6	126.8	82.2	242.7
4	66.1	841,125	61.0	18.7	34.9	109.0	74.2	72.5
5	951.3	1,767,980	938.3	113.1	755.8	1,140.7	384.9	530.7
6	468.5	571,400	440.7	86.6	298.7	601.7	303.1	771.2
7	255.7	199,150	255.3	53.6	164.4	374.8	210.4	1,281.7
8	585.3	816,375	587.6	44.7	512.0	657.5	145.5	719.7
9	116.4	3,374,750	113.1	11.6	92.4	134.5	42.1	33.5
China	2,712	9,422,830	2,663	182	2,451	3,173	721	283

[a] For watershed region names, see *Figure 1.5*.
[b] In billion m^3.
[c] In km^2.
[d] In mm.

Table 2.8. Summary of data needed to calculate the water resources indices described in *Table 2.5*.

Watershed region[a]	Supply	C_V[b]	Demand (1993)	Projected demand (2000)	Projected demand (2010)	Storage (billion m^3)	Population (million)
1	164.1	0.20	51.93	66.31	87.07	52.4	111
2	27.6	0.43	46.47	50.36	57.29	22.1	105
3	75.7	0.33	73.46	86.83	105.09	11.8	192
4	61.0	0.31	44.95	49.91	63.41	41.5	111
5	938.3	0.12	196.53	224.46	261.45	167.4	391
6	440.7	0.20	77.19	93.13	121.17	71.3	131
7	255.3	0.21	32.09	39.04	47.37	38.2	76
8	587.6	0.08	8.37	10.09	12.39	17.0	16
9	113.1	0.10	62.13	68.26	78.45	43.5	22
China	2,663.4	0.07	601.13	688.4	833.7	412.8	1155

Note: Supply and coefficient of variation (C_V) are from simulation with CHARM. Demand values and projections are from UN (1997). Storage values are from ICOLD (1984) and from personal correspondence with the Institute of Geography of the Chinese Academy of Sciences. Population data are from the 1992 China Statistical Yearbook (SSB, 1992).
[a] For watershed region names, see *Figure 1.5*.
[b] C_V = coefficient of variation.

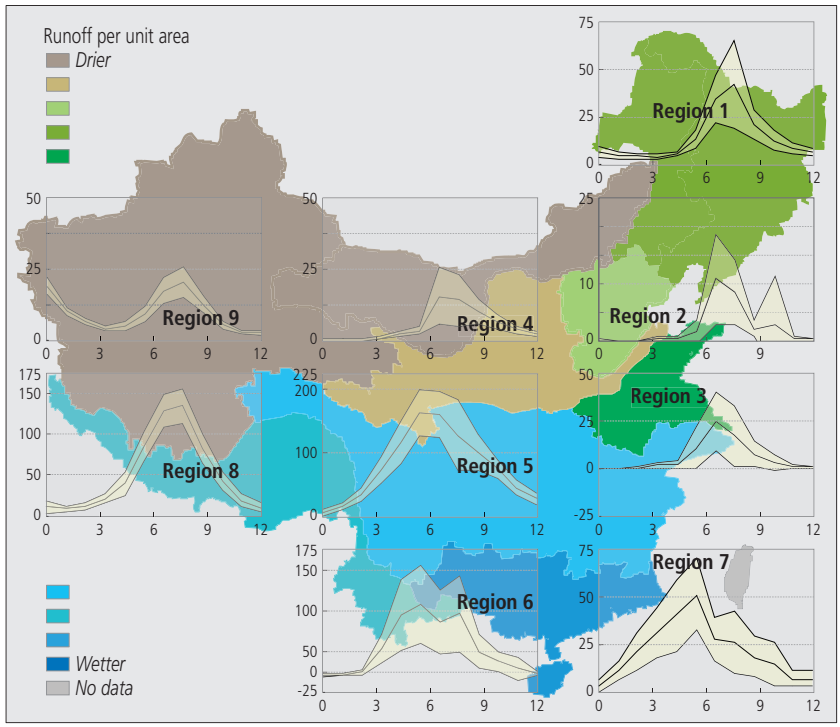

Figure 2.17. Results of CHARM simulation for nine watershed regions, 1965–1980. The month of the year is given on the horizontal axes. Monthly runoff is displayed on the vertical axes in billion m^3. One standard deviation is plotted on each side of the mean monthly value.

Table 2.9. Water stress factors and values of index calculations for major watershed regions of China.

Watershed region[a]	Factor 1 (Population)		Factor 2 (Use) 1993		2000		2010		Factor 3 (C_V)[b]		Factor 4 (Storage)		Factor 5 (Security)	Factor 6 1993	2000	2010
1	1	1,473	2	0.32	2	0.40	3	0.53	1	0.20	2	0.32	3	6	6	7
2	2	264	3	1.68	3	1.82	3	2.07	3	0.43	1	0.80	4	9	9	9
3	2	395	3	0.97	3	1.15	3	1.39	2	0.33	3	0.16	5	10	10	10
4	2	551	3	0.74	3	0.82	3	1.04	2	0.31	1	0.68	3	8	8	8
5	0	2,403	2	0.21	2	0.24	2	0.28	1	0.12	3	0.18	4	6	6	6
6	0	3,358	1	0.18	2	0.21	2	0.27	1	0.20	3	0.16	4	5	6	6
7	0	3,346	1	0.13	1	0.15	1	0.19	2	0.21	3	0.15	5	6	6	6
8	0	35,850	0	0.01	0	0.02	0	0.02	0	0.08	3	0.03	3	3	3	3
9	0	5,172	3	0.55	3	0.60	3	0.69	0	0.10	2	0.38	2	5	5	5
China	0	2,306	2	0.23	2	0.26	2	0.31	0	0.07	3	0.17	3	5	5	5

[a] For watershed region names, see *Figure 1.5*.
[b] C_V = coefficient of variation.

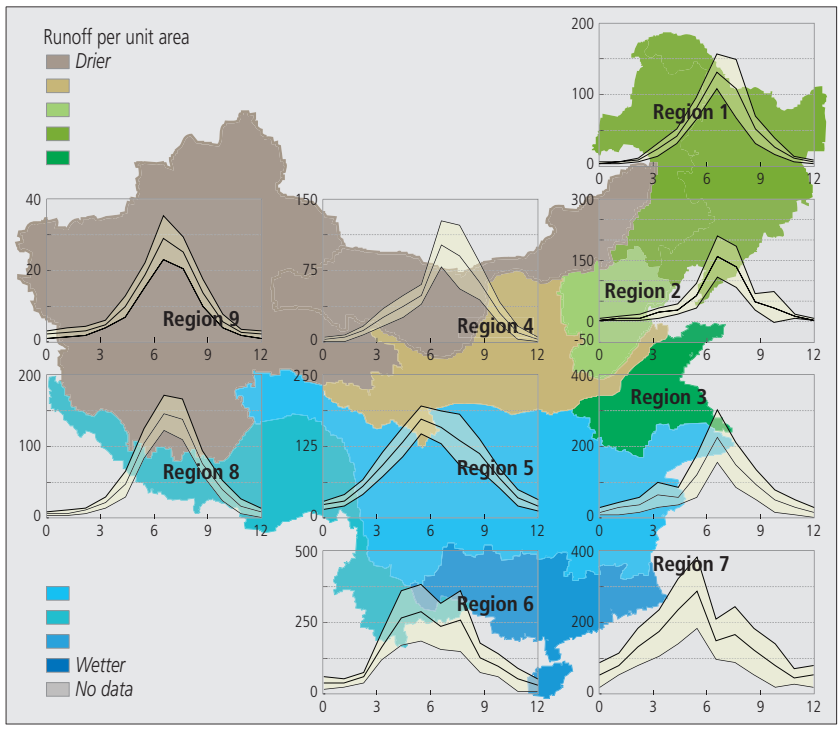

Figure 2.18. Average monthly precipitation (mm) for the nine watershed regions, 1965–1980. The month of the year is given on the horizontal axes. Monthly rainfall is displayed on the vertical axes in mm. One standard deviation is plotted on each side of the mean monthly value.

2.6.2 The Northeast

The Northeast region contains several major rivers, including the Heilong Jiang (Amur), Songhua (Sungari), Wusuli (Ussuri), Liao He, Yalu, and Tumen Rivers. The region covers approximately 13% of the total area of China, or about 1.25 million km^2. It contains about 10% of the population, but produces only 6% of China's surface water runoff. The per capita surface water runoff of 1,000 m^3 per person per year is below China's national average of 2,300 m^3 per person per year and is an indication of water stress.

The three major land uses in the region are timber forest, nonirrigated farmland, and grassland. Together, these account for 85% of the area. The average runoff per unit area, 132 mm, is currently sufficient for these uses. However, additional irrigation is planned for the region, with demand for irrigation water increasing by 20% between 2000 and 2010. The value of the combined water stress index (factor 6 in *Table 2.9*) is in the middle of its range at 6, but the water stress increases

with increasing demand by 2010, when the index value moves to 7. The factors all indicate stressed water resources in the region. However, with further expansion and improvement of water infrastructure, enough water does exist in the region to satisfy basic needs.

2.6.3 Hai He–Luan He basin

The Hai He–Luan He basin presents major challenges to water resources management in China. The region is significantly smaller, at only 3.4% of the total area of China, than the Northeast, but has a much greater population, more than 9% of the total population of China. This results in a per capita surface water availability of only 264 m^3 per capita per year. This certainly indicates a region of considerable water stress. The scarcity is exacerbated not only by the large population, but also by types of land use in the region and highly variable rainfall, and therefore highly variable runoff. More than 25% of the total area in the region is irrigated farmland, which accounts for two-thirds of the water use, or the entire stormflow produced in the region on average. Another 30% is nonirrigated farmland. Total water use in the region for 1993 was estimated to be 41 billion m^3, significantly more than the 28 billion m^3 of runoff produced in the region for that year. Furthermore, water demand in the region is expected to reach 57 billion m^3 by 2010. Groundwater has been used to bridge the gap between supply and demand in the region. However, this use cannot be sustained, as groundwater table levels have been dropping by 1–2 m per year.

The CHARM modeling exercise illustrates the additional problem of high runoff variability in the region. Although the per capita annual surface water runoff is 264 m^3 on average, the lowest runoff in the 15 simulated years is only 9 billion m^3 total, or 89 m^3 per capita. Intra-annual variability is also a concern, since nearly all the rainfall and runoff, 87% on average, occurs between July and October. Storage has been and continues to be built to reduce the variability in supply. In fact, only the large storage capacity built in the region to reduce water supply variability keeps the combined stress index of 9 below that of the Huai basin, but factors 1, 2, and 3 assume the worst values of all regions in China, with demand not being met by average runoff in the region. Furthermore, because of evaporation, seepage, and other losses, not even the average runoff can be delivered to where it is needed. This is a region of extremely high water stress that must import water to meet its needs.

2.6.4 Huai He basin

The Huai He basin has much in common with the Hai He–Luan He basin in that it also covers 3.5% of the nation's area and contains a large percentage of the population, in this case 17%. The region also contains some of the country's best arable land. The population is larger in the Huai He basin, but so is the runoff. At

395 m^3 per capita, runoff is actually 50% higher than in the Hai He–Luan He basin, but the region still suffers from water scarcity. In this basin, irrigated farmland is the primary land use, accounting for 31% of the area. Timber forest, paddy, and nonirrigated farmland are the other major land uses. Once again, demand is expected to outstrip surface water supply in 2010, with demand reaching 105 billion m^3, while average annual surface water supply is about 75 billion m^3. As in the Hai He–Luan He basin, and as shown in *Table 2.9* and *Figure 2.17*, the Huai He basin suffers from great variability in runoff. Modeled flows range from 45 to 127 billion m^3 per year, with 87% of the runoff occurring between June and October.

2.6.5 Huang He basin

The Huang He, or Yellow River, is the second longest river in China, being exceeded in length only by the Chang Jiang (Yangtze River). However, at 60 billion m^3 per year, the Huang He carries only 7% of the Yangtze's annual runoff. The Huang He basin is more arid than the Chang Jiang basin and the variability of rainfall and runoff is also much greater. In a year of low flows, the Huang He basin may produce only 50% of the surface water runoff of an average year. The flow is highly seasonal, with 77% occurring between July and October, and only 1% of annual flow occurring in the period from January to March. Since the entire volume of flow in these months has been diverted and used in recent years, the Huang He does not even flow to the sea during this period each year, and sometimes for even a longer period stretching into April and May.

The total area of the Huang He basin, about 8% of the country, is less than that of the Northeast, but the population is about the same. Per capita annual surface water runoff is 550 m^3, still well within the water-scarce range. Major land uses in the region include steppe grassland (41% of the area), nonirrigated farmland (17%), irrigated farmland (13%), and mountainous grassland (12%).

By 2010, demand for water will outstrip average surface water runoff by 4%. Compared with the Hai He–Luan He and Huai He basins, 4% is not much. However, the Huang He presents additional challenges to water management. The river obtained its name, Yellow River, from the huge quantities—1.6 billion tons per year—of yellow silt eroded from the Loess Plateau and carried by the river. Silt quickly fills the many reservoirs built on the river and diminishes their storage capacity. For example, begun in the late 1950s, "Yangouxia Dam lost almost one-third of its storage capacity before it was even commissioned. By 1966, three-quarters of Yangouxia's reservoir had been filled with sediment" (McCully, 1996:108).

2.6.6 Chang Jiang basin

The Chang Jiang, or Yangtze River, is China's largest river. The basin covers 19% of the country and carries 35% of the stormflow. Per capita annual runoff

is 2,400 m^3. Owing to the plentiful precipitation, irrigated dryland agriculture accounts for only a very small percentage of the land use in this region. Paddies, however, cover some 16% of the area. Timber forest covers the greatest area (28%), while nonirrigated farmland (11%), mountainous grassland (11%), steppe (15%), and brush (10%) make up much of the rest of the area.

The Chang Jiang has produced some of China's most disastrous floods because of the volume of water it carries. In 1931, for example, 3.3 million hectares of farmland were inundated, 140,000 people drowned, and 3 million people were rendered homeless (Gao *et al.*, 1992). However, the coefficient of variation in annual flows is low compared with those of the basins in the northern part of the country. The result is that, even in years of low runoff, water demand in the basin can easily be met. This, in turn, has made the basin a good candidate for water transfers to basins in the North, where demand is not being met. Several options for water transfers to the North are under consideration, with one, following the route of the ancient Grand Canal in the east, already beginning to be implemented.

2.6.7 Southern region

The southern watershed region is quite mountainous, with 17% of the area covered by mountainous grassland and 30% covered by timber forest. The basin is strongly affected by monsoons and the moisture from the South China Sea, producing the second largest runoff depth (close to 800 mm per year) and per capita runoff (3,300 m^3) of the nine watershed regions. The subtropical/tropical climate and high runoff make the area suitable for growing rice, which is done over 18% of the area. Nonirrigated farmland makes up another 10% of the region.

The variability of runoff in this region is greater than in the Chang Jiang basin. As in the case of the Chang Jiang, though, water demand can be met by surface water runoff even in low-flow years. As with much of China, however, the flow can vary greatly within a year, with only 1% produced from January through March. For this reason, storage and irrigation may be necessary for growing crops in these months.

2.6.8 Southeastern region

The southeastern region is 57% forest and 28% paddy. It is the smallest of the watershed regions, covering only 2.4% of the country, but has a higher population density than any other region except the Hai He–Luan He basin. Like all of the regions in the southern half of the country, the Southeast has more than enough water. Per capita stormflow is almost equal to that in the South watershed region, and average runoff depth is even higher at over 1,000 mm per year.

2.6.9 Southwestern region

The Southwestern watershed region, including major rivers originating from the Tibetan Plateau, is composed almost entirely of high-altitude prairie, forest, and bare land. The runoff depth is not the greatest in the southern half of China, but because of the very low population density in the region, the per capita runoff is by far the greatest of any region at 36,000 m^3 per capita per annum. The region also has the smallest interannual variability. The high precipitation, low variability, and low demand in the region ensure that water shortages will not occur here.

2.6.10 Interior basins

The largest watershed region in China, covering 35% of the country, contains no rivers that flow to the sea. The Interior basins are extremely arid, with an annual average of only 34 mm of runoff over an entire region that is 16% desert, 9% gobi, 50% steppe, and 12% bare land. It receives only 4% of China's total annual runoff but still contains irrigated land on 2% of its area. The population of the region is also very small, amounting to only 2% of China's total population. This, in turn, results in a higher per capita runoff, 5,000 m^3, than in the heavily populated basins farther east. Because water demand has been very low, the demand can currently be met by surface water supply in the region.

2.7 Conclusions

CHARM is a rainfall–runoff model designed to be as simple as possible for use in assessing the effects of land-use and climate change on water resources in China subject to limited data availability for model calibration and verification. After first calculating the stormflow, CHARM performs a water balance on the remaining water that does not immediately run off but infiltrates the soil. Evapotranspiration and subsurface flow remove water from the soil. If the soil is saturated, any additional water runs off over the surface. The effects of changing land uses are modeled by CHARM by changing the volume of water that runs off as stormflow. Climate change effects can be modeled by changing the precipitation, temperature, and radiation inputs to the model, which affect components of the major processes represented in the model.

The calibration and modeling of several sample basins, such as the Tao He and Yilou He, produced good results and also pointed to some challenges and areas where the model could be improved. Once calibrated, CHARM performed well in modeling stream flow in both these basins, tracking flows especially well for years prior to massive dam construction. As requested in the control input, the calibrated model produced flows within 5% of the annual runoff in both cases, also approximating the shape of the monthly hydrograph, even without using explicit

routing calculations. For the Yilou He, the simulated runoff hydrograph did not drop quite as quickly after the summer peak as the actual runoff did, suggesting that the model may underestimate direct runoff and overestimate water retention in the soil in this particular region. The simulation also missed a small runoff peak in May, which could have come from a local storm for which no data were recorded in 1951, the calibration year. Another possibility is that dams already existed on the river, which would explain both these differences. The other interesting conclusion from the sample basins is that stormflow constitutes a relatively small portion of the total simulated runoff. Since the direct runoff is the component that is sensitive to land-use changes, this may indicate that changes in runoff due to changes in land use are small. Furthermore, the calibration coefficient (α), and therefore subsurface flow, could also change with land use, but the nature of this relationship is still unknown. The effects of land-use change on water resources, therefore, may be underestimated by CHARM.

CHARM provides a means of calculating the amount of and variability in surface water resources in China. The average amount of surface water resources is certainly an important characteristic of the water sector and already shows that water shortage is a problem in some areas. If receiving less than 2,740 liters per person per day is considered an indication of water scarcity (Postel, 1992), then at least three of the nine watershed regions in China suffer from water scarcity, even if all of the average surface water runoff could be considered water supply. However, the average runoff cannot be delivered consistently as water supply, and there is considerable variability in the runoff, which poses an even greater challenge to water managers. Variability can be simulated by CHARM by first calibrating large regions in China using actual data. Then runoff can be calculated by CHARM for different years based on the climatic inputs. The simulations provide information about the variability of runoff in China, which is needed for efficient management of water resources.

Runoff does indeed prove quite variable in both time and space. The northwest Interior basin region produces only about 34 mm of runoff annually on average, whereas the Southeast produces over 1,200 mm. Interannually, the variation is also significant, with the coefficient of variation as high as 0.4. Within the year, 60% of the runoff in almost all basins is generated in only three months. This variability in runoff is one of the major problems faced by water resources managers, who need steady resource supplies. The simulation results obtained with CHARM show that China is facing serious water supply problems, which most likely will worsen in the future with a growing population. Land-use and climate change could exacerbate or help mediate the variability of runoff. CHARM provides a tool to aid in measuring these effects in future studies.

3

Impacts of Storage on Regional- and National-Level Water Availability: An Analysis of Reservoir Area–Volume Relationships and Evaporative Losses

3.1 Introduction

A number of global water assessments have been produced supplying numbers for regional- or national-level water availability (Gleick, 1993; Shiklomanov, 1999; Cosgrove and Rijsberman, 2000). These studies generally report average annual renewable water resources as a measure of the water available to meet water demand, where renewable water resources "represent the water entering a country's river and groundwater systems" (Cosgrove and Rijsberman, 2000). However, the *World Water Vision* document points out that not all of the renewable water resources will be available to meet demand for the following reasons:

1. Of global water resources, a large fraction is available where human demands are small, such as in the Amazon River basin, Canada, and Alaska.
2. Rainfall and river runoff occur in large amounts during very short periods, such as during the monsoon periods in Asia, and are not available for human use unless they are stored in aquifers, reservoirs, or tanks (the traditional system in the Indian subcontinent).
3. The withdrawal and consumption figures do not show the much larger share of water resources "used" through degradation in quality—that is, polluted and of lower value for downstream functions.
4. Water not used by humans generally does not flow to the sea unused. Instead, it is used in myriad ways by aquatic and terrestrial ecosystems—forests, lakes, wetlands, coastal lagoons—and is essential to their well-being. (Cosgrove and Rijsberman, 2000:7)

The result is that another quantity, called usable water, must be calculated to represent the potential amount of water available, even after future development. Usable water never seems to be reported in global water studies, primarily because of the difficulty of calculating and defining it, and the lack of tools and precedence for doing so. Defining and calculating renewable water resources is difficult enough, with large uncertainties. However, this report will look at the challenges and the approaches necessary to move from renewable water resources to at least an engineering estimate of usable water resources at a regional scale, based on reservoir development.

How much water supply can be developed in a region is a very contentious issue. Theoretically, the entire surface area could be covered with an impermeable material and flow could be immediately directed to pipes and then to covered, impermeable storage tanks, so that the actual volume of rainfall could be nearly completely captured, resulting in a quantity of water even greater than the generally estimated total renewable water resources figure. The volume of rainfall, then, is really the maximum potential freshwater renewable resources. However, although conceivable, this is neither practical nor realistic. Engineers may argue that the potential usable water resources are the renewable water resources minus losses to the developed system. Economists would argue that the usable water resources are the water resources that are economically feasible to develop. Finally, environmentalists would argue that the sustainable usable water resources are below any of these levels, since many ecosystems rely on the water in lakes and rivers. As humans, we cannot use all of this water at will without destroying the environment that supports us. Of course, economists can still argue that if the right economic controls are in place, it would not be economically feasible to exploit so much water that the environment would be destroyed.

The debate on how much water is usable will undoubtedly continue. Fueling this debate is the great uncertainty in any measured and/or calculated value for renewable water resources. The renewable water resources are extremely difficult to measure and are made even more difficult to measure because they are so difficult to define precisely. When reporting freshwater resources in *Water in Crisis: A Guide to the World's Fresh Water Resources*, Gleick (1993:128) states that the "data should be viewed with healthy skepticism," a sentiment that is repeated in many other documents that provide data on renewable water resources. The errors in renewable water resources values should be kept in mind when trying to estimate usable water resources.

Some of the limitations to using the full renewable water resources mentioned in the *World Water Vision* document, and listed above, can be worked around. The first point, for example, is only relevant in a global study, not when the development of large watershed regions or countries is considered. Point 2 states that the

temporal variation can be mediated by engineering, and point 3, on water quality, can also be mediated by engineering. Reducing the impacts of temporal variation and poor water quality in order to increase the water supply to its full potential is generally the goal of developing a basin, anyway. Points 2 and 3, then, do not directly limit the potential resources available, although they may indirectly reduce the resources through losses to the developed system.

The largest of these losses is evaporation. To calculate evaporation from reservoir storage, the relationship between the storage in reservoirs and the surface area of those reservoirs must be known. Approximating this relationship at different scales—that is, for single reservoirs, multiple reservoirs, or entire watersheds—is the focus of this report. Since point 4 is the most controversial of the limitations, this report will take the engineering approach and leave out the environmental reductions in water availability. Environmental reductions to usable water can always be added once the possible reductions due to engineering have been calculated.

3.2 Storage versus Surface Area

In arid regions, evaporation causes a significant loss of water in developed river basins. For instance, about 4% of the annual runoff of the entire Colorado River basin evaporates from Lake Powell, only one of many reservoirs on the Colorado River in the United States (Linsley *et al.*, 1992). Such losses due to evaporation should be incorporated in the calculation of potential usable water from a watershed. At existing reservoir sites, losses due to evaporation from reservoirs can be calculated by directly measuring evaporation and surface area. At sites that are planned for reservoir development or potential development, evaporation can be estimated by developing reservoir water surface elevation versus surface area and elevation versus storage curves. Once these curves have been created from the topology of the potential reservoir site, evaporation depth can be calculated using an evaporation model such as the Penman–Monteith method (Allen *et al.*, 1998; FAO, 2001) and multiplied by the surface area of the reservoir. The question arises as to how to calculate potential usable water resources in a basin without having a detailed development plan or an analysis of all potential reservoir sites. Is it possible to make an estimate of evaporation from storage in a generic watershed, and how accurate could the estimate be?

To make an estimate of evaporation from storage in a watershed, the first step is to determine how much water surface area is exposed for each level of storage built in a basin. As previously mentioned, this is a relatively straightforward computational task at a known reservoir site or combination of sites. Here, though, we are trying to find a generic relationship between surface area and storage applicable to an entire watershed region without having information on the individual reservoir

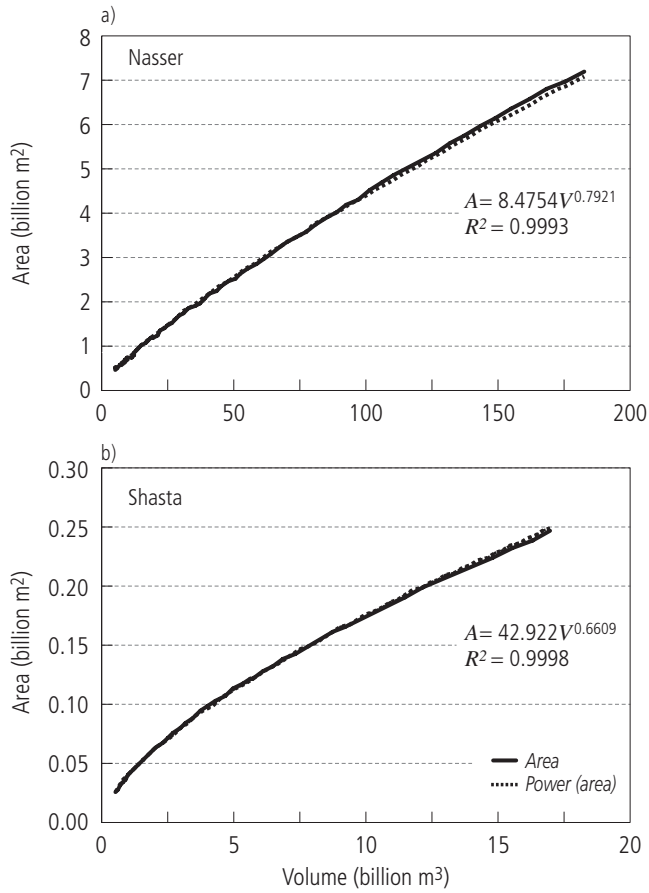

Figure 3.1. Surface area versus storage curves for (a) Lake Nasser and (b) Shasta Reservoir.

sites. The first step is to look at existing reservoirs and watersheds and the nature of the area–volume relationship.

3.3 Area–Volume Relationship for Individual Reservoirs

The area–volume relationships for two reservoirs, Lake Nasser in Egypt and Shasta Reservoir in the United States, will be used as examples of typical area–volume relationships. *Figure 3.1* shows surface area versus storage curves for the Aswan Dam (Lake Nasser) in Egypt and for Shasta Dam in California.

Both curves show a slightly steeper slope for the area versus volume curve at low volume. The slope decreases with increasing volume, indicating that in

most reservoirs, water first floods the low, broad floodplain before rising up the steeper hills and slopes at the edge of the valley. Curves can easily be fit to the data to describe the relationship between area and volume. A power formula of $A = 42.922V^{0.6609}$ describes the relationship for the Shasta Reservoir nicely, with $R^2 = 0.9998$. The same form of equation, $A = aV^b$, can also be used to fit the data from Aswan Dam at Lake Nasser, in which case $a = 8.4754$ and $b = 0.7921$, producing $R^2 = 0.9993$. The simple power formula approximates the area–volume relationship for a single reservoir very well.

The power formula, however, contains two parameters, a and b, which were found by obtaining the best fit from given data at known reservoir sites with readily available detailed data on elevation, area, and storage at small increments of elevation. If we do not have data for the exact reservoir shape, we need at least two points of volume and area data besides area = volume = 0 to fit a curve. Only one point with storage and surface area data is provided in global reservoir datasets such as the *World Register of Dams*, compiled by the International Commission on Large Dams (ICOLD, 1989), or datasets from other sources like the Food and Agriculture Organization of the United Nations (FAO), if surface area data are provided at all. However, if we use only area = volume = 0 as the second point, the result is simply a straight line. For this reason, it is necessary to find another relationship to describe storage area–volume curves. The most obvious method would be to use a straight line, since we only have one data point in addition to the origin to fit to. *Figure 3.2* shows how well the Nasser and Shasta data fit using a straight line.

The straight line fit is worse than the power formula but still quite good. When we are forced to set the intercept at 0:0 because of a lack of data, the fit degrades even further, but it can still be useful to approximate the curve.

Assigning a generic shape to a reservoir may be another method of improving the area–volume curve estimate. As an example, a triangular pyramid, shown in *Figure 3.3*, can be used to approximate a reservoir shape.

The volume of the triangular pyramid is

$$V = \frac{1}{3} \cdot A_s \cdot d = \frac{1}{6} \cdot l \cdot w \cdot d \,. \tag{3.1}$$

The angles between all sides remain the same as the reservoir is drained, so that the ratio of length to width and the ratio of width to depth remain the same. Since these values are constants, we can set $c_1 = l/w$ and $c_2 = w/d$ and rewrite Equation (3.1) using the new constants:

$$V = \frac{1}{6} \cdot c_1 \cdot c_2^2 \cdot d^3. \tag{3.2}$$

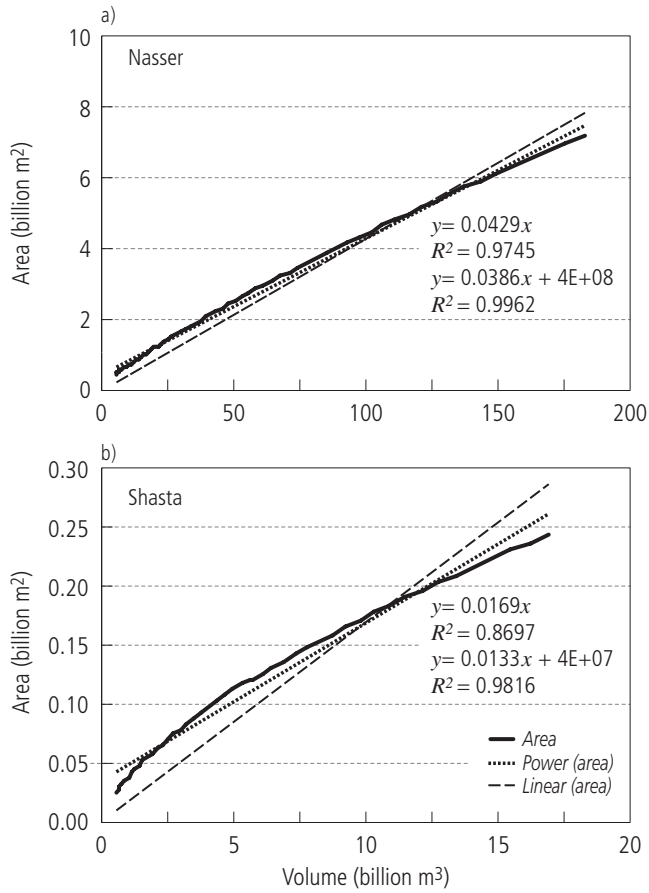

Figure 3.2. Results of fitting straight lines to the surface area versus storage curves for (a) Lake Nasser and (b) Shasta Reservoir. Two lines are fit in each case, one of which is forced to go through the origin.

We can now find an equation for the surface area of the reservoir based on the known volume and the constants c_1 and c_2. From Equation (3.1),

$$V = \frac{1}{3} \cdot A_s \cdot d \,, \tag{3.3}$$

so,

$$A = \frac{3V}{d} \,. \tag{3.4}$$

Solving Equation (3.2) for depth results in

$$d = \sqrt[3]{\frac{6V}{c_1 \cdot c_2^2}} \,. \tag{3.5}$$

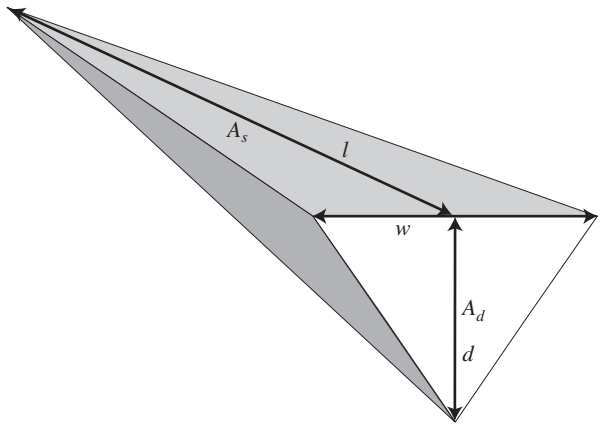

Figure 3.3. The triangular pyramid, a geometric shape that could possibly be used to approximate a typical reservoir.

Substituting Equation (3.5) into Equation (3.4) and simplifying yields

$$A = 3 \cdot \sqrt[3]{\frac{c_1 c_2^2 V^2}{6}} = 3 \cdot \sqrt[3]{\frac{c_3 V^2}{6}} = c_4 V^{\frac{2}{3}}, \tag{3.6}$$

where

$$c_3 = c_1 c_2^2 = \frac{l_1 w_1}{d_1^2} = 2\frac{A_1}{d_1^2} = \frac{2A_1^3}{9V_1^2} \tag{3.7}$$

and

$$c_4 = \sqrt[3]{\frac{27 c_3}{6}} = \frac{A_1}{V_1^{2/3}} \, . \tag{3.8}$$

In Equations (3.7) and (3.8), the subscript "1" is used to show that the values with the subscript come from a single given reference point. If this geometric shape is effective at describing the relationship between area and volume, it is an improvement over having to fit a power series to existing data and is as simple to use as the straight line. Like a line passing through the origin, Equation (3.6) requires only a single parameter. Further inspection of Equation (3.6) shows that it is, in fact, a power formula, suggesting that it may provide a very good fit. We only need to know the surface area at one volume level to calculate c_4. Alternatively, width, depth, and length or several other combinations of data could provide the necessary information.

A comparison of the actual volume and area data from the Shasta Reservoir and the area produced from the triangular pyramid shape is displayed in *Figure 3.4*.

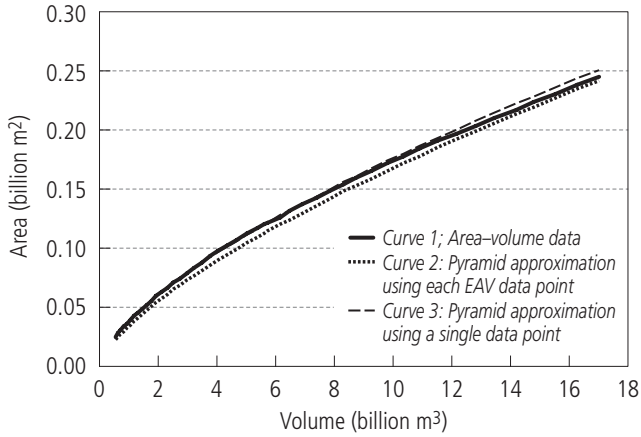

Figure 3.4. Results of applying the generic reservoir shape to the Shasta Reservoir in California. The coefficient of determination (R^2) for the generic reservoir shape used for Curve 3 is 0.9996, with $c_4 = 37.9245$. EAV = elevation–area–volume.

Three curves are shown in the figure. The first curve shows the actual area–volume data. The second curve simply tests the validity of the triangular pyramid shape by using Equation (3.4) to calculate the area from each point of known depth and volume from the actual depth–volume data. The final curve applies the geometric shape completely, showing the area–volume curve with the area calculated from Equation (3.6), when c_4 is calculated from the one point of maximum area and volume, according to Equation (3.8). The length and surface area of the Shasta Reservoir were available at normal storage, providing the necessary data for the pyramid. The fit of this curve with the original data is excellent, with a coefficient of determination, R^2, equal to 0.9996. This generic reservoir geometry, which we will call the pyramid approximation, provides an accurate estimate of the area–volume relationship for the Shasta Reservoir.

The results of applying the pyramid shape to Lake Nasser, however, produce less satisfactory results, as shown in *Figure 3.5*. The data for Lake Nasser indicate that Lake Nasser does not conform nearly as well to the triangular pyramid as does Shasta. The chosen shape does not, in fact, explain the data better than a line through the origin in the case of Lake Nasser. The coefficient of determination in this case is 0.9106. Lake Nasser is the exception, however. Appendix B shows that the pyramid approximation successfully fits the area–volume of a wide range of reservoir curves.

Volume and surface area at a single point are the most likely to be provided in reservoir databases such as that of ICOLD (1989) or the US Army Corps of Engineers' National Inventory of Dams (USACE, 2001). However, reservoir surface

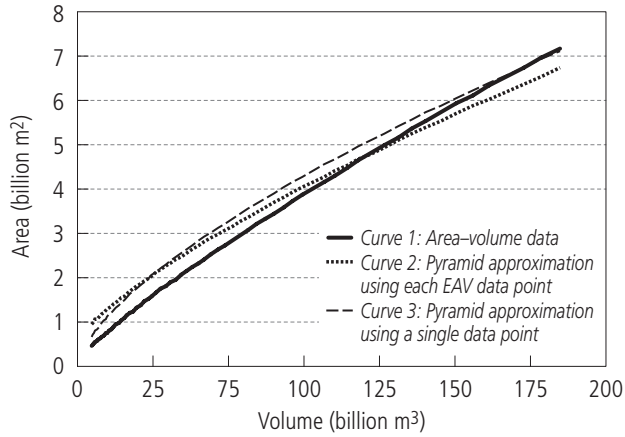

Figure 3.5. Results of applying the generic reservoir shape to the Lake Nasser in Egypt. $R^2 = .91063174$ and $c_4 = 220.94372$.

area is often not provided in these datasets. Furthermore, in undeveloped or incompletely developed watersheds with no further detailed development plans, not even the maximum surface area data would be available to match with the maximum storage required. Therefore neither the value of parameter c_4 for the pyramid case nor the slope of the line for the linear curve can be calculated directly. The examples of Lake Nasser and the Shasta Reservoir also show that the slope of the area–volume curve, or the value of c_4, varies from reservoir to reservoir. A relationship between the slope or c_4 and other watershed parameters must then be found if this method is to be used to estimate the area–volume curve of an unplanned reservoir in the basin. Furthermore, assuming a single reservoir may be practical for small watersheds, but for the large watersheds and regions that are the focus of water availability assessments, the area–volume relationship must be appropriate for not one, but multiple reservoirs. The case of multiple reservoirs in a region is examined in the next section.

3.4 Area–Volume Curves for Multiple Reservoirs in Aggregate

Large regions with multiple reservoirs complicate the relationship between the total storage and surface area in the basin, since the relationship can be altered by the operating policies of the reservoirs. Several studies have attempted to aggregate multiple reservoirs into a single reservoir to simplify the analysis of operating policy on flows in the watershed (Smith, 1981; Houghtalen and Loftis, 1988; Behrens,

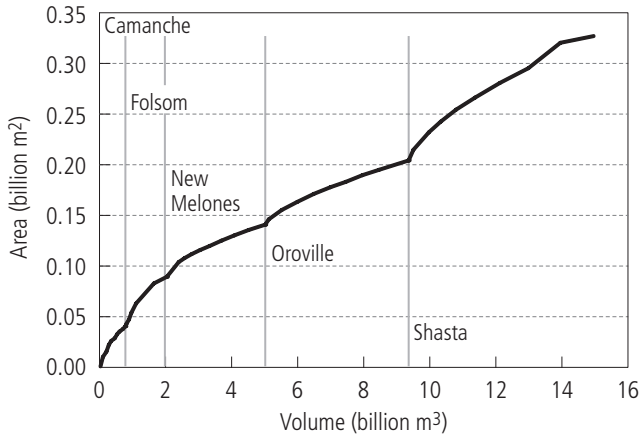

Figure 3.6. Cumulative area–volume curves for five reservoirs in the Sacramento River basin in California.

1991). Although these studies have concluded that aggregation is useful and functional for most parameters, they have also shown that area–volume relationships and the related losses due to evaporation are difficult to aggregate for use in accurately modeling the operation of several reservoirs as a single reservoir. Fortunately, our task in this report is much simpler and does not require such precision. We need only to obtain an estimate of losses to evaporation from storage in large regions.

Figure 3.6 shows the result of cumulatively plotting the surface area versus volume for five reservoirs in the Sacramento River basin in California, from smallest to largest. With all five reservoirs on one plot, we can clearly see that the slopes of the area–volume curves are different for each reservoir, as mentioned in the previous section. The largest reservoirs generally have the smallest slope.

The differing slopes enable managers to adjust the total surface area of the combined reservoirs through operational policy. If the management objective is to minimize evaporation, for example, reservoirs with the steepest area–volume curve would be drained first when releases from the reservoir system were required. This would result in the most rapid reduction of surface area exposed to evaporation. At the other extreme, if the management objective is to maximize the hydropower obtained from the reservoirs, all of the reservoirs would be kept as full as possible to maximize head. The results of applying different policies to these five reservoirs in the Sacramento River basin are plotted in *Figure 3.7*.

The figure shows a range of drawdown possibilities, including drawing water from the largest reservoir until it is completely empty, then taking from the next largest reservoir, and so on; drawing water first from the smallest reservoir and then on up to the largest; drawing down all the reservoirs equally, proportionate to their

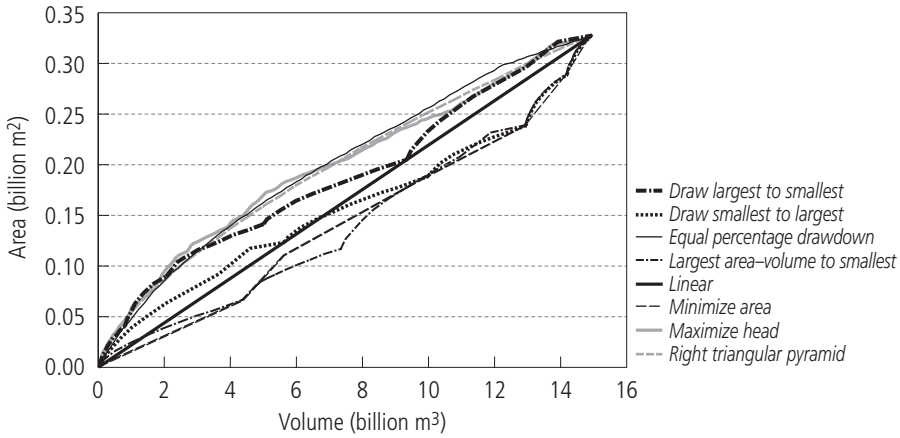

Figure 3.7. Impacts of different operational policies on cumulative area–volume curves for five reservoirs in the Sacramento River basin. Outer curves show extremes of the envelope in which the area–volume relationship could fall at any point in time.

maximum storage capacities; drawing water from the reservoir with the largest ratio of maximum area to maximum volume and then down to the smallest, which is one way to minimize surface area; minimizing surface area using a simple "pseudo-optimization" algorithm; and maximizing head, also using a simple optimization algorithm. The simple optimization routine used to minimize area and maximize head is referred to as "pseudo-optimization" because it does not actually maximize or minimize the area under the curve, but simply sets a reservoir release step size and releases water from the reservoir with the largest ratio of area to volume in that step for the area minimization case and the smallest ratio of area to volume in that step for the head maximization case. Because the largest ratio of area to volume is found at the lowest volumes in any one reservoir, the step size for the area minimization case had to be initially set to the entire volume of the smallest reservoir and then reduced when there was not enough volume available in any one of the reservoirs to cover the entire step. The optimization routines could certainly be improved, but the results of a better optimizer would be only slightly different, making it nonessential to establishing the point.

Although a large number of curves indicating different release possibilities are plotted in *Figure 3.7*, the purpose of the figure is simply to show the boundaries of the range of area–volume possibilities achievable by managing the system of reservoirs. The ability to manage these reservoirs assumes that all reservoirs are managed by a single organization for a single downstream purpose. In reality, this is not the case. The reservoirs are on different rivers in different areas and have

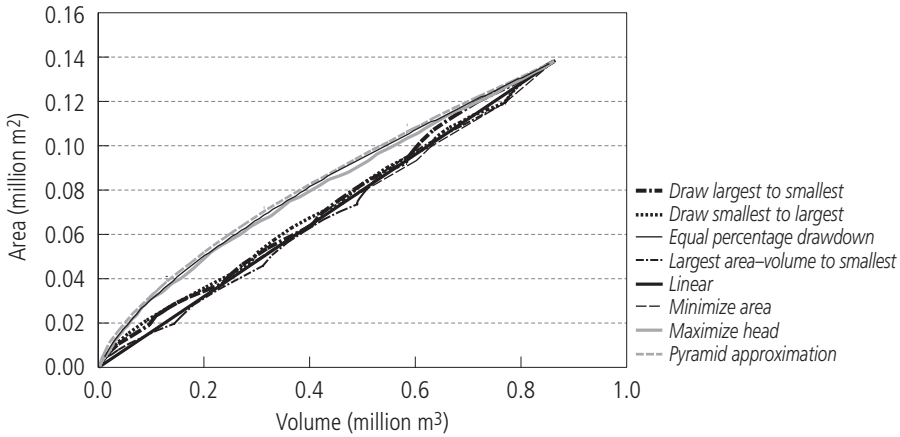

Figure 3.8. Impacts of different operational policies on the cumulative area–volume curves of reservoirs in the Limpopo River basin in Botswana.

different owners and different purposes. Much of the water from four of five of these reservoirs is used for irrigation, which generally takes place near the reservoir site, at least before the outflow of one of the other reservoirs. With each reservoir operated separately for different purposes, the combinations of drawdowns from the individual reservoirs will most likely fall between the extreme cases shown in *Figure 3.7*. The case of an equal percentage drawdown in all reservoirs, which is near the upper boundary of the range of possibilities, would still be quite possible and reasonable, though. Furthermore, since most reservoirs have some dead storage, which can be as high as 30–40% of the total storage, draining a reservoir completely is unlikely. Since the largest ratios of area to volume are easily within the lowest third of the reservoir volume, this suggests that the curves with greater area per volume at the upper half of the range shown in *Figure 3.7* are more likely.

Three other tested watersheds show similar results, as shown in *Figure 3.8*, *Figure 3.9*, and *Figure 3.10* for the Limpopo River, the Missouri River, and the Colorado River, respectively.

The best elevation–area–volume (EAV) relationships were obtained for reservoirs in the Sacramento and Limpopo Rivers. *Figure 3.8* includes data from the Shashe, Letsibogo, Bokaa, Gaborone, and Molatedi Dams in Botswana. The Missouri River data on the Fort Peck, Gavin's Point, Fort Randall, Big Bend, Oahe, and Garrison Dams came from a paper fax and were difficult to read. The resulting guesswork produced many errors in the curves. For the Colorado River, the actual data on the Blue Mesa, Crystal, Flaming Gorge, Fontenelle, Havasu, Mead, Mohave, Morrow Point, Navajo, and Powell Reservoirs were not available from the US Bureau of Reclamation; instead, the data shown were produced from

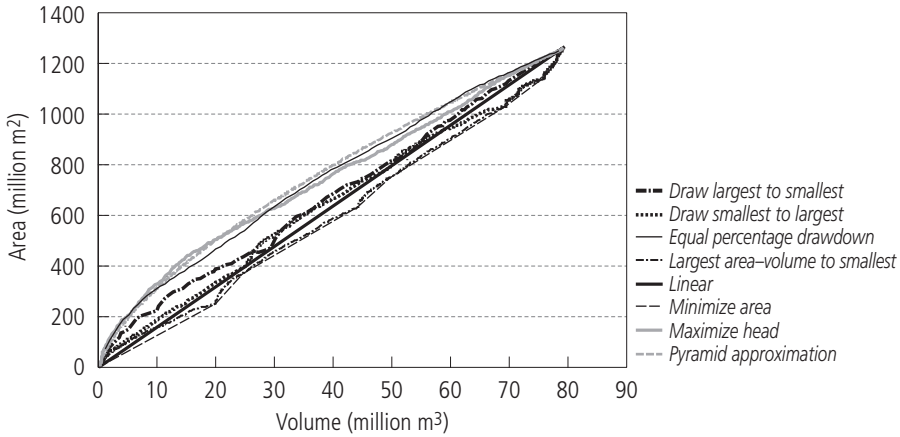

Figure 3.9. Impacts of different operational policies on the cumulative area–volume curves of reservoirs in the Missouri River basin.

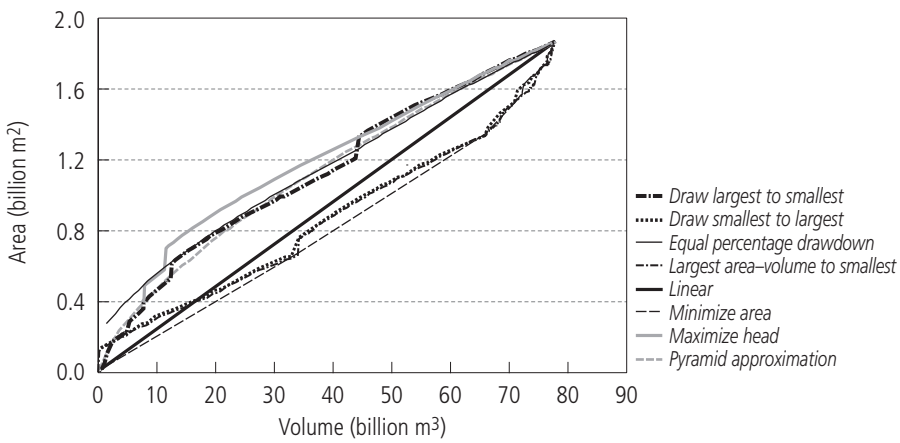

Figure 3.10. Impacts of different operational policies on the cumulative area–volume curves of reservoirs in the Colorado River basin.

polynomials that the Bureau had created for the curves. As a result, the curves for individual reservoirs do not go through the origin, and in some cases they have negative values for area at low storage.

The figures indicate that either a line or the pyramid approximation can be used to approximate the aggregate area–volume curves for multiple reservoirs. As discussed, the curves showing greater ratios of area to volume at the upper part of the envelope are more plausible because reservoirs are often managed separately for separate purposes, so that they are all drawn on at similar times rather than only being drawn down one at a time. If all are similarly drawn from, then the

area–volume relationship will be close to the equal percentage drawdown curve shown in *Figures 3.7* to *3.10*, suggesting that the pyramid approximation to the total volume and area of the combined reservoirs is a realistic approximation of the area–volume relationship for the aggregated reservoirs. The fact that the linear approximation runs through the center of the policy scenarios, however, along with its ease of use, present a good argument for using the linear relationship. Depending on the problem under consideration, either of the methods could be appropriate for obtaining a rough approximation of the area–volume relationship for multiple reservoirs when the actual locations, area–volume curves, and operating policies are not known. A more accurate estimate can only be obtained when the locations and operating policies of all the reservoirs are known.

3.5 Regional Area–Volume Curves

The multiple reservoir analysis indicates that either a line or the pyramid approximation can be used to represent the area–volume curve from multiple reservoirs. We must remind ourselves that the objective is to calculate losses to evaporation for an entire region. For this purpose, we need a relationship that fits the entire region, not just a single reservoir or group of reservoirs. The analysis on aggregating reservoirs presented above only considers a few reservoirs that are parts of much larger watersheds and regions. How well do these reservoirs represent the larger watershed regions that they are a part of?

The National Inventory of Dams (NID) provides data for all the reservoirs in the United States, although complete data are not available for all reservoirs (USACE, 2001). Watershed boundaries were obtained from the HYDRO1K Database (USGS, 2002). Using GIS software, the total normal storage and surface area were calculated for all reservoirs in the watersheds having data on both normal storage and surface area. For the three US watersheds examined—namely, the Sacramento, Missouri, and Colorado Rivers—only 84%, 44%, and 64% of the dams, respectively, had both area and storage data, but these dams accounted for 99%, 97%, and 98% of the total storage in the watershed, respectively. The dams analyzed in Section 3.4 for these three watersheds represent about 37% of the total normal storage for the Sacramento River, 64% for the Missouri River, and 84% for the Colorado River. *Figures 3.11* to *3.13* show a comparison of the linear approximation of the area–volume relationships for the reservoirs discussed in the previous section and the linear approximation of the area–volume relationships for their respective watersheds, based on the total known normal storage and surface area in the watersheds.

Figures 3.11 to *3.13* show several different measurements of area and volume in the watershed from different sources. The EAV data line is the linear approximation

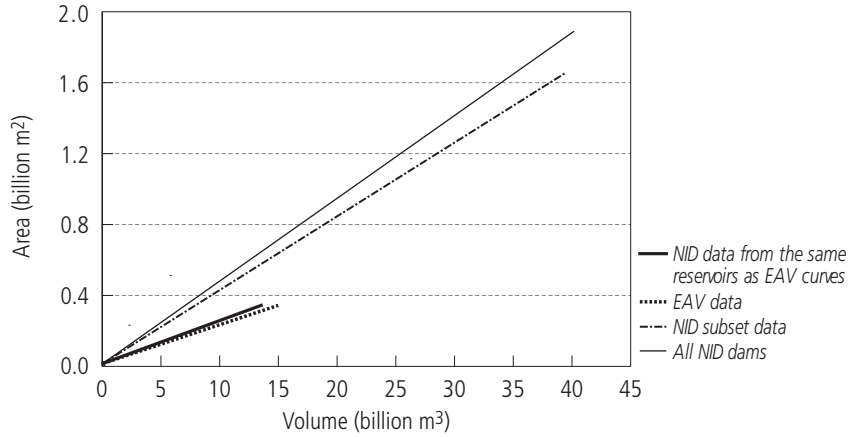

Figure 3.11. Comparison of total area and volume of reservoirs in the Sacramento River watershed from different data sources.

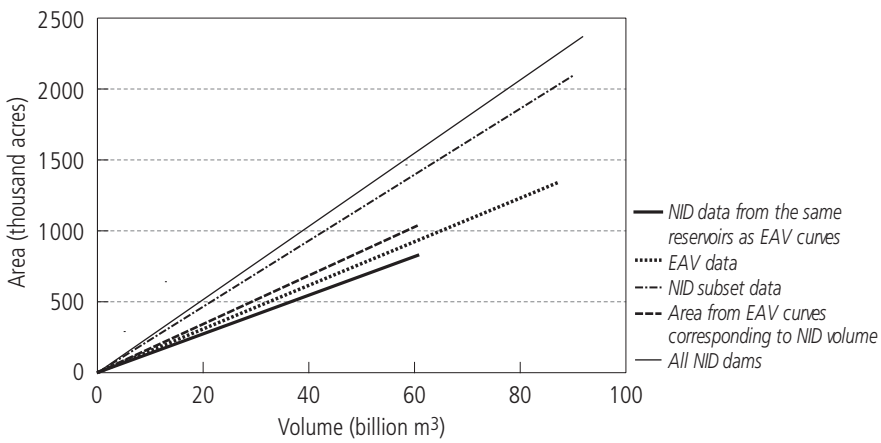

Figure 3.12. Comparison of total area and volume of reservoirs in the Missouri River watershed from different data sources.

to the multiple reservoirs from the previous section. The area and volume data came from the EAV data for the dams. The line marked "NID data from the same reservoirs as EAV curves" shows the total area and volume from the NID of the dams included in the EAV line. There is some discrepancy between the two lines from different datasets, but this is particularly clear in the Missouri River basin. The EAV data for reservoirs in the Missouri River watershed pagebreak obviously extend significantly beyond the normal storage of the reservoirs. For this reason, an additional line was plotted in *Figure 3.12* to show what the EAV data state is for the total surface area at storage levels taken from the NID for each reservoir. Here

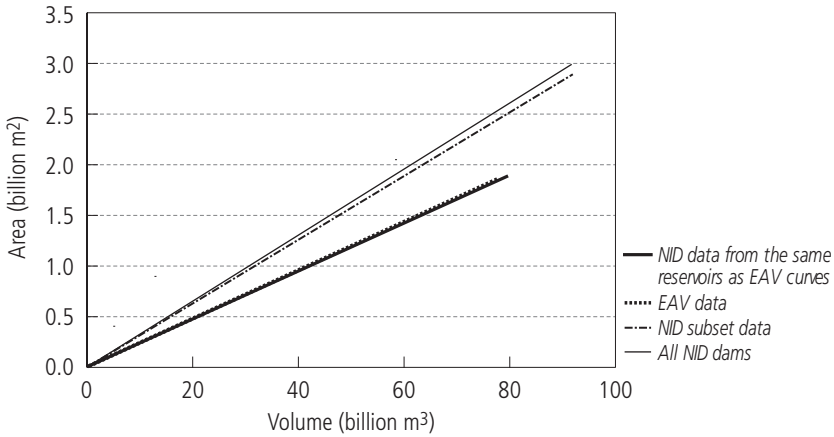

Figure 3.13. Comparison of total area and volume of reservoirs in the Colorado River watershed from different data sources.

there is also a large discrepancy, which is at least partially the result of the poor quality of the fax from which the data were obtained.

The final two lines in *Figures 3.11* to *3.13* are taken from a subset of the NID and the NID itself. The NID subset is from the *National Atlas of the United States* (US Department of the Interior, 2002), containing only large reservoirs of the type that would be included in the ICOLD database of large dams. These are dams 50 feet (∼15 m) in height or taller, or with a normal storage capacity of at least 5,000 acre-feet (∼6 million m^3), or with a maximum storage capacity of at least 25,000 acre-feet (∼30 million m^3). Although the data for the two lines are taken from the same dataset, the data are from different years. Both lines are included for two reasons. The main reason is that the subset data are the only data that are readily available at the global level, and it is important to recognize that larger dams generally have a smaller ratio of surface area to volume than do smaller dams. Therefore, a linear approximation to the total surface area and volume of all large dams in a watershed will generally underestimate the amount of reservoir surface area in the watershed. The second reason is to show that data taken from the same database in different years will show discrepancies, as databases are continually updated and improved. This is evident in *Figure 3.13* for the Colorado River, where the NID subset shows greater storage in the basin than the entire NID.

The danger of extrapolating an area–volume curve beyond the known area and volume in the watershed is clearly shown in *Figures 3.11* to *3.13*. The more storage and surface area data available in the watershed, the better the estimate will be if one is forced to extrapolate an area–volume line without complete data. A large portion of the storage in the Colorado River basin is in the reservoirs included in the EAV

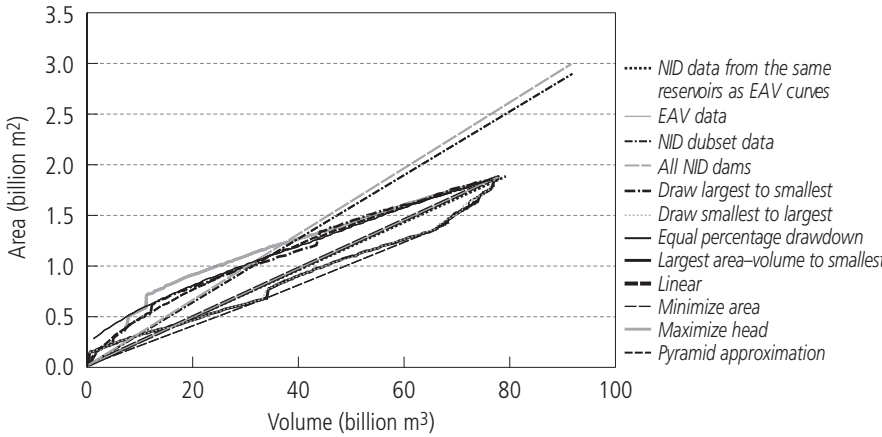

Figure 3.14. Error produced by using only a subset of reservoirs to predict the area–volume curve versus potential error due to different operating policies.

data curve, for example. If we only had data for these reservoirs, extrapolating from them to the total storage in the basin would produce the least error of the three watersheds listed. Even in this best-case scenario, though, the error produced by extrapolating an area–volume line produced from a few reservoirs to the total storage in a watershed is enough to dwarf the error in the area estimate due to different policy scenarios, as shown in *Figure 3.14*.

Extrapolation error is also the reason that we have focused on a linear area–volume curve in this section. As shown in *Figure 3.15*, extrapolating a power curve such as the pyramid approximation produces greater error at high storage volumes. The primary reason is that data are usually available on only the large dams, which generally have less surface area per volume than do smaller dams. The extrapolated curve from reservoirs with known area and volume, then, will always be below the actual area–volume curve for the watershed. The pyramid approximation would still be useful if the known storage surface area and volume in the watershed were a large percentage of the total; but the fewer surface area data available, the worse the extrapolation error will be from a power curve.

One final question remains in the analysis of regional area–volume curves: Can an estimate of the regional area–volume curve be made when neither the volume nor the area is known for any of the reservoirs in the watershed? To answer this question, we may be able to find a relationship between the slope of the area–volume curve, using the linear approximation, or the constant c_4, using the pyramid approximation, and watershed parameters. The most obvious watershed parameter for this purpose is the average slope within the watershed. We would expect the ratio of area to volume to decrease with increasing slope in the watershed. Average

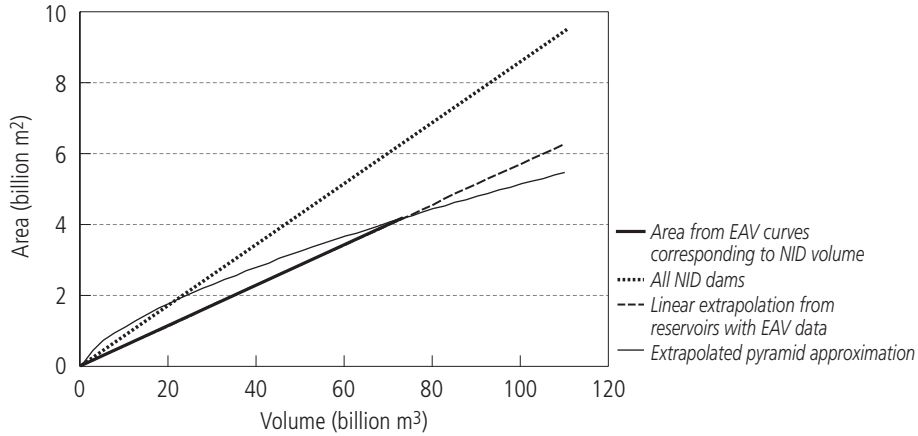

Figure 3.15. Error resulting from extrapolating a line past the combined storage of the reservoir with complete data for their elevation, area, and volume (EAV) relationships.

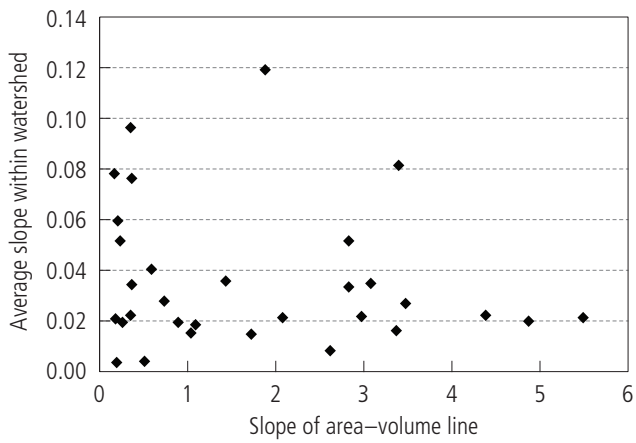

Figure 3.16. Average slope within a watershed versus slope of area–volume line for level 2 watershed from the HYDRO1K dataset.

slopes were obtained from the HYDRO1K database, which provides the average slope within 1 km by 1 km grid cells. These average slopes were then calculated for "level 2" watersheds, such as the Colorado, Missouri, and Sacramento/San Joaquin River basins in the United States. *Figure 3.16* shows the results of plotting the average slope in the watershed against the area–volume slope for level 2 watersheds.

It is evident from *Figure 3.16* that there is no clear relationship between the average topographic slope within a level 2 watershed and the slope of the aggregate

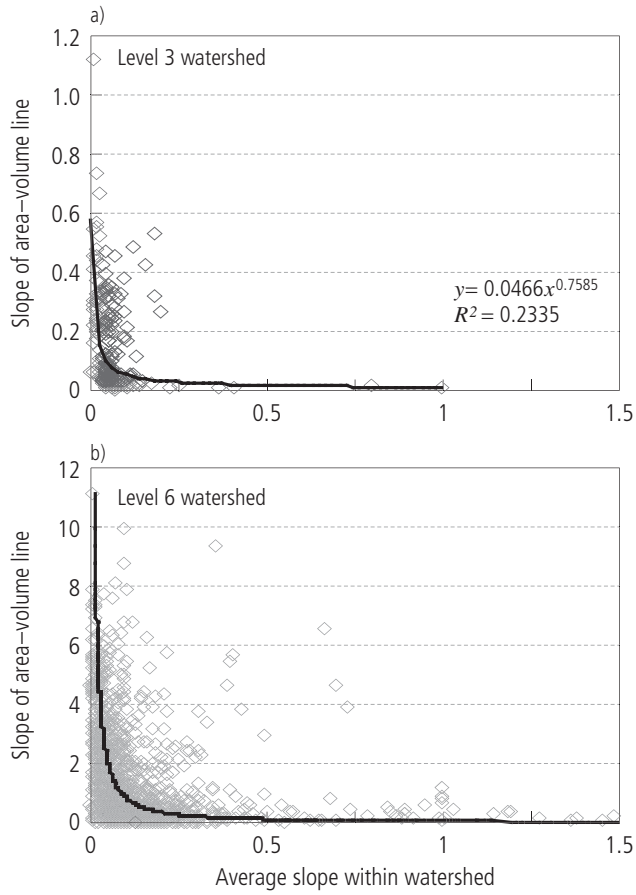

Figure 3.17. Average slope within a watershed versus slope of area–volume line for level 3 and level 6 watersheds from the HYDRO1K dataset.

reservoir area–volume line in the watershed. This indicates that the best estimate of the linear area–volume curve in a watershed may come from simply taking the average of the area–volume curves in similarly sized watersheds. Although this will result in substantial error, the only way to improve the estimate is by obtaining some data on the area and volume of reservoirs in the watershed or at least the location of reservoirs within the watershed. If the location of a reservoir is known, the local slope of the land around the reservoir should provide a good estimate of the area–volume relationship. Analyzing data for smaller watersheds does provide the expected relationship between slope and area–volume slope, as shown in *Figure 3.17* for level 3 and level 6 watersheds, but there is still extremely high variability. A power series relationship again seems appropriate, but any fit is rather poor due to the wide variation in the data points.

3.6 Summary

Evaporation from storage is a substantial source of water loss in developed watersheds, particularly in arid regions. In some watersheds, such as the Nile River basin, as much as 15% of the total available water can be lost due to evaporation from reservoirs. Evaporation must then be considered when assessing the usable water in a watershed. To calculate evaporation from storage, however, we must know or be able to estimate the relationship between storage surface area and storage volume. In this chapter, the area–volume relationship at different scales has been analyzed to provide methods for estimating the area–volume relationship for individual reservoirs, multiple reservoirs, and entire watersheds when precise data on elevation, area, and volume for the reservoirs are not available.

For individual reservoirs, the pyramid approximation was found to provide an excellent estimate of the area–volume curve. The coefficient of determination between the pyramid approximation and the actual area–volume relationship on the tested reservoirs averaged 0.983, with the worst fit of 0.911 in Lake Nasser. In addition, the pyramid approximation has the advantage that it has only one parameter and therefore requires only one data point of area and volume. Normal storage volume and area are often included in reservoir databases, providing the necessary information for applying the pyramid approximation.

For multiple reservoirs, either a linear approximation or the pyramid approximation can be used to estimate the aggregate area–volume relationship. In the case of multiple reservoirs, however, the operating policy or policies for the reservoirs play an important role in determining the combined surface area of the reservoirs at any point in time. Different policies result in a range of area and volume—between a condition of maximizing head and minimizing surface area—within which the combined reservoirs could fall. The pyramid approximation may give a more conservative estimate of evaporation (i.e., greater evaporation) for planning purposes, since it falls on the higher side, or greater surface area portion, of this range. It may also be a more accurate estimate than a linear approximation, especially if the reservoirs are operated independently. A linear approximation for the area–volume relationship to the maximum area and volume point of the combined reservoirs falls more in the center of the range, however, so there are also good reasons for applying it. Familiarity with the reservoir system and the particular issue being investigated can determine which is more appropriate on a case-by-case basis. Both produce only estimates, and the actual area and volume point at any particular time could be somewhat different from the estimate.

The greatest uncertainty by far is introduced when trying to approximate the aggregate area–volume relationship for an entire large watershed where no existing storage area and volume data are available for any reservoir. In this case, the best estimate may be to apply the average slope of the linear area–volume relationship

in watersheds of similar size. The estimate can be improved greatly if an area–volume point is available at one or more reservoirs in the watershed. The area–volume line can then be extrapolated from the total known area and volume. This will still produce considerable error, but the more reservoirs with an area–volume point there are, the more the error can be reduced. Because so much water can be lost to evaporation in arid regions, even a rough estimate of evaporation is better than ignoring evaporation from storage completely.

4

The Development of Regional Cost Curves for Watershed Storage and the Impacts of Evaporation: A Case Study of China

4.1 Introduction

This chapter focuses on water supply and develops a methodology that can be used to estimate supply curves from storage reservoirs in large watershed regions. There are three steps in this process:

1. Determine the storage–yield relationship for the watershed.
2. Determine the regional cost curve for reservoir storage.
3. Determine the water–yield production function.

These three steps are performed on major watersheds in China. China was chosen as a case study because of its large population, its policy of 95% self-sufficiency in grain production, its great regional disparity in water resources (dry in the North, very wet in the South), its rapid development, and the limited availability of data on its watersheds, which is common throughout much of the world.

4.2 Developing Storage–Yield Relationships for the Major Watershed Regions of China

A storage–yield curve shows the amount of water storage necessary to provide, or yield, a "reliable" amount of water in each time period. The storage requirement is a function of the variability of the runoff. Natural runoff is highly variable, so storage is built to mediate the variability and to retain the runoff until it is needed. Logically, the minimum steady flow that can be delivered is the minimum flow of the river in the time period being considered. The maximum steady flow that can be delivered by a reservoir is the average runoff flowing into the reservoir, although

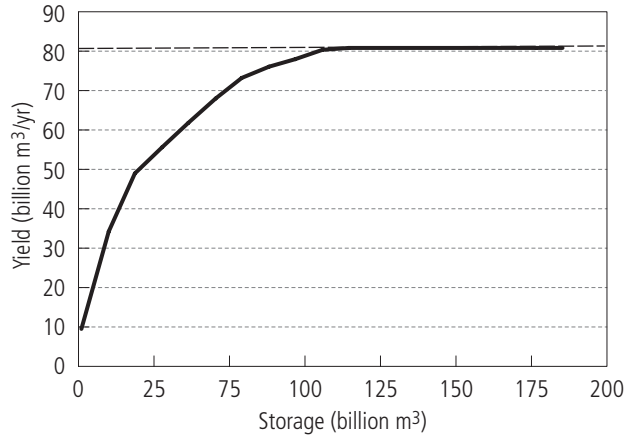

Figure 4.1. Typical shape of storage–yield curve, exhibiting diminishing returns to scale. This curve was calculated from data for Lake Nasser and excludes evaporation and other losses, so that the yield reaches the average annual inflow to Lake Nasser.

in reality, losses such as those from evaporation, bank storage, and seepage make this theoretical maximum difficult to achieve even when adequate storage exists. To achieve a yield close to the average runoff, the storage must be large enough to be able to contain the largest flood flow and must be able to keep releasing water through the longest and deepest drought. Generally, storage–yield curves exhibit diminishing returns to scale, as shown in the sample curve in *Figure 4.1*, created using data from Lake Nasser in Egypt (Wiberg, 1998).

Evaporative losses from reservoir storage can have a significant impact on the yield in semi-arid and arid regions. Furthermore, because of evaporative losses, building too much storage can result in decreasing yields. Continuing with the Lake Nasser example, *Figure 4.2* shows the impact of evaporation on the storage–yield curve.

If the operating policy of the reservoir is simply to provide a reliable yield, the storage–yield curve reaches a maximum level below the average inflow to the reservoir. If additional storage is built beyond what is needed to supply this maximum yield, the additional storage need not be used. However, if the dam was built for hydropower and managers want to keep the dam full to maximize head, then yield from the reservoir can actually decrease at higher storage levels as a result of evaporation from the greater surface area. *Figure 4.2* shows the importance of considering evaporation when calculating storage–yield curves in arid or semi-arid regions.

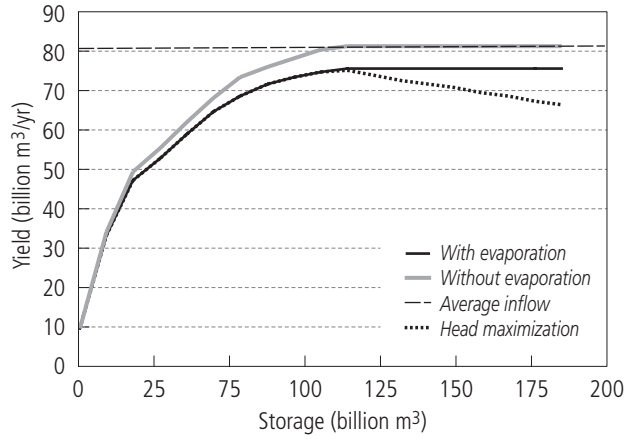

Figure 4.2. Impact of evaporative losses on storage–yield curve for Lake Nasser. If the policy is to maximize head for hydropower while at the same time delivering a reliable yield, then the reliable yield actually declines with increased storage at higher storage levels due to the greater surface area and higher evaporation.

A common technique for calculating storage–yield curves is the sequent peak algorithm (Thomas and Fiering, 1963). Equation (4.1) is the equation for this algorithm:

$$S_t = \begin{cases} R_t - Q_t + S_{t-1} & \ldots \text{if positive} \\ 0 & \ldots \text{otherwise.} \end{cases} \tag{4.1}$$

Here, S is the storage, R is the release, and Q is the inflow. The subscript t represents the current time period. Equation (4.1) is applied for every time period and the maximum S_t over all time periods is the storage required for the series of inflows applied.

The t of Equation (4.1) naturally leads to the question of what time period to use. *Figure 4.3* compares the result of using monthly versus yearly time series for sequent peak analysis. Generally, the seasonal variability in flow is greater than the annual variability. For this reason, monthly flows should be used to calculate the required storage. If only annual flows are used, the yield will be overestimated for each level of storage, since the storage may not be able to handle the variability within the year. The monthly time series used should cover as many years as available on record, so that the storage–yield curve takes the annual variability as well as the seasonal variability into account.

For China, data were available on the average annual runoff for the nine major watershed regions shown in *Figure 1.5* in Chapter 1 of this report (UN, 1997). Because time series data are necessary to determine the storage requirement, the

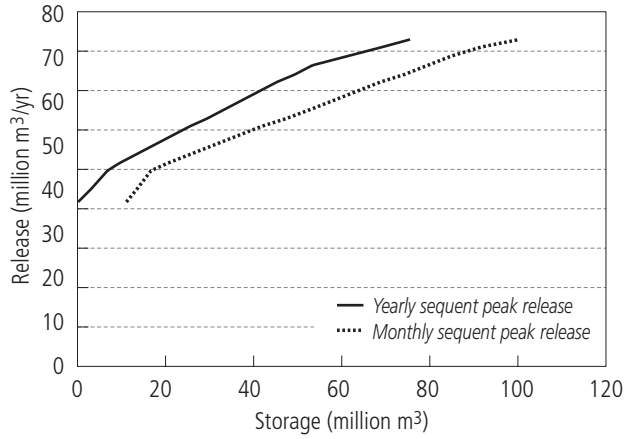

Figure 4.3. Yearly versus monthly runoff data for the Qingshu River in China at Quanyanshan. If only an annual time series is used, the amount of yield at each level of storage will be overestimated, since intra-annual variability is usually greater than interannual variability.

Climate- and Human Activities-sensitive Runoff Model (CHARM) was used to obtain the time series runoff values using the climate data discussed in Chapter 2.

Evaporation should also be incorporated into the sequent peak algorithm when calculating required reservoir storage, since evaporation can have a significant impact on the storage–yield curve, as shown in *Figure 4.2*. Evaporation and other losses can be incorporated into Equation (4.1) by adding them to the right-hand side of the equation, as shown in Equation (4.2):

$$S_t = \begin{cases} R_t + E_{t-1} - P_{t-1} - Q_t + S_{t-1} & \ldots \text{if positive} \\ 0 & \ldots \text{otherwise.} \end{cases} \tag{4.2}$$

The P in Equation (4.2) is the precipitation falling on the reservoir surface. Precipitation adds to storage on the surface and therefore must be included in the water balance. Precipitation and evaporation can be combined and simply called net evaporation. The term "evaporation" is used to mean net evaporation in this report.

Evaporation from a reservoir is dependent on the surface area of the reservoir. Therefore, to calculate the volume of evaporative losses from storage for an entire region, the evaporation and surface area for every reservoir in the region must be known at all time periods. However, as was pointed out in Chapter 3, there are some serious problems with obtaining these data. One problem is that most reservoir databases do not include information on the relationship between reservoir surface area and volume. In fact, for most reservoirs not even a single point of

matching surface area and volume is given. The second problem is that, even with full knowledge of the relationship between surface area and volume for every reservoir in the region, the surface area of the combined reservoirs at any point in time would still be highly dependent on the operating policies of the reservoirs. Operating policy information is even more difficult to obtain for thousands of reservoirs. Finally, and most important, the purpose here is to calculate the amount of storage necessary to make full use of the available resources in the region. Much of this storage may not yet be built, and there may be no information on where it might be built or no plan to build additional storage at all. In these cases, the parameters of the additional storage are not known. For this reason, we must be able to estimate a relationship between the total storage in the watershed and the total surface area. Such an approximation was developed in Chapter 3. For large regions where few reservoir data are available, it was shown that a linear approximation is simple to use and provides a reasonable estimate of the area–volume relationship, particularly when only data from large dams are available. It was also shown that the best estimate could be obtained if there were at least a few dams in the region containing one point of matching area and volume information. Once the relationship between surface area and volume is calculated, an evaporation methodology such as the Priestley–Taylor or Penman–Monteith method can be used to calculate the evaporation depth (FAO, 2001). Multiplying the evaporation depth by the surface area of the reservoir gives the evaporation volume lost from storage.

For China, some data were available from the International Commission on Large Dams (ICOLD) for dams greater than 15 meters in height. Information on additional reservoirs in the Huang He basin was also obtained from the Chinese Academy of Sciences. Although exact coordinates for the reservoirs were not available from ICOLD's publication (ICOLD, 1989), the location of the nearest town was listed. With help from the members of the Chinese Academy of Sciences and other Chinese experts, the locations of the towns were found and matched with the dams so that the dams could be mapped onto the watershed regions of *Figure 1.5*. For each region, we calculated the sum of the surface area and volume of all dams having information on both. *Table 4.1* shows the results of these calculations.

Table 4.1 shows that the total number of dams in China that had storage information and that could be located was 1,347. This seems to be a rather small number compared with the more than 83,000 dams that exist in China (UN, 1997). The dams with storage information, however, are all large dams (more than 15 meters in height) and account for a substantial portion (about 85%) of the total storage in China, according to the *1994 Statistical Yearbook of China* (SSB, 1995). Furthermore, of the dams that were located and had storage information, only about 12% also had data on area. However, these reservoirs accounted for 70% of the storage of the located reservoirs, and therefore about 60% of the total storage in China.

Table 4.1. Available reservoir data by region.

Region	R_v	R_{v+a}	R_{v+a}/R_v	V_v (billion m^3)	V_{v+a} (billion m^3)	V_{v+a}/V_v	A_{v+a} (billion m^2)	A/V slope
1	36	8	22.22%	52.38	38.92	74.30%	12.46	0.32
2	39	7	17.95%	19.83	0.01	0.04%	0.01	1.15
3	57	6	10.53%	11.82	1.04	8.76%	0.24	0.23
4	207	23	11.11%	41.51	35.29	85.01%	22.97	0.65
5	468	42	8.97%	167.43	110.28	65.87%	13.77	0.12
6	304	47	15.46%	71.25	47.39	66.51%	3.07	0.06
7	185	16	8.65%	38.21	29.22	76.48%	1.47	0.05
8	31	8	25.81%	16.96	16.55	97.60%	0.14	0.01
9	19	2	10.53%	46.49	37.46	80.59%	0.39	0.01
China	1,347	160	11.88%	468.15	327.72	70.00%	62.94	0.24

Note: R = number of reservoirs; V = volume; A = surface area; v = reservoirs with volume data; and $v + a$ = subset of reservoirs with both volume and area data. See *Figure 1.5* for names of regions.

As recommended in the previous chapter, a line through the origin with slope equal to the total surface area divided by the volume of all reservoirs with information for both was used to approximate the area–volume curve. The slopes of the resulting lines are given in *Table 4.1*. Because the hydrologic model CHARM applies the Penman–Monteith equation to calculate evapotranspiration according to the method recommended by the Food and Agriculture Organization of the United Nations (Allen *et al.*, 1998), the Penman–Monteith equation is also used to calculate evaporation depth from the reservoir surface. Although evaporation can vary with storage level and water temperature, a k_c coefficient of 1.0 is acceptable for an average open water evaporation coefficient over the year and is used for the sake of simplicity (FAO, 2001). Since all the reservoirs in a large region are aggregated together and the locations of unbuilt storage, as well as most of the built storage, are not known with certainty, it is difficult to obtain a better estimation of evaporation depth.

Combining the sequent peak method with the estimated evaporation from the area–volume curve and Penman–Monteith methodology, the storage–yield curves with and without evaporation were calculated using the monthly time series data output by CHARM. The results are shown in *Figure 4.4*.

Figure 4.4 shows the storage–yield curves for the nine major watershed regions in China, as displayed in *Figure 1.5*. For each region, the sequent peak methodology was performed both with and without evaporation to show the impact that evaporation has on the reservoir yield. To put the curves into context, information on annual average renewable water resources is provided in *Table 4.2*.

Table 4.2 shows the spatial disparity in water resources in China. Water in northern China is very scarce, with the worst water scarcity evident in the Hai He–Luan He watershed, which surrounds China's capital city, Beijing. The Hai He

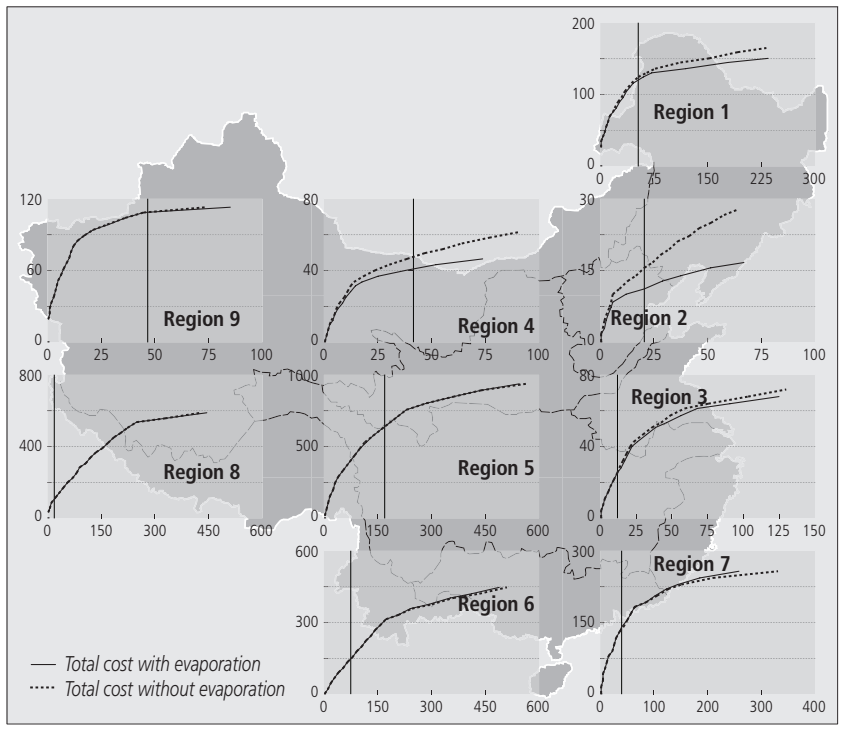

Figure 4.4. Storage–yield curves, with and without evaporation, for the nine watershed regions of China. Required storage is displayed on the horizontal axes in billion m^3. Annual release, or yield, is on the vertical axes, also in billion m^3. The vertical axis crosses the horizontal axis at the current storage level.

and the Huai He and a small eastern portion of the Huang He regions (regions 2, 3, and 4, respectively) also produce over half of China's wheat and a third of its corn (Brown, 2001). These three regions are the most water scarce, with demand already exceeding renewable water resources in the Hai He and Huai He regions. Since these regions are the driest, it should be no surprise that the yield from storage is impacted by evaporation the most in these regions, as shown in *Figure 4.4*. The Hai He–Luan He watershed shows an exceptionally high evaporative loss of about 40% of the runoff. Southern China, on the other hand, has no concern about water scarcity, with more than 30,000 m^3 of water per capita in the Southwest region (region 8). Incorporating net evaporation into the sequent peak calculations in some of the southern watersheds of China results in an increase in yield, because the precipitation is greater than the evaporation.

Figure 4.4 also shows the level of storage development in each region. Even with the limited reservoir information that is available, it is clear that China's

Table 4.2. Distribution of water resources in China.

Region	Annual precip. (mm)	Annual runoff[a] (billion m^3)	C_V[b] year series	C_V[b] month series	Range[b] (billion m^3)	Projected demand[c] (2010)	Population (million[c])	Runoff[c] per capita (m^3/yr)
1	510.8	165.3	0.20	1.05	94.81	87.07	111.76	1,479
2	559.8	28.8	0.43	2.16	34.74	57.29	127.97	225
3	859.6	74.1	0.35	1.74	57.07	105.09	190.50	389
4	464.4	66.1	0.30	1.32	46.61	63.41	100.79	656
5	1,070.5	951.3	0.12	0.75	309.39	261.45	401.55	2,369
6	1,544.3	468.5	0.20	1.28	262.33	121.17	135.21	3,465
7	1,758.1	255.7	0.21	0.84	105.46	47.37	85.26	2,999
8	1,097.7	585.3	0.08	0.95	167.76	12.39	18.48	31,679
9	157.7	116.4	0.10	0.70	32.33	78.45	24.09	4,832
China	648.4	2,711.5	0.07	1.20	94.81	833.7	1,167.38	2,323

[a] Data from Ministry of Water Resources and Electric Power (1997).
[b] Coefficient of variation C_V and range were calculated using a 16-year time series or runoff generated using the hydrologic model CHARM. C_V is reported both for the monthly time series and annual time series of flows. The range is reported only for the monthly time series.
[c] Per capita runoff and demand projections from Nanjing Institute of Hydrology and Water Resources (1996) as reported in UN (1997). Population for each region calculated from per capita runoff and runoff from each region.

watersheds are generally well developed. The northern regions have all approached a very high level of storage development, with current storage levels at the high end of the storage–yield curve, particularly the Huang He and the Interior basins regions (regions 4 and 9, respectively). The easy and cheap storage, where substantial increases in yield are obtained for relatively little increase in storage, has already been built. Increasing yield another unit now in these regions would require a much larger increment in storage capacity. It should be noted, however, that the storage reported in the reservoir databases is total storage and not just the active storage of the reservoirs. Because no data on dead storage in the reservoirs were available, the level of current storage for these reservoirs is overstated. Ideally, only active storage would be included in the current storage level, since active storage is the only storage available for storage and flow control.

4.3 Developing Cost Curves for the Nine Major Watershed Regions of China

Now that the storage–yield curves have been developed for the nine major watershed regions of China, the next step is to calculate the cost of storage. Although

Table 4.3. Storage costs in 1964 US dollars per acre-foot (Wollman and Bonem, 1971).

	Size class (1,000 acre-feet)										
Physio-graphic zone	I (0–20)	II (20–40)	III (40–60)	IV (60–100)	V (100–200)	VI (200–400)	VII (400–1,000)	VIII (1,000–2,000)	IX (2,000–4,000)	X (4,000–10,000)	XI (Over 10,000)
A	288	238	219	203	181	163	141	125	110	96	75
B	250	200	181	165	144	125	106	94	80	69	54
C	221	169	150	138	119	100	83	70	61	50	39
D	200	150	131	116	98	81	65	53	44	35	21
E	194	144	123	106	91	75	59	48	40	31	19
F	181	133	113	100	81	69	54	43	35	26	15
G	178	129	109	94	75	63	48	38	31	24	13
H	154	108	91	78	63	50	38	30	23	18	10
I	119	81	69	58	48	38	28	23	19	13	8
J	76	54	46	40	31	25	19	15	13	10	5

storage cost data are not readily available for China, a simple approach to estimating regional storage cost is developed in this section, following a methodology developed by Löf and Hardison (1966) and modified by Wollman and Bonem (1971) to study the outlook for water resources in the United States.

Since the cost of storage varies by local physiography and the size of the reservoir, Löf and Hardison (1966) developed storage cost curves for 11 size classes and 10 physiographic zones in the United States. The cost curves were then modified by Wollman and Bonem and based on the US construction technology of the 1960s and 1964 US dollars. *Table 4.3* shows the original storage cost table from Wollman and Bonem (1971).

The costs were then normalized by the average unit cost over all physiographic zones and class sizes so that the units of dollars and acre-feet were no longer an issue, and the size classes were converted to cubic meters. *Table 4.4* is the converted table.

The data from *Table 4.4* were plotted and power functions were fit to the data for each physiographic zone to create a continuous function for the average unit cost for each zone. The plot and fitted functions are displayed in *Figure 4.5*.

Assuming that the relationship between physiographic zone, size, and relative unit storage cost remains the same, the cost of any size reservoir can now be estimated using information on the topography in the region along with information from *Table 4.4* or the fitted curves from *Figure 4.5*. The technique involves the following steps:

Table 4.4. Normalized storage cost.

	Size class (million m^3)										
Physio-graphic zone	I (0–25)	II (25–49)	III (49–74)	IV (74–123)	V (123–247)	VI (247–493)	VII (493–1,233)	VIII (1,233–2,467)	IX (2,467–4,934)	X (4,934–12,335)	XI (Over 12,335)
A	3.31	2.73	2.51	2.33	2.08	1.87	1.62	1.43	1.26	1.10	0.86
B	2.87	2.30	2.08	1.89	1.65	1.43	1.22	1.08	0.92	0.79	0.62
C	2.54	1.94	1.72	1.58	1.37	1.15	0.95	0.80	0.70	0.57	0.45
D	2.30	1.72	1.50	1.33	1.12	0.93	0.75	0.61	0.51	0.40	0.24
E	2.23	1.65	1.41	1.22	1.04	0.86	0.68	0.55	0.46	0.36	0.22
F	2.08	1.53	1.30	1.15	0.93	0.79	0.62	0.49	0.40	0.30	0.17
G	2.04	1.48	1.25	1.08	0.86	0.72	0.55	0.44	0.36	0.28	0.15
H	1.77	1.24	1.04	0.90	0.72	0.57	0.44	0.34	0.26	0.21	0.11
I	1.37	0.93	0.79	0.67	0.55	0.44	0.32	0.26	0.22	0.15	0.09
J	0.87	0.62	0.53	0.46	0.36	0.29	0.22	0.17	0.15	0.11	0.06

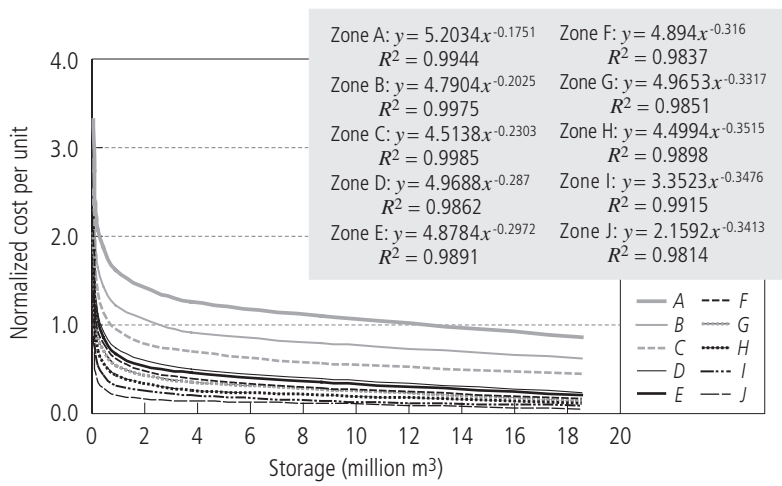

Figure 4.5. Curves of the storage cost by reservoir size for each physiographic zone.

1. First, the average unit storage cost for the country or region of interest should be obtained. The values in *Table 4.3* were normalized to produce *Table 4.4* for this reason. It is easier to obtain an average unit storage cost from national statistics or global datasets than to obtain unit storage cost values for each zone and each reservoir size.
2. Step two is to decide on the physiographic zone of the region for which storage costs are being considered. This can be done by using a digital elevation model

to calculate the average slope of the topography and correlating that with the physiographic zones provided.
3. The third step is to obtain the normalized unit cost from *Table 4.4* or the fitted curves from *Figure 4.5* and multiply by the average unit cost of the country or region that was obtained in step 1.

To validate the technique, we applied it to China and investigated the cost of the Three Gorges Dam, for which several studies with cost data are available. Although the final cost for the Three Gorges Dam remains unclear, with unofficial estimates running as high as US$75 billion, supporters of the project insist that it is within budget at 203.9 billion yuan, or US$24.6 billion at the current exchange rate. The storage capacity of the reservoir is 39.3 billion m^3, which sets the unit cost of storage at 5.19 yuan per m^3. The topography of the land in the vicinity of the Three Gorges Dam and the Chang Jiang (Yangtze River) watershed fits the slope of physiographic zone A. Therefore, the normalized cost curve for physiographic zone A can be used to calculate the cost. Using the equation for zone A from *Figure 4.5*, the normalized cost for a 39.3 billion m^3 reservoir in zone A is 0.086. To obtain the average per unit cost over all zones and reservoir sizes, one can divide the unit cost for the Three Gorges Dam of 5.19 yuan per m^3 by 0.086. A figure of exactly 6 yuan per m^3 is obtained. The budget estimate of 203.9 billion yuan includes present-value calculations of price inflation and interest payments on loans. The baseline currency year is uncertain, but the estimate was first reported in 1994.

As an additional check to see if 6 yuan is reasonable, Keller *et al.* (2000) report that the median cost of large storage around the world is about US$0.27 per m^3. They report that the median is 2.5 times the reported low value and that the average is 4 times the low value, placing the average cost at about US$0.43 per m^3 in 1998 US dollars, or about 3.58 yuan per m^3. This is the cost of construction and conveyance alone. Since only 55%, or 3.3 yuan per m^3, of the Three Gorges Dam project is construction costs, with the other 45% going to relocation costs, this cost is quite reasonable.

We can also update the original tables from Wollman and Bonem (1971) to 1998 US dollars. The mean cost of storage from *Table 4.3* is US$87.12 per acre-foot. If we use the consumer price index for the United States to update this figure to 1998 US dollars, the result is US$458.08 per acre-foot of storage, which corresponds to just over 3 yuan per m^3.

For the purposes of this study, we will retain the rough estimate of 6 yuan per m^3 of storage on average in China. Although this figure is above the construction costs of reservoir projects, we hope that the higher estimate takes into account some of the additional costs of reservoir construction, operation, and maintenance. In the case of the Three Gorges Dam, these additional costs include relocation of people and cities. Furthermore, since full capacity information was used for the

Table 4.5. Corresponding physiographic zone and cost per unit storage for each of the nine major watershed regions in China.

Watershed region	Physio-graphic zone	Total storage (billion m^3)	Total cost (billion yuan)	Cost/unit storage (yuan/m^3)
1	F	52.38	135.83	2.59
2	F	19.83	72.36	3.65
3	B	11.82	112.30	9.50
4	B	41.51	300.24	7.23
5	A	167.43	1451.58	8.67
6	A	71.25	673.79	9.46
7	B	38.21	266.55	6.98
8	A	16.96	138.56	8.17
9	A	46.49	314.50	6.77

Note: For watershed region names, see *Figure 1.5*.

reservoirs instead of active storage in developing the storage–yield curves, the cost of building the necessary active storage will be underestimated. The higher cost estimate, if indeed it is too high, will only help counter this original underestimate. Unfortunately, any estimate of cost in this report must be viewed only as a rough estimate, which could be improved with better data on reservoir costs, storage, and area. Now that we have decided on a cost estimate, we can proceed to step 2.

For each of China's nine major watershed regions, the average physiographic slope was calculated from the HYDRO1K database. The slope was then used to match each region with the corresponding physiographic zone as defined by the US Army Corps of Engineers (Löf and Hardison, 1966; Wollman and Bonem, 1971). Using the average storage cost of 6 yuan per m^3, the physiographic zone, and the normalized unit cost curve, the cost of each reservoir of known storage was calculated for each region. The total storage and total cost were used to calculate the unit cost of storage in each region. The results are given in *Table 4.5*.

Assuming that the distribution of dam sizes remains the same as more dams are built in each region, the unit cost for each region can be used to estimate the cost of additional storage in the region. In other words, a linear cost curve, with slope equal to the cost per unit storage from *Table 4.5*, can be applied to each region.

4.4 Water Supply from Storage for the Nine Watershed Regions of China

To construct the supply curves for the nine major watershed regions of China, the storage–yield curve is combined with the linear cost curve to produce the cost–yield

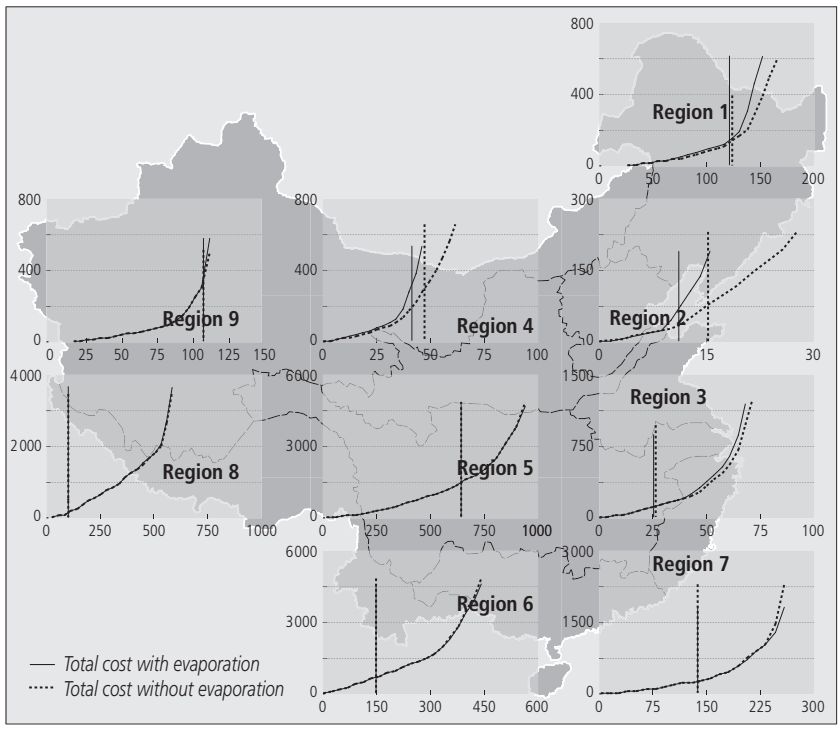

Figure 4.6. Total cost curves for China, with and without evaporation. Horizontal axes show yield from storage in billion m^3; vertical axes show total cost in billion yuan. The vertical axis crosses the horizontal axis at the estimated yield from current storage levels.

curve, otherwise known as the total cost curve. Each level of storage in the storage–yield curve was multiplied by the cost per unit of storage. The cost was then plotted versus yield to obtain the total cost curves for reservoir storage in China shown in *Figure 4.6*.

For each region, the curves essentially become vertical beyond the points shown on the plots, implying that no more yield can be obtained from the current level of runoff in these regions. If more water is needed in a particular region, it must be transferred from another region with spare capacity. Region 9 is a good example of a region that cannot increase its yield beyond its current level. Since not all of the storage reported is active storage, however, the plot may overestimate the storage level.

Like *Figure 4.4*, *Figure 4.6* shows the impact of evaporation on the yield from storage, this time in terms of yields and costs. In the southern regions, evaporation from storage makes very little difference in the cost of achieving any level of yield.

The difference in cost between scenarios with and without evaporation in regions 5, 6, 7, and 8 is less than 1%. The situation in the North, though, is substantially different. Using the current storage level to assess the impact of evaporation on yield at constant costs, we find that the yield is reduced by only 1.64% in region 1 and 3.32% in region 3. In region 2, however, the decrease in yield is as high as 26% at current storage levels. Region 4 also has a substantial drop in yield of about 14%.

How does evaporation affect the cost of supplying a specified level of yield in each region? Again, in the South, the impacts are not significant, with less than a 1% difference at current yield levels. Using the current yield level, calculated by including evaporation, as the fixed yield level, we find that in region 1, evaporation increases the cost of the current yield by over 4%. In region 2 the increase in cost is over 40 billion yuan, or more than 127%. The increased cost due to evaporation in region 4 is about 66%. If we were to attempt to achieve the level of yield comparable to what the current amount of storage could achieve without evaporation, the cost would be 150% in region 2 and over 17,000% in region 4.

The total cost curve for reservoir storage in each of the regions has now been developed and analyzed, but the economic supply curve has not actually been developed. The supply curve for a competitive firm, which is the marginal cost curve, or the derivative of the total cost curve, will be used. The marginal cost, or supply, curve can reinforce what we have learned from the total cost curve by telling us directly what the cost of an additional cubic meter of water would be in each region.

There are a number of methods for calculating the marginal cost curve from the total cost curves given. A function could be fitted to the total cost curve and the derivative could be taken of the functional form. Alternatively, with this method, a curve could even be fitted to the storage–yield curve and the total cost curve could be derived from that. Another method is to simply calculate the slope between two points on the total cost curve and use the actual data to form the marginal cost curve. Although a functional form is mathematically easier to work with, the second method of calculating the marginal cost curve has a few advantages. One is that fitting a curve to the data results in another source of error, which is unnecessary here. The full curve is captured with the data and there is no need to extrapolate beyond the data. Another reason is that viewing and analyzing the actual data can sometimes result in findings and conclusions that would be missed when working with a fitted, smooth functional form. The calculation of the supply curves, or marginal cost curves, results in the curves shown in *Figure 4.7*.

One should be careful about calling the curves in *Figure 4.7* supply curves and about the conclusions drawn from them. Marginal cost should equal price for the supply curve. However, in this case the supply continues over the lifetime of the project. If the management plan is to recoup the cost of the project, then the costs

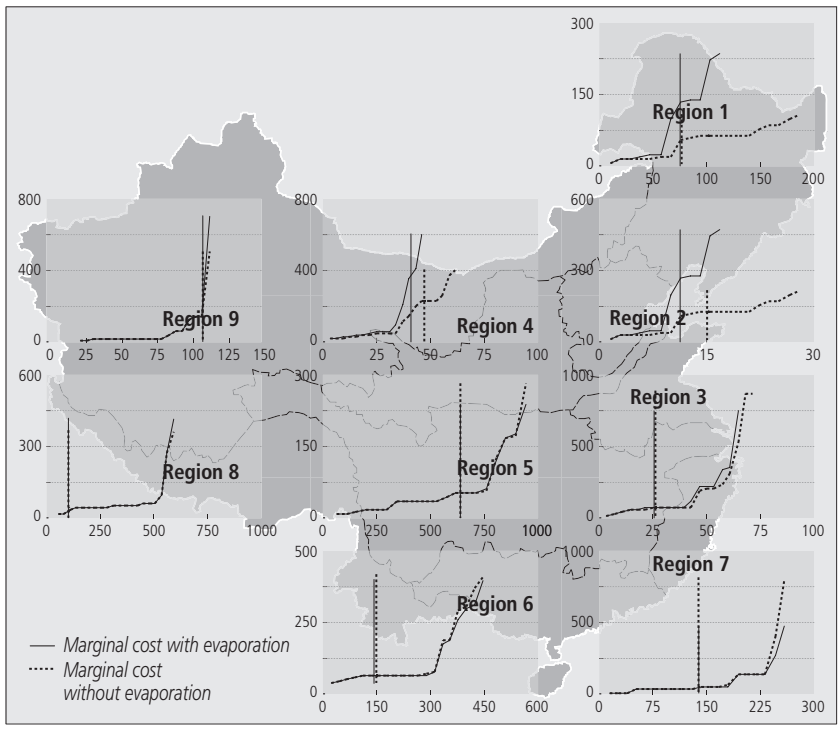

Figure 4.7. Supply, or marginal cost, curves for storage in the nine major watershed regions of China. Horizontal axes show yield from storage in billion m^3; vertical axes show marginal cost in billion yuan. The vertical axis crosses the horizontal axis at the estimated yield from current storage levels.

should be annualized over the lifetime of the project and the price should be set equal to these costs. The marginal cost shown here is the increase in total cost, *over the lifetime of the project*, to increase the *annual* yield by 1 m^3.

With information on the interest rate and project lifetime, the plots can be converted to show the price that should be charged for each unit of water over the project lifetime to match the marginal costs. The present value of a stream of revenue, equal to the water price times the yield, for the lifetime of the project needs to be calculated. The present value of this stream of revenue must equal the cost of storage, so the price is calculated to fit this condition. The present value (PV) formula for a series of constant cash payments (PMT) for n time periods at interest rate r is

$$PV(1+r)^n - PMT\left(\frac{(1+r)^n - 1}{r}\right) = 0. \tag{4.3}$$

Solving Equation (4.3) for PMT, the result is

$$PMT = PV\left(\frac{r(1+r)^n}{(1+r)^n - 1}\right). \tag{4.4}$$

In our case, the present value of the revenue is the cost, since our cost estimate was the present value of the project costs. We can use this technique to calculate the average price necessary to cover the cost of the project from the total cost curve or to find the water price that would match the marginal cost. The present-value calculation only needs to be performed for one point on the curve to find a multiplier, which can be used to convert the rest of the curve. If we use a project lifetime of 50 years and an interest rate of 3%, for example, the multiplier to convert the marginal cost curve from a cost per additional cubic meter of annual yield to a cost per cubic meter of water delivered by the project is 0.0389. In region 4, then, for marginal revenue to equal marginal cost, the price for water should be 14 yuan per m^3. In region 5, the price would be only 2 yuan per m^3.

Once again, scarcity is shown in regions 2 and 4 by high marginal costs for additional storage. In region 2, the cost to add an additional cubic meter of storage is about 260 yuan, while in region 4, the marginal cost is over 370 yuan. Without evaporation, the marginal cost at this same level of yield would drop about 60% in each case, but would still be greater than the marginal cost in other regions. With water so scarce in the North and the cost of increasing the supply so high, it is no wonder that China has decided to divert water via three routes from the Chang Jiang (Yangtze River) basin to the northern basins. When complete, the three diversions will transfer 38–48 billion m^3 of water to the North at an estimated cost of more than 480 billion yuan, although estimates vary. The results of the cost analysis are summarized in *Table 4.6*.

4.5 Summary

In this chapter, a methodology was developed for calculating the marginal cost curve for providing water from reservoir storage, using nine major watershed regions in China as examples. The impact of evaporation in these regions was also investigated. The first step in developing the marginal cost curve is to obtain time series runoff data. If time series data are not available, they can be obtained from a hydrologic model. The length of the time period used depends on the size of the region under investigation and the use of storage in the region. However, in the large regions and entire countries that this methodology is designed for, monthly time series flows over as many years as possible provide the necessary information. If we assume that many reservoirs are distributed throughout the entire region, a routing model is not necessary.

Table 4.6. Total cost of obtaining current yield under net evaporation and cost of same yield with no evaporation, and marginal cost at current yield.

Region	Yield (billion m^3)	Cost (billion yuan)	Cost for equivalent yield without evaporation (billion yuan)	Increase due to evaporation (%)	Marginal cost (yuan)	Marginal cost for same yield without evaporation (yuan)	Increase due to evaporation (%)
1	80.84	51.42	49.34	4.22	19.04	18.01	5.40
2	11.22	72.36	31.80	127.55	258.72	100.56	61.13
3	25.61	112.30	106.74	5.21	79.85	75.99	4.83
4	40.91	300.24	180.87	66.00	370.91	158.40	57.29
5	640.04	1,451.58	1,448.43	0.22	52.13	52.02	0.21
6	146.24	673.79	671.43	0.35	66.48	66.20	0.43
7	138.54	266.55	267.46	–0.34	37.26	37.96	–1.86
8	104.22	138.56	138.44	0.09	28.73	28.69	0.13
9	108.86	314.50	309.14	1.73	166.04	157.17	5.34
China	1,296.49	3,381.31	3,203.65	5.55	119.91	77.22	55.28

Once time series runoff data have been obtained, the sequent peak method or a reservoir model can be applied to estimate the storage requirement for the region as a whole. Any losses to the system, such as evaporation, that can be estimated should be included in the storage requirement calculation. Egypt, for example, loses about 12% of its total annual renewable water resources to evaporation at Lake Nasser (FAO, 1997; Gleick, 1998). Since evaporation depends on the surface area of water in reservoirs, however, the relationship between surface area and storage for the combined reservoirs must be estimated. This can be done using the estimation technique presented in Chapter 2 of this report. The output of the sequent peak methodology is a curve relating total storage to annual yield from storage in the region.

The next step is to determine the cost of storage in a region. Curves were developed for reservoir cost in relation to the physiography of the region and the size of the reservoir, based on average cost tables from the US Army Corps of Engineers. The tables and curves provide data that are normalized to the average per unit cost, so that data on costs from the region under investigation can be quickly applied by multiplying by the average per unit cost in the region.

The final step of the procedure is to combine the storage–yield curve with the storage cost data to obtain the total cost curve, which shows the total cost to create any level of yield. The derivative of the total cost curve is the marginal cost curve, which can be considered the supply curve, with some stipulations. The curve shows the cost of supplying an additional unit of water. This is the price that a competitive

firm should charge for the water. However, the price, or cost, must be spread over the lifetime of the project, because the yield is an annual yield that will be delivered every year for the duration of the project. The price per unit of water necessary for a competitive firm to produce the current yield can be obtained by using present-value calculations using the marginal cost at the current yield as the present value. Generally, water projects do not need to take price as given, however, so planners calculate the price of water necessary to repay the project costs. This can be done using present-value calculations and the total cost curve.

The marginal cost curve methodology described above was applied to assess the impacts of evaporation on storage costs in the nine major watershed regions of China. The results show that evaporation has a large impact on reservoir storage in some of the northern regions where water is already scarce. Low precipitation and a high level of development in these regions make it very expensive to increase yield. Evaporation in the Hai He–Luan He watershed surrounding Beijing (region 2) results in a cost increase, at current yield, of 130% over what it would cost to achieve the same yield without evaporation. The marginal cost of increasing yield by 1 m^3 annually is greater than 250 yuan, while in other regions, particularly in the South, the marginal cost is as low as 20 yuan. The impact of net evaporation is also much lower in the South. In fact, in the Southeast region (region 7), net evaporation actually increases yield slightly, since precipitation is greater than evaporation.

The cost figures in this paper can only be viewed as very rough estimates. Few data were available on reservoir location, surface area, cost, or active storage in the reservoirs. Many approximations, assumptions, and estimates were made to obtain these values throughout the several steps of the methodology of calculating the marginal cost curves. The methodology itself will result in some error due to the many different operating policies possible and the fact that it is simply an estimation technique for large regions. However, the estimate can be greatly improved with better data, particularly on active storage, surface area, and costs.

5

The Impacts of Climate Change on Regional Surface Water Supply from Reservoir Storage in China

5.1 Introduction

The previous chapters have described the spatial and temporal diversity of China's water resources, showing how scarce water is in the North and how abundant it is in the South. In the northern regions of China, the renewable water resources were estimated by Chinese studies to be as low as 225 cubic meters (m^3) per capita, the value in the Hai He–Luan He watershed surrounding Beijing (Nanjing Institute of Hydrology and Water Resources, 1996). The analysis of the impacts of evaporation in Chapter 3 suggests that this figure for per capita water resources could be reduced by one-third as a result of evaporation from reservoirs in the region. Three of nine major watershed regions show signs of severe water scarcity. The estimated annual renewable water resources are not even enough to satisfy demand in these regions, and the usable water resources are much less than the renewable water resources figures.

Another important issue in China is the variability of its water resources. China's rivers are known for floods and droughts. China's Huang He, or Yellow River, is named for the amount of sediment it carries. However, it is also known for its disastrous floods and droughts—and it is not alone in producing floods and droughts. In its response to the Dams and Development Report of the World Commission on Dams, the Chinese National Committee on Large Dams (CHINCOLD, 2001) lists some of the catastrophic floods and droughts China has survived:

- A drought in 1876–1879 halted food production in 1 million square kilometers (km^2) of nine provinces.
- A serious drought in northern China in 1920 affected 20 million people and caused 500,000 deaths.
- A drought in 1928 affected 120 million people in 13 provinces.
- In 1931, flooding of the Chang Jiang (Yangtze River) caused more than 300 dike bursts, affecting 28 million, and causing 145,000 deaths.

- In 1933, flooding of the Huang He affected 11,000 km^2, causing more than 50 dike bursts, affecting 3.64 million, and leading to 18,000 deaths.
- In 1935, flooding of the Huang He inundated 27 counties and affected 3.4 million.
- In 1935, flooding of the Chang Jiang affected six provinces with a total area of 29,000 km^2, affecting more than 10 million, and causing 140,000 deaths.
- A serious drought in 1942–1943 in Henan province caused more than 1 million deaths.

Water scarcity and variability problems have prompted China to construct tens of thousands of reservoirs to reduce the impacts of floods and droughts, to provide a reliable water supply, and to produce power. In addition, China has begun work on two of three huge diversion projects that will eventually bring 38–48 billion m^3 of water per year from the Chang Jiang (Yangtze River) watershed region north to the Huang He, Huai He, and Hai He–Luan He watershed regions.

In light of this massive capital spending and planning on long-term water resources supply projects, it is important to consider the impacts that climate change might have on water resources in the future. Will the scarcity in the northern regions of China worsen with climate change? Will climate change result in more or fewer floods and droughts in these regions? How might climate change impact the yield from storage and current supply projects, and how much will it cost to maintain the same yield if the climate changes? These are some of the questions that water resources planners need to consider in planning long-term water resources supply projects and the type of questions that will be investigated in this report.

5.2 GCMs and Climate Change in China

A recent study of climate change impacts on agricultural land potential and water resources in the North China Plain used outputs from three general circulation models (GCMs) for its assessment of climate change (Fischer and Wiberg, 2001). The GCM outputs were obtained from the Data Distribution Centre (DDC) of the Intergovernmental Panel on Climate Change (IPCC). Scenarios from these same models will be used here, so that comparisons between the land productivity assessment and water availability can be made. The three models are as follows:

- *The ECHAM4 Model.* This model was developed at the German Climate Research Centre of the Max Planck Institute for Meteorology in Hamburg, Germany (Roeckner *et al.*, 1992, 1996; Oberhuber, 1993). Here, we use the results of the "greenhouse gases plus sulfate aerosols forcing" scenario.

- *The First Generation Global Coupled Model (CGCM1)*. This model was developed at the Canadian Centre for Climate Modelling and Analysis. The average "ensemble forcing" scenario was taken for the "greenhouse gases plus sulfate aerosols" model run (Boer *et al.*, 1998; Flato *et al.*, 1998).
- *The HadCM2 Model*. This model is based on recent experiments performed at the Hadley Centre for Climate Prediction and Research (Murphy, 1995a, 1995b; Murphy and Mitchell, 1995). The average of "ensemble forcing" scenarios is used for greenhouse gases plus sulfate aerosols.

Since "current demographic and socioeconomic trends suggest that the next 30–50 years will be decisive for managing viable transitions towards sustainable land use systems" (Fischer and Wiberg, 2001:317), this chapter will focus on the second model period, 2040–2069. For this period the HadCM2, ECHAM4, and CGCM1 scenarios predict an average temperature increase of 2.5°C, 3.0°C, and 4.6°C, respectively. The increase in temperature in the northern regions is slightly greater at 2.6°C, 3.0°C, and 5.7°C, respectively. The increasing temperature will result in higher evapotranspiration in these already dry regions, resulting in further drying.

The increased temperature is countered, however, by increased rainfall. More evaporation results in more precipitation. Although the North is dry, more water is also evaporated farther south, and weather patterns can transport this moisture to the North. This seems to be the case with these scenarios, since the HadCM2 model predicts an increase in precipitation of 11.3% in the northern regions. For the CGCM1 model, the increase is 9.4%, and for the ECHAM4 model it is 16.4%. For the whole of China the increase is 10.4% for the ECHAM4 and HadCM2 models and 4.7% for the CGCM1 model scenario.

This chapter discusses the impacts of climate change on water resources and storage costs in the nine major watershed regions of China by first analyzing the impacts of temperature and precipitation changes alone and then applying the GCM scenarios. To test the impacts of temperature changes, a sensitivity analysis will be performed using three temperature changes. As 2°C and 3°C are common estimates for average global temperature increases over the next 50–100 years, and as these amounts are also the changes predicted for China by two of the three scenarios, temperature increases of 2°C and 3°C will be used to see what impact changes in temperature alone could have. A 2°C temperature decrease will also be added to assess what may happen in the case of cooling and to determine whether the impact is similar in the reverse direction. For precipitation, 15% and 30% increases in precipitation and a 15% decrease in precipitation will be discussed. The results of the GCM model runs, which provide monthly time series changes in temperature and precipitation, will then be applied and discussed.

Table 5.1. Impact of temperature changes on annual average surface water resources of nine major watershed regions in China.

Watershed region	Surface water resources (billion m^3)						
	Current	+2°C	Change (%)	– 2°C	Change (%)	+3°C	Change (%)
1	165.33	153.60	–7.10	178.51	7.97	148.17	–10.38
2	27.87	26.94	–3.35	29.02	4.09	26.53	–4.81
3	71.49	68.89	–3.65	74.46	4.15	67.71	–5.29
4	61.62	58.11	–5.70	65.63	6.51	56.51	–8.30
5	943.26	909.84	–3.54	978.11	3.70	893.57	–5.27
6	444.44	427.84	–3.74	461.59	3.86	419.75	–5.55
7	257.47	251.51	–2.32	263.50	2.34	248.53	–3.47
8	588.77	582.79	–1.01	595.07	1.07	579.85	–1.52
9	113.40	104.68	–7.69	123.57	8.97	100.70	–11.20
China	2,673.66	2,584.20	–3.35	2,769.46	3.58	2,541.32	–4.95

Note: For watershed region names, see *Figure 1.5*.

5.3 Temperature Changes

A rise in temperature increases the evaporation from water surfaces and land, and generally increases transpiration from plants. The quantity of water resources over large regions should therefore be inversely related to temperature, decreasing with increasing temperature or increasing with decreasing temperature. To test this hypothesis, the hydrologic model CHARM (Climate- and Human Activities-sensitive Runoff Model) was run for the nine watershed regions in China, first adding 2°C for each time period, then adding 3°C, and finally subtracting 2°C from the baseline, historic time series temperature. *Table 5.1* shows the impact of these changes on the average annual surface water resources of each region.

According to the information in *Table 5.1*, for China as a whole, the annual runoff decreases by approximately 1.7% per 1°C rise in temperature. In some of the drier regions—the Northeast, Huang He, and Interior basins regions (regions 1, 4, and 9, respectively)—the change is more than double this amount.

Changes in the average runoff do not provide a complete picture of the impacts of temperature changes, however. Floods and droughts are the results of the variability of flows, and calculations of the reservoir storage capacity necessary to capture runoff and release it when needed are based on runoff variability. For storage capacity calculations, the range of flows is the most important statistic, since reservoirs must be able to handle the maximum flow but still store water through the period of lowest flow. Can a simple change in temperature impact the variability of runoff? *Table 5.2* shows the changes in the coefficient of variation and range of monthly flows in the nine regions.

Table 5.2. Changes in coefficient of variation and range of monthly flows under temperature change.

Re-	Baseline		+2°C				–2°C				+2°C			
gion	C_v	Rng	C_v	%	Rng	%	C_v	%	Rng	%	C_v	%	Rng	%
1	1.1	94.8	1.1	4.1	92.4	–2.5	1.0	–4.1	97.5	2.8	1.1	6.3	91.3	–3.7
2	2.2	34.7	2.2	2.0	34.7	–0.1	2.1	–2.3	34.8	0.2	2.2	3.0	34.7	–0.2
3	1.7	57.1	1.8	1.3	55.7	–2.4	1.7	–1.4	58.5	2.6	1.8	1.9	55.0	–3.7
4	1.3	46.6	1.4	2.9	46.2	–0.8	1.3	–2.9	47.0	0.9	1.4	4.4	46.1	–1.2
5	0.8	309.4	0.8	1.1	302.7	–2.2	0.7	–1.1	316.3	2.2	0.8	1.6	299.4	–3.2
6	1.3	262.3	1.3	1.5	257.0	–2.0	1.3	–1.5	267.5	2.0	1.3	2.2	254.4	–3.0
7	0.8	105.5	0.8	1.0	104.6	–0.8	0.8	–1.0	106.3	0.8	0.8	1.6	104.1	–1.3
8	1.0	167.8	1.0	0.2	166.5	–0.8	0.9	–0.3	169.0	0.8	1.0	0.3	165.8	–1.1
9	0.7	32.3	0.7	2.3	30.9	–4.4	0.7	–1.9	33.9	4.7	0.7	3.6	30.2	–6.5

Note: C_V = coefficient of variation; Rng = range, in billion cubic meters. Other columns show the percentage difference between the given scenario and the baseline, or historic, value. For watershed region names, see *Figure 1.5*.

The coefficient of variation does increase with increasing temperature, but interestingly, at the same time that the coefficient of variation increases, the range of flows decreases. An explanation for this may be found in the soil water balance. During wet periods, if the soil quickly becomes saturated and the rain continues, excess runoff flows quickly over the surface. However, evaporation more quickly depletes the soil moisture, resulting in new and more frequent dry periods. In the baseline scenario, the soil may have stayed saturated for a longer time. Conditions can then change very quickly from excess runoff to dry soil, creating greater variability. At the same time, peak flows are reduced, since storms must saturate the soil before the excess runoff state is achieved. Since there is a natural limit to how low a low-flow period can be, the range decreases.

The fact that temperature and flow range respond in opposite directions has competing influences on the storage–yield curve. If the range decreases, less storage will be needed to hold the same amount of water. However, greater evaporation from the increased water surface area will result in lower yields. The storage–yield curves for the nine regions under the three temperature change scenarios are shown in *Figure 5.1*.

Despite the slight decrease in range, the results shown in *Figure 5.1* are as expected. As temperature increases, evaporation increases, resulting in reduced runoff and reduced yield from storage. The areas with the greatest surface area per unit volume of storage, such as regions 2 and 4, fare the worst. The decrease in yield per 1°C increase in temperature in region 2 is about 3%. For region 4, it is closer to 4%. Region 9 also has a substantial reduction in yield, also 4% per 1°C increase in temperature. In order to achieve the same yield, storage in region 4 would have to be increased by a substantial 77% if the temperature were to rise

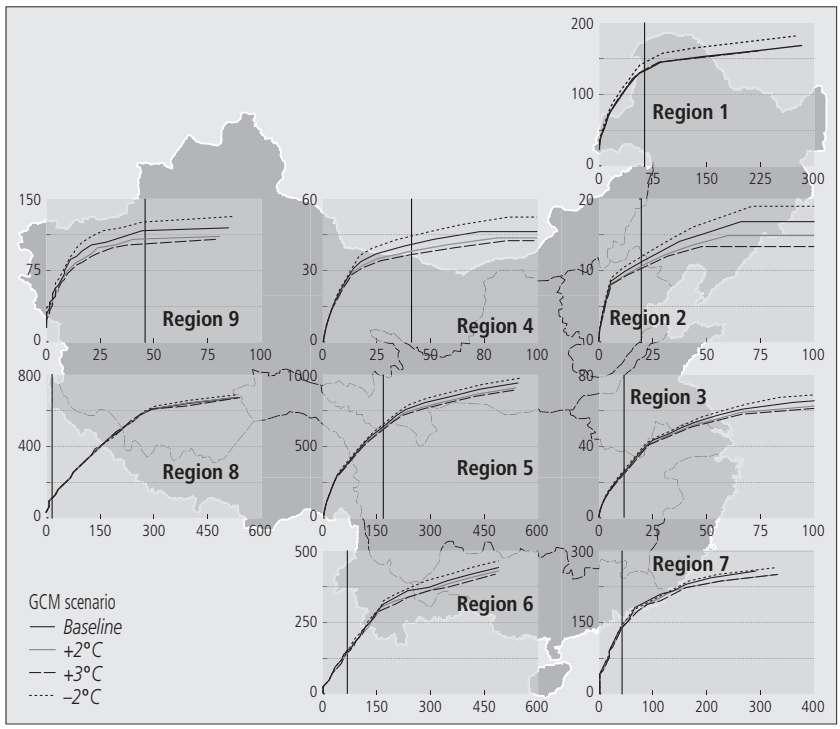

Figure 5.1. Impact of temperature change on storage–yield curve. Horizontal axes show storage in billion m^3; vertical axes show yield in billion m^3. The vertical axes cross the horizontal axes at the current storage level.

by 3°C. This would cost more than 230 billion yuan, or about 56 yuan per m^3. In the Interior basins region (region 9), achieving the same yield after a 3°C rise in temperature would not even be possible.

5.4 Precipitation Changes

The impact of precipitation changes on runoff is clearer than the impacts of temperature changes. If precipitation is increased in each period, runoff should also increase and vice versa.

The results shown in *Table 5.3* offer no surprises. Runoff does increase with increasing precipitation. When precipitation is increased by 15% for every time step, the result is an increase in runoff of almost 40%. The increase in runoff is larger than the precipitation increase, because multiplying the precipitation for each time step by a fixed factor results in much greater precipitation, in absolute terms, during the seasons that are already wet. Since the soil is already wet at these times, the

Table 5.3. Results of increasing precipitation of baseline period by 15% and 30% and decreasing it by 15%.

	Surface water resources (billion m^3)						
Region	Current	+15%	Change (%)	–15%	Change (%)	+30%	Change (%)
1	165.33	213.60	29.19	123.92	–25.05	268.04	62.12
2	27.87	38.41	37.79	19.39	–30.43	50.86	82.46
3	71.49	95.70	33.85	50.97	–28.71	123.00	72.05
4	61.62	82.98	34.66	44.04	–28.53	107.99	75.25
5	943.26	1,166.91	23.71	733.69	–22.22	1,401.24	48.55
6	444.44	568.79	27.98	325.79	–26.70	696.56	56.73
7	257.47	305.10	18.50	211.37	–17.91	353.91	37.46
8	588.77	659.77	12.06	518.93	–11.86	732.12	24.35
9	113.40	138.61	22.23	91.71	–19.12	167.03	47.29
China	2,673.66	3,269.86	22.30	2,119.81	–20.71	3,900.74	45.90

Note: For watershed region names, see *Figure 1.5*.

increased rainfall runs off directly and adds to the increased subsurface flow from the wet soil, resulting in a much higher peak runoff. Because of the increased range of flows, the increase in yield from existing storage due to precipitation increases of 15% and 30% is smaller than the increase in runoff, but still substantial, as shown in *Figure 5.2*.

5.5 GCM Scenarios and Reservoir Yield

The preceding sections provide a clear picture of what happens to runoff and reservoir yield under precipitation and temperature changes. The GCM scenarios provide a complex mix of changes to climatic parameters. As mentioned previously, both average temperature and average precipitation increase in the scenarios of climate change surrounding 2050. The increase in average temperature will decrease runoff and yield, while the increase in precipitation will increase runoff and yield, so that the direction of change in the end is unclear. From the results of the preceding sections, we can surmise that, because of the magnitude of the changes in precipitation, precipitation will most likely have a greater influence on runoff than will changes in temperature. However, the temperature and precipitation predicted by the GCM scenarios are not uniform over the months of the year. Thus, the shape of the hydrograph could be modified to produce unexpected results.

Table 5.4, which is similar to *Table 5.1* and *Table 5.3*, summarizes the changes in average annual runoff obtained by using the changes in climate parameters between the three GCM scenarios mentioned and the baseline scenario runs of the GCMs.

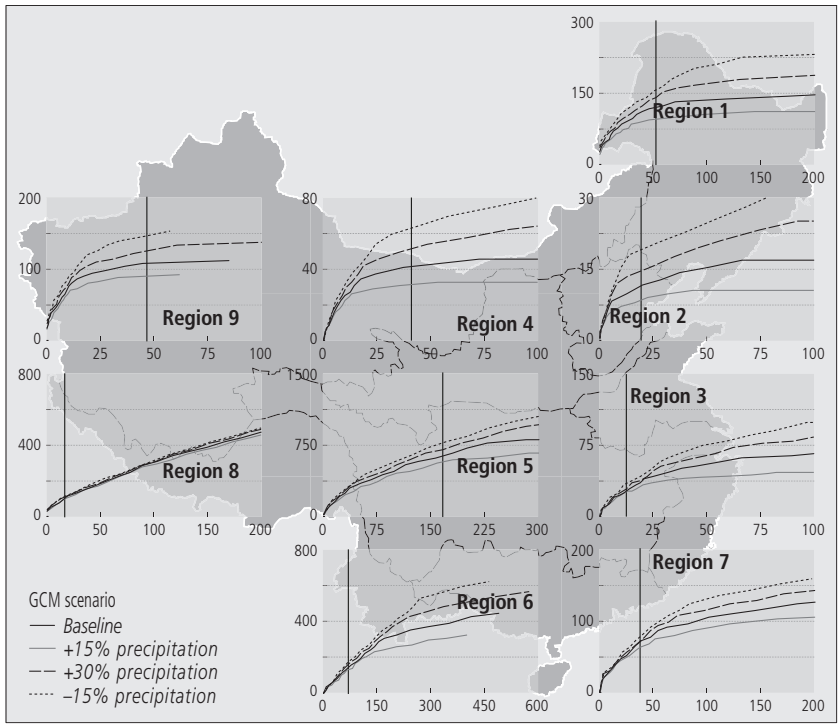

Figure 5.2. Impact of increasing precipitation by 15% and 30% and decreasing it by 15%. Horizontal axes show storage in billion m^3; vertical axes show yield in billion m^3. The vertical axes cross the horizontal axes at the current storage level.

Table 5.4. Results of applying combined changes in temperature and precipitation from GCM scenarios to hydrologic model CHARM.

	Surface water resources (billion m^3)						
Region	Current	HadCM2	Change (%)	CGCM1	Change (%)	ECHAM4	Change (%)
1	165.33	172.42	4.29	149.41	–9.63	178.40	7.90
2	27.87	26.96	–3.26	29.93	7.36	35.50	27.36
3	71.49	68.56	–4.10	76.63	7.19	86.48	20.96
4	61.62	59.00	–4.25	66.42	7.79	69.85	13.35
5	943.26	1,000.40	6.06	948.01	0.50	992.81	5.25
6	444.44	469.30	5.59	451.12	1.50	461.54	3.85
7	257.47	267.46	3.88	254.85	–1.02	257.32	–0.06
8	588.77	605.32	2.81	562.81	–4.41	647.61	9.99
9	113.40	110.50	–2.55	99.31	–12.42	118.92	4.87
China	2,673.66	2,779.94	3.97	2,638.48	–1.32	2,848.41	6.54

Note: For watershed region names, see *Figure 1.5*.

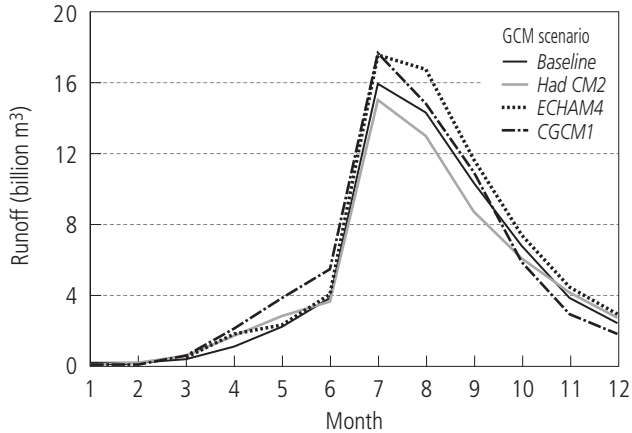

Figure 5.3. Average monthly flows in the Huang He watershed, historical and for three GCM scenarios.

Table 5.4 shows some interesting results. Although all scenarios predict an increase in precipitation for the regions of greatest water scarcity (regions 2, 3, and 4), the HadCM2 scenario results in a decrease in runoff for these regions. A look at the flow hydrograph might provide a reason for this. *Figure 5.3* shows a plot of the average monthly flows in the Huang He watershed (region 4) from the output of CHARM for the historical data and the three GCM scenarios.

The figure shows that although the HadCM2 scenario predicts an increase in rainfall, the rainfall is more evenly dispersed throughout the year. Less precipitation occurs in the wettest period, so the peak runoff is lower. If there is more precipitation in the dry periods, the precipitation can easily evaporate or infiltrate into the drier soil. More rainfall during the dry periods, then, may not produce additional runoff. If more rain falls when the soil is already wet, however, all of the additional precipitation will quickly run off over the surface, since it cannot infiltrate into the soil. The changes in the timing of precipitation, then, are at least as important as the amount of precipitation.

Figure 5.4 shows the impacts of the changes in runoff on the storage–yield curves graphically, while *Table 5.5* lists the impacts on yield from storage from each GCM scenario at current known storage capacity levels.

Figure 5.4 and *Table 5.5* indicate that even if the average runoff is reduced in a region, the yield from current storage capacity can still increase. In regions 2 and 3, the changes in precipitation and temperature from the HadCM2 scenario result in an annual average decrease in runoff due to less rainfall and runoff during peak periods and higher evaporation. However, because of the reduced range of flows, more yield is possible from the current storage capacity, but only to a certain

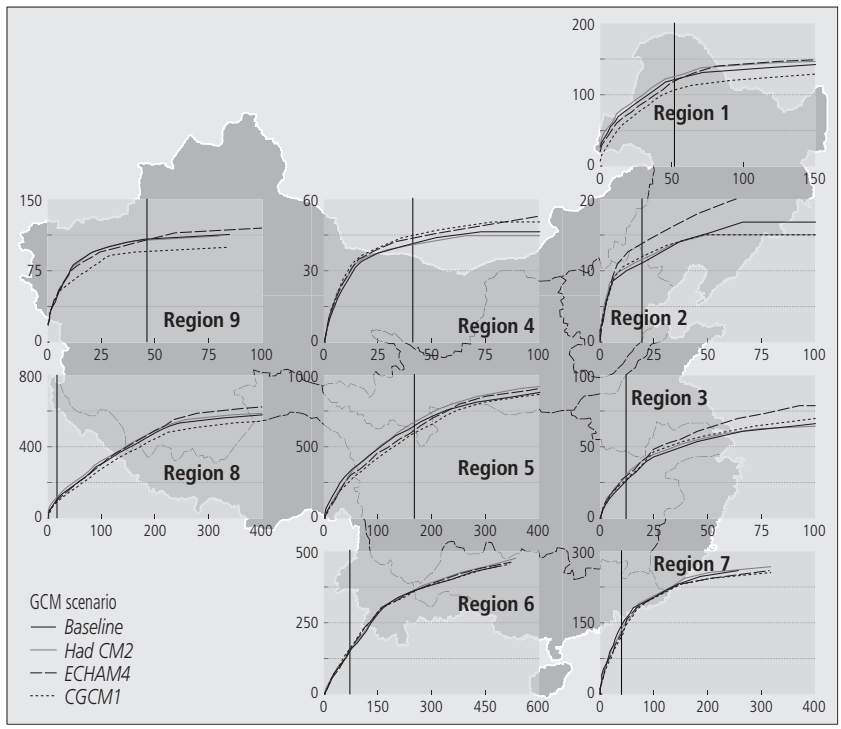

Figure 5.4. Impact of changes in runoff on storage–yield curves for the nine watershed regions in China, historical and three GCM scenarios. Horizontal axes show storage in billion m^3; vertical axes show yield in billion m^3. The vertical axes cross the horizontal axes at the current storage level.

Table 5.5. Changes in release from current known storage capacity under three GCM scenarios.

	Yield at known storage levels (billion m^3)						
Watershed region	Baseline release	HadCM2	Difference (%)	CGCM1	Difference (%)	ECHAM4	Difference (%)
1	120.36	126.38	5.00	107.22	–10.92	119.71	–0.54
2	11.60	11.86	2.24	12.29	5.98	14.14	21.97
3	25.61	30.40	18.70	26.80	4.67	28.39	10.85
4	40.91	40.77	–0.35	44.17	7.95	43.48	6.28
5	640.04	665.67	4.00	586.46	–8.37	612.85	–4.25
6	146.24	149.97	2.55	160.01	9.41	152.64	4.37
7	138.54	130.94	–5.49	120.15	–13.27	126.33	–8.81
8	104.22	115.54	10.87	84.95	–18.49	96.55	–7.36
9	108.86	106.65	–2.03	95.66	–12.13	106.34	–2.32
China	1,336.37	1,378.17	3.13	1,237.70	–7.38	1,300.43	–2.69

Note: For watershed region names, see *Figure 1.5*.

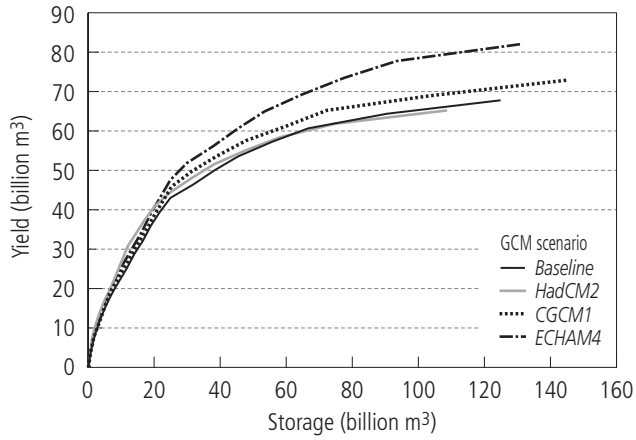

Figure 5.5. Effect of differences in climate from GCM scenarios on storage–yield curve in the Huai He watershed.

point. If the maximum possible yield is developed, the scenarios with greater average runoff will generally produce greater yield, although this can also depend on evaporation and timing of flows into and out of the reservoir. *Figure 5.5* provides an enlargement of the storage–yield curve for the Huai He watershed (region 3), which shows that although the HadCM2 scenario results in greater yield at the known storage level, at higher storage levels the yield would be lower than the baseline case because of the lower average runoff.

In the southern regions, the increase in precipitation is not as great as in the North, even decreasing in some regions in some scenarios. The temperature increase, however, is still large. Since temperatures are higher in the South in any event, the change in evaporation is even greater there than in the North. This results in decreasing runoff in these regions, with the decrease as high as 20% in region 8 under the CGCM1 scenario. Since the southern regions are already very wet, however, and more prone to flooding than to droughts, the decrease in runoff could actually be beneficial. The storage levels are low in these regions because water is not scarce and there has been little need to develop storage for supply reasons. This could put these regions at greater risk of flooding and drought, however, if the flow variation increases due to climate change. The next section will investigate this possibility further.

5.6 GCM Scenarios and Extreme Events

As discussed in the previous section, some GCM scenarios result in greater increases during peak flows than during low-flow periods, and other scenarios result

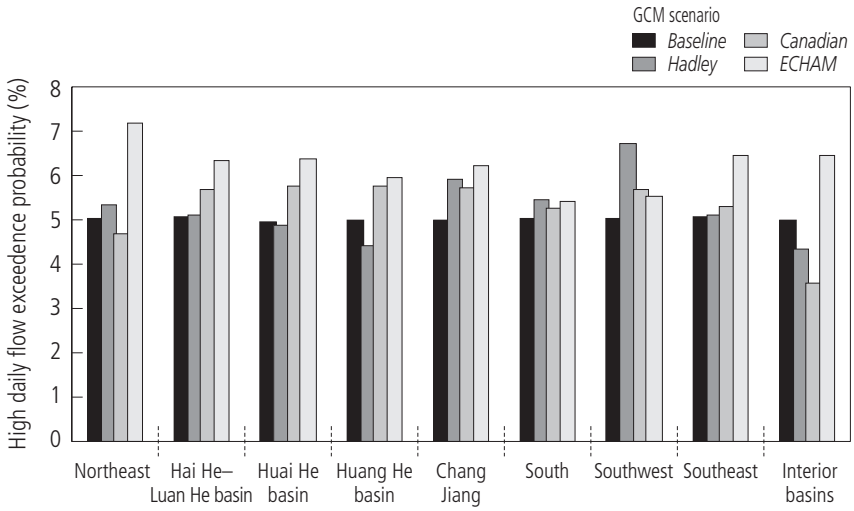

Figure 5.6. Probability of a daily flow's exceeding the 5% probable flow of baseline scenario.

in a more even distribution of runoff throughout the year, lowering the peak flow but increasing flow during low-flow periods. The changes in the variability of flows result in changes in the level of yield that is possible at existing storage levels. The changes in variability should also result in changes in flood and drought flows and the frequencies of these flows. This could be of great concern, considering that China's water resources are already highly variable in both time and space, and that China has a long history of flood and drought disasters.

To investigate the impact of climate change on the frequency of floods and drought, we took the level of runoff that had a 5% probability of occurring on any given day under the baseline scenario and the level of runoff that had a 95% probability of occurring on any given day under the baseline scenario. We then counted the number of events in the daily runoff series for each scenario that were greater than the 5% probable daily flood and the 95% probable daily flood from the baseline scenario. This was done to calculate the probability that the same flood would be exceeded under the climate change scenarios. This provides some measure of the change in frequency of peak flows and low flows. The same was done for a 14-day flood from the 14-day moving sum of the daily runoff series, since both flood flows and droughts usually last longer than one day. The results are shown in *Figures 5.6* through *5.9*.

These figures show that the number of flood flows generally increases under the GCM scenarios. This result should be expected because of the higher precipitation and runoff. There are exceptions, however, the reasons for which have already been

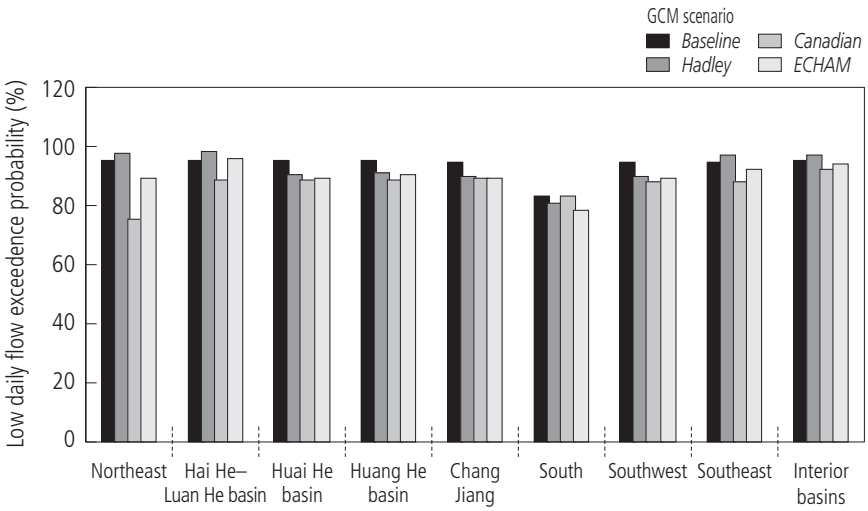

Figure 5.7. Probability of a daily flow's exceeding the 95% probable flow of baseline scenario. This is a measure of the occurrence of low flows; a higher number of low flows occurs when the probability is lower.

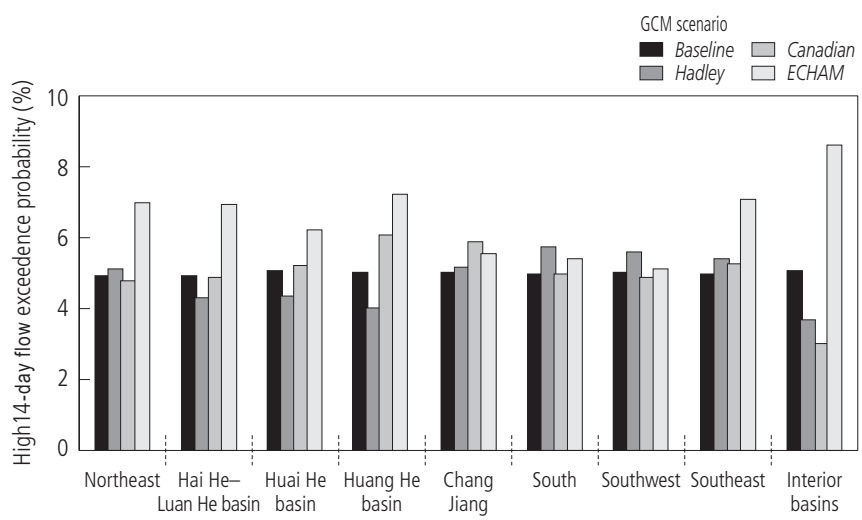

Figure 5.8. Probability of a 14-day flow's exceeding the 5% probable flow of baseline scenario.

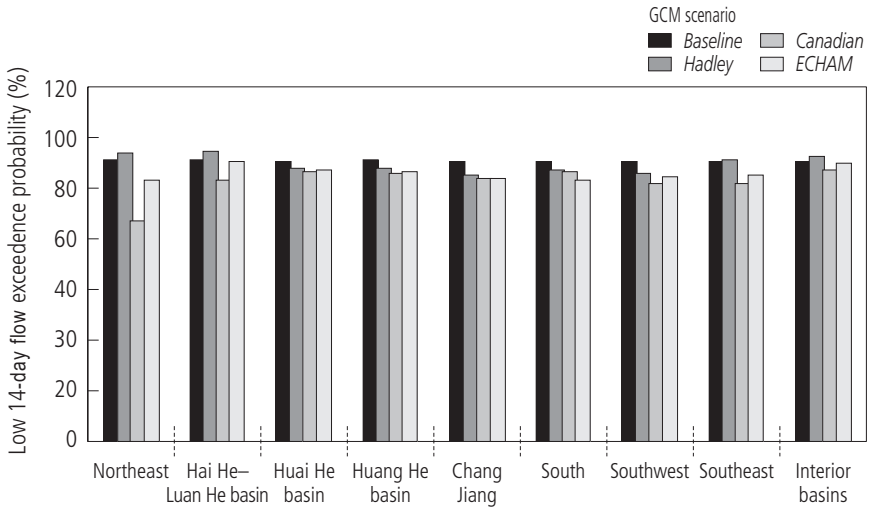

Figure 5.9. Probability of a 14-day flow's exceeding the 95% probable flow of baseline scenario. This is a measure of the occurrence of low flows; a higher number of low flows occurs when the probability is lower.

mentioned. The HadCM2 scenario produces a decrease in flood flows in the Hai He–Luan He, the Huai He, and the Huang He watersheds. This is again due to the decrease in the peak flow in the HadCM2 scenario. Since the HadCM2 evens out flow somewhat more throughout the year than the other scenarios do, the number of low-flow periods is also reduced in the Hai He watershed under this scenario. The CGCM1 scenario also reduces the peak flow in some regions, particularly in the Northeast, which reduces the occurrences of floods in that region. However, as a result of higher evaporation during the rest of the year, the number of low-flow periods increases.

In the majority of cases, the number of low-flow periods, or droughts, increases. Not only is there an increase in the number of floods in most of the regions, then, but there is also an increase in the number of droughts. The increase in the numbers of floods and droughts could make it necessary to build more storage capacity to prevent damage, particularly in the South. The additional storage will result in additional evaporative losses from reservoirs, but in at least one of the southern regions, the net evaporation was negative anyway.

5.7 GCM Scenarios and Storage Costs

In most cases the regions of greatest water scarcity in China receive more water in the climate change scenarios tested than in the baseline scenario. In the southern

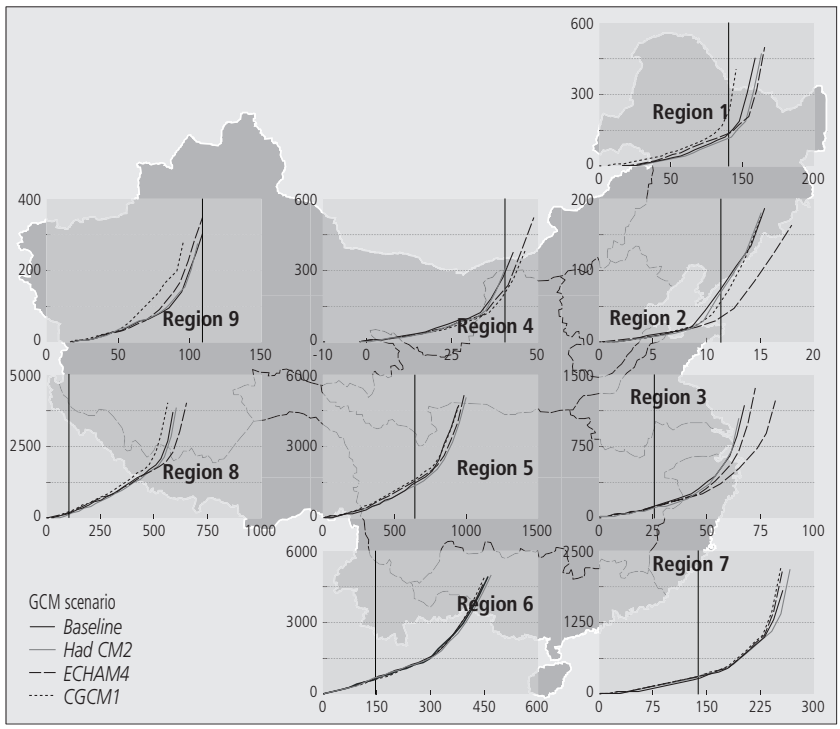

Figure 5.10. Impact of climate change from GCM scenarios on costs of supplying current yield. Horizontal axes show yield from storage in billion m^3; vertical axes show total cost in billion yuan. The vertical axis crosses the horizontal axis at the current yield level.

regions, however, the yield from existing reservoirs is reduced in many scenarios. Throughout the country, the scenarios also increase the probability of extreme events. Some regions may have to increase storage, then, to maintain the same yield or limit the vulnerability to floods and droughts, while others benefit with greater yield from existing storage. This section looks at the costs of maintaining the current yield under the climate change scenarios.

The total cost curve for each region and each GCM scenario is shown with the baseline case yield in *Figure 5.10*. The figure indicates that there can be high costs associated with delivering the current yield under climate change. This is particularly true of regions where storage is already highly developed, such as in the Interior basins (region 9), the Huang He watershed (region 4), and the Hai He–Luan He watershed (region 2). Because the change in many regions is quite small and difficult to read from the figure, *Table 5.6* provides the cost of maintaining the same yield under the different scenarios.

Table 5.6. Cost of maintaining original yield under each climate scenario and cost difference between each scenario and baseline case cost.

Watershed region	Yield (billion m^3)	Cost of maintaining current yield (billion yuan)						
		Baseline cost	HadCM2 cost	HadCM2 – base	CGCM1 cost	CGCM1 – base	ECHAM4 cost	ECHAM4 – base
1	120.37	135.87	109.05	–26.82	175.09	39.21	130.26	–5.62
2	11.22	72.36	27.14	–45.22	24.62	–47.74	22.86	–49.50
3	25.61	112.30	87.91	–24.39	99.90	–12.41	91.64	–20.66
4	40.91	300.24	169.16	–131.08	134.34	–165.90	146.43	–153.81
5	640.04	1,451.58	1,356.34	–95.24	1,647.75	196.16	1,545.03	93.44
6	146.24	673.79	650.95	–22.84	604.94	–68.85	640.11	–33.68
7	138.54	266.55	294.50	27.96	319.26	52.71	301.68	35.14
8	104.22	138.56	110.25	–28.31	200.88	62.32	155.90	17.34
9	108.86	314.50	395.79	81.30	519.57	205.07	341.02	26.52
China	1,336.01	3,465.76	3,201.10	–264.66	3,726.34	260.59	3,374.94	–90.82

Note: For watershed region names, see *Figure 1.5*.

Table 5.6 indicates that substantial investment would be required to maintain the current yield in some of the southern regions. In the northern regions, the cost of storage decreases. Since this storage is already built, however, there are no real savings in the regions with excess storage capacity to offset the additional expense in the regions that require more storage. If the negative differences are ignored, the cost of climate change according to these scenarios is 109.25, 555.48, and 172.44 billion yuan for the HadCM2, CGCM1, and ECHAM4 scenarios, respectively.

The marginal cost curves will also shift to show which regions benefit and which are harmed by the climate changes predicted by the climate scenarios. *Table 5.6* indicates that water will become less scarce in the northern regions and scarcer in the southern regions. This should also be apparent in the marginal costs of storage in these regions. In some regions, the reservoirs are able to yield more water than before climate change. In these regions, the marginal cost of additional yield would be zero until the release is increased to the point that the existing storage can no longer support that yield. In these regions, then, the marginal cost curve could be set at zero until that level is reached. However, in the following figures and tables, the marginal cost curve is kept in a form that does not acknowledge the existing storage, so that the impacts of climate change on the entire curve can be examined.

Although the northern regions, except for region 9, generally benefit from climate change, *Figure 5.11* and *Table 5.7* show that they remain the most expensive regions in which to increase storage capacity. Region 1, however, is the least expensive region in which to add storage in two of the scenarios. Yet in the CGCM1 scenario, it is one of the regions with the highest marginal cost. Region 9 has

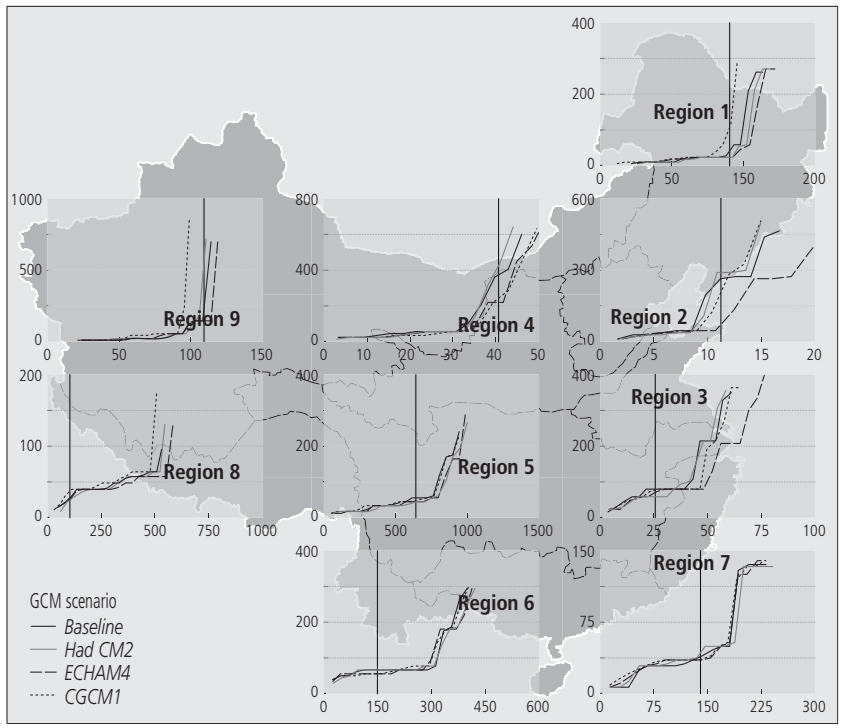

Figure 5.11. Effect of climate change on marginal cost curves for each region. Horizontal axes show yield from storage in billion m^3; vertical axes show marginal cost in billion yuan. The vertical axis crosses the horizontal axis at the current yield level.

Table 5.7. Change in marginal costs between baseline case and GCM scenarios of increasing the yield 1 cubic meter.

Watershed region	Yield (billion m^3)	Marginal cost at current yield (yuan)						
		Baseline cost	HadCM2 cost	Change (%)	CGCM1 cost	Change (%)	ECHAM4 cost	Change (%)
1	120.37	42.27	21.71	–48.64	110.55	161.52	21.84	–48.32
2	11.22	258.72	291.50	12.67	197.42	–23.69	60.62	–76.57
3	25.61	79.85	57.69	–27.75	76.56	–4.12	69.60	–12.84
4	40.91	370.91	418.69	12.88	239.31	–35.48	219.07	–40.94
5	640.04	52.13	42.24	–18.98	46.11	–11.54	43.54	–16.48
6	146.24	66.48	66.48	–0.01	57.03	–14.21	57.04	–14.20
7	138.54	37.26	41.12	10.36	34.99	–6.11	34.04	–6.25
8	104.22	28.73	25.66	–10.69	36.38	26.64	27.09	–5.68
9	108.86	166.04	525.16	216.29	935.18	463.23	143.47	–13.59
China	1,336.01	122.49	165.58	35.18	192.61	57.25	75.25	–38.57

Note: For watershed region names, see *Figure 1.5*.

already achieved a yield close to its maximum, so that obtaining additional yield is very complicated and expensive.

Overall, the marginal cost values support the fact that water is scarcer in the North than in the South, so that the cheapest method of improving the yield in the North probably is to transfer water from the southern regions. This is precisely what China intends to do, with its South–North diversion schemes. Even if the cost of the project to transfer the water adds an additional 10 yuan per m^3 in addition to the cost of the water in the Chang Jiang watershed, it is still below the cost of trying to increase yield in the northern regions.

5.8 Summary

China's water resources are highly variable in both time and space. The northern half of China suffers from severe water scarcity, while the southern half has more than enough water. Most of the water arrives in the monsoon months between July and October and can cause severe flooding. Both the South and North are prone to severe flooding and drought. The concern about climate change, then, is whether it will exacerbate the problems caused by this spatial and temporal variability in water resources.

The average temperature change in China for the scenario period 2040–2069, according to the HadCM2, CGCM1, and ECHAM models, is an increase of about 3.4°C. Increases in temperature cause increases in evaporation and transpiration, thereby reducing available water resources. The result of running the hydrologic model CHARM, applying temperature changes of +2°C, –2°C, and +3°C, was a decrease in runoff of about 2.2% for each 1°C increase in temperature. Regional results varied from a high of about 4% for each 1°C increase in the Northeast region (region 1) to a low of about 0.5% for each 1°C increase in the wet and mountainous Southwest region (region 8).

Precipitation changes predicted by the GCMs were quite favorable for China, with an average increase in precipitation of 8.5% across all the GCM scenarios. CHARM showed an increase in runoff of 1.74% on average across all regions for each 1% increase in precipitation. The greater increase in runoff is primarily a result of multiplying the precipitation in each time period by a fixed multiple. This results in greater increases in periods that are already very wet than in dry periods. The increase in runoff per 1% increase in precipitation varied from 2.24% in the Huang He watershed (region 4) to 0.8% in the Southwest region (region 8).

The GCM scenarios provided mixed results, with the runoff increasing in some regions and decreasing in others. Often even within the same region, one scenario showed increased runoff, while another scenario showed decreased runoff. In general, though, the runoff increased in the water-scarce northern regions and

decreased slightly in the water-rich southern regions. This is good news for China. However, in some cases, although the rainfall increased in a region, the runoff decreased because the rainfall was more evenly spread throughout the year. More rain is projected to fall during dry periods and less during peak periods. Generally, this is also good, but less runoff occurs because the water can be retained in the soil and evapotranspired without ever reaching the streams. Although very few people live in the Interior basins region (region 9), this is the region that suffers the most under the scenarios, with an average decrease in runoff of about 3.4%. For the whole of China, the average increase in runoff predicted is 3.1%.

There are other problems with the increased runoff, however. The number of extreme events increases along with it. The number of daily flows that exceed the 5% probable daily flow of the baseline case increased 11% on average across all regions and scenarios. The increase was as much as 43% in the Northeast region (region 1) under the ECHAM scenario, but there were actually reductions in some of the northern regions under the HadCM2 scenario. The occurrence of droughts also increased by an average of 4% over all regions and scenarios.

In China as a whole, the yield from existing storage capacity was reduced by an average of 2.3%. The regions of greatest water scarcity—namely, the Hai He–Luan He, Huai He, and Huang He watersheds (regions 2, 3, and 4, respectively)—increased their yield at current capacity. The southern regions, on the other hand, need to add more storage to counter the effects of decreased runoff and increased variability. Keeping the current yield level throughout China under the climate change scenarios would cost an average of 280 billion yuan. Increasing frequency of floods and droughts may warrant the building of even more storage in the South, beyond what is necessary to maintain the current yield.

The marginal costs of additional storage in the nine watershed regions support the construction of water diversions from southern China to the North. Water is much more readily available and much cheaper in the South than in the North. Many of the northern regions cannot obtain much more yield by building more storage. Marginal costs range from a low of about 22 yuan per m^3 increase in yield in the Northeast region (region 1) under the HadCM2 scenario to a high of 935 yuan per m^3 increase in yield in the Interior basins region (region 9), where not much more yield can be obtained.

The costs in this report must only be viewed as rough estimates. Changes are more reliable than absolute numbers at this point. More data on reservoirs, large and small, including location, surface area, active storage as opposed to total capacity, project costs, and operation and maintenance costs in China, could greatly improve the estimates. The results of this study do show, however, that climate change can present China with some benefits as well as some additional challenges to water management and additional costs.

6
Summary

In this report, a methodology for creating regional cost and supply curves for yield from storage has been developed and applied to study the potential cost of maintaining current yield levels under climate change in nine major watershed regions in China. Contributions were made in each of the major steps necessary to produce the supply curves. The major steps and contributions are as follows:

1. Step 1 is obtaining time series runoff values. For this purpose, the Climate- and Human Activities-sensitive Runoff Model (CHARM), a new hydrologic model that is sensitive to changes in land use and climate, was created.
2. Step 2 is calculating storage–yield curves. Because evaporation is important in obtaining a realistic level of yield in arid and semi-arid regions, a methodology was developed to estimate regional water surface area versus storage volume relationships. In the process, a technique was devised to estimate surface area–volume relationships for both individual reservoirs and aggregated groups of reservoirs.
3. Step 3 is calculating total cost curves and marginal cost, or supply, curves. A methodology was developed to estimate storage costs in the region.
4. Step 4 is applying the methodology and analyzing the results. Here the methodology was used to assess the impacts of evaporation on reservoir storage in China, to assess the impacts of climate change on the storage–yield and cost curves for the nine major watershed regions in China, and to estimate the costs of maintaining the same level of yield in each region.

The examples of the calibration and use of CHARM on the Tao He and Yilou He watersheds show that the model, which is calibrated against a yearly runoff value, simulates monthly flows quite well in these small watersheds. Sensitivity testing showed the model produced decreases of 2.4% per 1°C increase in temperature in the Tao He and 3.4% per 1°C increase in the Yilou He. The change in runoff due to a 1% change in precipitation was approximately 1.7% for both basins. Land-use changes were shown to produce the largest impact on annual runoff when the land cover in the basin is already highly impermeable and the hydrograph is highly variable with sharp peaks in runoff. However, land-use change impacts the timing of flows more than the average runoff. Because of the simplicity of CHARM, and the minimal data requirements, the model may not capture the entire impact of

land-use changes. Changes in runoff due to climate changes predicted by general circulation model (GCM) scenarios varied with the scenario and no general trend was seen.

Designed to be a simple model, CHARM proved effective at modeling the sample watersheds and showed its sensitivity to land use, land cover, and climate. With data that are available in global datasets, CHARM can be used to provide time series runoff for regions or countries where such data are not available. The flow variability is important in water management, as shown in the case of China. China is famous for its floods and droughts, and time series runoff analysis shows that the annual coefficient of variation in runoff is as high as 0.4 in one of the critical watershed regions, namely, the Hai He–Luan He region surrounding Beijing, where a sizable amount of China's agricultural production is located. CHARM output also shows that the intra-annual variation in runoff is very high, with 60% of the runoff occurring in only three months.

The time series runoff data output by CHARM makes the calculation of storage–yield curves possible for each region of China. Evaporation, however, is a substantial loss to stored water and should be included in the calculation of the storage required to meet a target yield. Chapter 3 and Appendix B show that for individual reservoirs, the area–volume relationship can be approximated very well by applying the equations for a triangular pyramid shape. On all tested reservoirs with known area–volume relationships, the coefficient of determination between the actual area–volume relationship and that predicted by the pyramid approximation was greater than 0.9.

Approximating the area–volume curve for aggregated reservoirs, however, is more complicated, since the surface area in the combined reservoirs for the same storage level can be controlled by operational policy. However, Chapter 3 showed that the range of area at each storage volume point is bracketed between a case where the reservoirs are managed to maximize head for hydropower and a case where the policy is to minimize the surface area. Since reservoirs in large regions are usually not managed to supply water for only one downstream demand, the actual area–volume relationship lies close to the relationship predicted by the pyramid approximation using the combined area and storage of the reservoirs.

The area–volume curve analysis for entire regions, though, showed that a linear approximation may be more appropriate. The reason for this is that data are generally only available for large reservoirs. Although a few large reservoirs may account for a large percentage of the storage in a region, small reservoirs generally have larger surface area per unit storage, and there are many more small reservoirs than large ones. If data on area and volume are only available for a few large reservoirs, then the surface area in the region will be underestimated when extrapolating beyond the known total area and volume using the estimated area–volume curve. The extrapolation error will be larger with the pyramid approximation than with

the linear approximation, so the linear approximation may be more appropriate in this case. If no surface area data exist at all for the region of interest, so that extrapolation is not even possible, then a curve comparing the slope of the watershed to the slope of the area–volume curve can be used to obtain a linear estimate for the area–volume curve. However, this estimate would only be very rough.

Using the area–volume curve methodology described above, the storage–yield and cost curves for the nine watershed regions of China were developed and compared with the case of no evaporation to assess the impact evaporation has in these regions. Average costs of reservoir storage were calculated using the cost tables originally created by the US Army Corps of Engineers. Costs in the table vary by physiographic zone and reservoir size. The table was normalized to the average cost per unit storage. If the average costs per unit storage in a region are known, then multiplying the average costs by the normalized values in the cost table produces a cost table for that region or country. For China, this average cost was calculated to be about 6 yuan/m^3. By matching the average slope of a watershed in China to the average slopes of the physiographic zones in the table, the costs of storage for each reservoir in the region can be estimated. To obtain the average cost for storage in that region, the total cost of all reservoirs in the region is divided by the total storage in the region. Assuming new reservoirs will be built according to a similar distribution of reservoir sizes and locations within the region, the average cost in the region can be used to estimate the cost of new storage.

The impact of net evaporation on water yield from storage in China proved to be quite substantial in the drier northern regions. The regions with the largest ratio of area to volume naturally are affected most severely. The Hai He–Luan He basin (region 2), for example, is in the plains, and the total surface area divided by volume for reservoirs with data on both is 0.73, the largest value of the nine regions. At current storage levels, the yield in this region has been reduced by 26% by evaporation from the reservoirs. The Huang He basin (region 4) also has substantial evaporative loss, reducing yield by 14%. Supplying the same yield that could be achieved without evaporation would cost an additional 40 billion yuan in the Hai He–Luan He basin. In the South region (region 6), however, including net evaporation in the calculations actually increases yield, since the region receives more water from precipitation than it loses to evaporation.

The marginal cost of increasing the annual yield by 1 m^3 provides a good indication of the relative water scarcity in the different regions. The marginal cost of yield is highest in the Huang He basin at over 370 yuan, followed by the Hai He basin at close to 260 yuan. Surprisingly, the lowest marginal cost is found in the Northeast region (region 1), at only 19 yuan. According to the available reservoir data, more storage could still be built before the costs start increasing markedly.

The marginal cost curve can be converted to a supply curve for a competitive firm using a simple multiplier. The multiplier comes about because the marginal

costs described are the costs of supplying another cubic meter of water per year. If one wants to know the costs per unit supplied or the price that should be charged per unit, then the expected lifetime of the project must be known. Present-value calculations can be done to find the price that, when charged over the lifetime of the project, is equal to the marginal cost, assuming that the cost estimate has already included the present value of all project costs. Performing the calculation on region 4 and region 5 produces prices of 14 yuan per m^3 and 2 yuan per m^3, respectively. This analysis makes it clear why China wants to divert water from the South to the North. Water supply, however, is usually managed by the government and is not subject to perfect competition. Generally, the goal is simply to generate enough revenue to pay the original cost of the dam, so that price is simply set equal to average cost of storage in the region.

The impacts of climate change on reservoir yield investigated in this study are generally favorable for China, although storage costs should still increase. The sensitivity of runoff to temperature in the regions is similar to that in the sample basins tested with CHARM. On average, the decrease in runoff due to a 1°C increase in temperature is about 2.2%, while runoff increases about 1.7% for a 1% increase in precipitation, although the sensitivity varies substantially by region.

With the GCM scenarios, however, greater rainfall does not always translate into increased runoff. The GCM scenarios vary the timing of rainfall during the year, which can result in less runoff with greater rainfall if the increased rainfall occurs during dry periods, as shown by the HadCM2 model scenario in the Huang He watershed. In general, however, the changes in climatic parameters indicated by the three GCM scenarios used resulted in increasing yields in the northern regions experiencing the greatest water scarcity and only slightly decreasing yields in the South. However, the decreasing yields are enough to reduce yield on average in China as a whole by 2.3%. Worse news for China is that, according to these scenarios, with climate change comes an increase in the number of extreme events. The number of flood flows greater than the 5% probable daily flow of the baseline case increases by an average of 11% across the scenarios. The number of drought periods also increases, and China is already known for its history of flood and drought disasters. The storage that has already been built has helped alleviate some of the damage in recent years, and additional storage now being built will improve the situation further. However, in order simply to maintain the existing yield throughout China, an additional 280 billion yuan will be needed for storage development, using the average figure from the three climate scenarios. Although the northern regions have excess yield under the climate scenarios, the storage cost in these regions is already a sunk cost. More storage needs to be built in the regions where yield decreases as a result of climate change. Even more storage than what is needed to maintain yield may be desired in the South to prevent the possible increase in flood and drought damage.

As a note of caution, the costs in this paper must only be viewed as rough estimates. The magnitude and direction of changes are more reliable than absolute numbers at this point. Each step in the procedure produces additional error. Because of its simplicity, CHARM produces error through the calibration coefficient, through the evapotranspiration estimation techniques, and through the choice in curve number for the stormflow component. The value for annual renewable water resources that CHARM is calibrated to could also be significantly in error. The possible error in the different area–volume estimation techniques was explained thoroughly in Chapter 3. The more reservoir information that is available, the more the error can be reduced; however, some error will always exist in the area–volume estimate from operational procedures of the reservoirs. Finally, the average cost estimate is only a rough estimate, since very few data on costs were available. More data on reservoirs, large and small, including location, surface area, active storage as opposed to total capacity, project costs, operation and maintenance costs, and operating policies in China could greatly improve the estimates. Additional runoff data, surface and subsurface, and more climate data, such as more daily precipitation data over longer time periods and some evaporation data, could also improve the estimate by improving the hydrologic modeling. Of course, the GCMs used cannot predict the future with perfect accuracy and precision.

The objective of the study, however, was to develop a methodology that could be applied over entire regions where few data are available, and this has been done. The rough estimates produced by this methodology provide far more information than simply average available water resources and can be used to identify regions of concern where more study is needed. The results of the climate change study on China, for example, show that although the changes to the climate in China predicted by the GCM scenarios are generally favorable, China still needs to increase storage, at considerable cost, to counter the negative impacts that climate change could produce in some of the regions. Surprisingly, much of this storage must be added in the South, while most studies focus on the more water-scarce North. As more data are gathered on these regions of interest, the estimates produced by this method can be continually improved.

Appendix A:

Calculation of Evapotranspiration

The first step in calculating evapotranspiration is to calculate the reference evapotranspiration (ET_0). The reference evapotranspiration in the Climate- and Human Activities-sensitive Runoff Model (CHARM) follows the Penman–Monteith method as recommended by the Food and Agriculture Organization of the United Nations (Smith, 1992; Allen *et al.* 1998), the same method that IIASA's Land Use Change Program uses for the agro-ecological zones (AEZ) methodology (Fischer *et al.*, 2000). The Penman–Monteith equation can be written as

$$ET_0 = ET_{ar} + ET_{ra} \ , \tag{A.1}$$

where ET_{ar} is the aerodynamic term, or

$$ET_{ar} = \frac{\gamma}{\upsilon + \gamma^*} \cdot \frac{900}{T_a + 273} \cdot U2 \cdot (e_a - e_d), \tag{A.2}$$

and ET_{ra} is the radiation term, or

$$ET_{ra} = \frac{\upsilon}{\upsilon + \gamma^*} \cdot (R_n - G) \cdot \frac{1}{\lambda}, \tag{A.3}$$

and

γ $\equiv$ psychrometric constant (kPa/°C),
γ^* $\equiv$ modified psychrometric constant (kPa/°C),
υ $\equiv$ slope of the vapor pressure curve (kPa/°C),
T_a $\equiv$ average daily temperature (°C),
e_a $\equiv$ saturation vapor pressure (kPa),
e_d $\equiv$ vapor pressure at dew point (kPa),
$e_d - e_a$ $\equiv$ vapor pressure deficit (kPa),
$U2$ $\equiv$ wind speed (m/sec),
R_n $\equiv$ net radiation flux at surface (MJ/m^{2}d),
G $\equiv$ soil heat flux (MJ/m^{2}d), and
λ $\equiv$ latent heat of vaporization (MJ/kg).

The calculation of the variables listed above is performed as follows:

Average daily temperature (°C)

$$T_a = 0.5(T_{\max} + T_{\min}), \tag{A.4}$$

where T_{min} and T_{max} are the maximum and minimum daily temperatures, respectively, and are given as inputs.

Latent heat of vaporization (MJ/kg)

$$\lambda = 2.501 - 0.002361T_a. \tag{A.5}$$

Psychrometric constant (kPa/°C)

$$\gamma = 0.0016286 \cdot \frac{P}{\lambda}, \tag{A.6}$$

where the atmospheric pressure (P) at elevation (A), given as input, is calculated by the following equation:

$$P = 101.3 \left(\frac{293 - 0.0065A}{293} \right)^{5.256}. \tag{A.7}$$

Modified psychrometric constant (kPa/°C)

$$\gamma^* = \gamma \left(1 + \frac{r_c}{r_a} \right), \tag{A.8}$$

where r_a is the aerodynamic resistance defined by

$$r_a = \frac{208}{U2}, \tag{A.9}$$

where $U2$ is the wind speed (m/s) which is input to the program, r_c is the crop canopy resistance,

$$r_c = \frac{R_l}{0.5LAI}, \tag{A.10}$$

and LAI is the leaf area index, assumed to be 2.88.

Saturation vapor pressure (kPa)

$$e_a = 0.5(e_{ax} + e_{an}), \tag{A.11}$$

$$e_{ax} = 0.6108 \exp\left(\frac{17.27 T_{\max}}{237.3 + T_{\max}}\right), \tag{A.12}$$

$$e_{an} = 0.6108 \exp\left(\frac{17.27 T_{\min}}{237.3 + T_{\min}}\right). \tag{A.13}$$

Vapor pressure at dew point (kPa)

$$e_d = \frac{RH}{100} \cdot \frac{2.0}{\left(\frac{1}{e_{ax}} + \frac{1}{e_{an}}\right)}. \tag{A.14}$$

Relative humidity (RH) is given as an input or calculated by the following regression:

Slope of the vapor pressure curve (kPa/°C)

$$\upsilon_a = 0.5(\upsilon_x + \upsilon_n), \tag{A.15}$$

where

$$\upsilon_x = \frac{4096 e_{ax}}{(237.3 + T_{\max})^2}\ , \tag{A.16}$$

$$\upsilon_n = \frac{4096 e_{an}}{(237.3 + T_{\min})^2}\ . \tag{A.17}$$

Net radiation flux at surface (MJ/m^{2}d)

$$R_n = R_{ns} - R_{nl}\ . \tag{A.18}$$

Here, R_{ns} is the net incoming shortwave radiation and R_{nl} is the net outgoing long-wave radiation. The shortwave radiation term will be developed first, followed by the long-wave term:

Net incoming shortwave radiation (MJ/m^{2}d)

For a reference crop with assumed albedo coefficient α =0.23,

$$R_{ns} = 0.77 R_s, \tag{A.19}$$

and the shortwave radiation (R_s) is

$$R_s = \left(.25 + .5\frac{SD}{DL}\right) R_a. \tag{A.20}$$

SD is the bright sunshine hours per day given as an input, DL is the maximum daylight hours, and R_a is extraterrestrial radiation. The calculations for DL and R_a are shown below:

Maximum daylight hours

$$DL = \frac{24}{\pi}\psi\ , \tag{A.21}$$

where ψ is the sunset hour angle described by

$$\psi = \arccos(-\tan\varphi \tan\delta), \tag{A.22}$$

ϕ is the latitude expressed in radians,

$$\varphi = \frac{L\pi}{180}\ , \tag{A.23}$$

and δ is the solar declination angle,

$$\delta = 0.4093 \sin\left(\frac{2\pi}{365}J - 1.405\right). \tag{A.24}$$

Extraterrestrial radiation (MJ/m^{2}d)

$$R_a = 37.586 d(\psi \sin\varphi \sin\delta + \cos\varphi \cos\delta \sin\psi), \tag{A.25}$$

where d is the relative distance between the earth and sun, calculated by

$$d = 1 + 0.033 \cos\left(\frac{2\pi}{365}J\right). \tag{A.26}$$

Net outgoing long-wave radiation (MJ/m^{2}d)

$$R_{ne} = 4.903 \cdot 10^{-9} \left(0.1 + 0.9\frac{SD}{DL}\right) (0.34 - 0.139\sqrt{e_d}) \cdot \frac{(T_{kx})^4 + (T_{kn})^4}{2}, \tag{A.27}$$

where

$$T_{kx} = 273.16 + T_{\max}\ , \tag{A.28}$$

$$T_{kn} = 273.16 + T_{\min}\ . \tag{A.29}$$

Soil heat flux

$$G = 0.14(T_{a,n} - T_{a,n-1}), \tag{A.30}$$

where $T_{a,n}$ and $T_{a,n-1}$ are average monthly temperatures of the current and previous months, respectively.

Once the potential evapotranspiration of a reference crop has been calculated, it is transformed into actual evapotranspiration by multiplying it by a soil moisture coefficient (k_s) and a crop coefficient (k_c):

$$Et = k_s k_c Et_0. \tag{A.31}$$

The calculation of these coefficients is quite simple in CHARM. The crop coefficient is set to an annual constant value currently, and the soil moisture coefficient is calculated as pictured in *Figure A.1* (Smith, 1992).

As the soil moisture is depleted, further evapotranspiration becomes increasingly difficult. Water is retained in the soil by capillary action, adhesion, and cohesion. As *Figure A.1* shows, in CHARM once the soil moisture is 50% depleted, evapotranspiration is assumed to decrease linearly until there is no more water left in the soil to deplete. The soil moisture coefficient can be described mathematically by the following equation:

$$k_s = \begin{cases} 1 & \text{if } z > 0.5 \\ 2z & \text{if } z <= 0.5, \end{cases} \tag{A.32}$$

where, from Equation (A.1), z is the relative soil storage, or $z = S/S_{max}$.

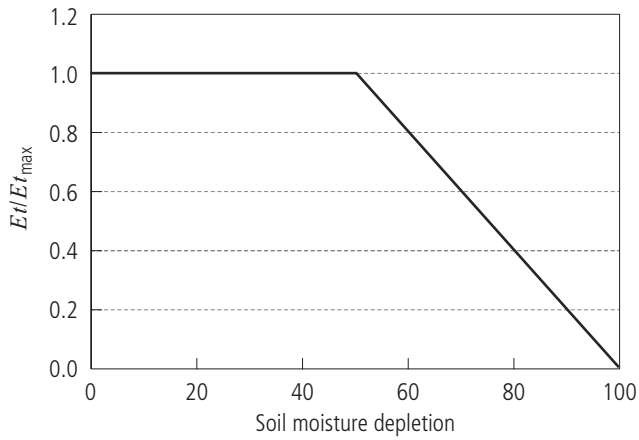

Figure A.1. Actual evapotranspiration rate as a function of soil moisture depletion, where soil depletion is 0 at field capacity and 100 at wilting point.

Appendix B:

Examples of the Pyramid Approximation

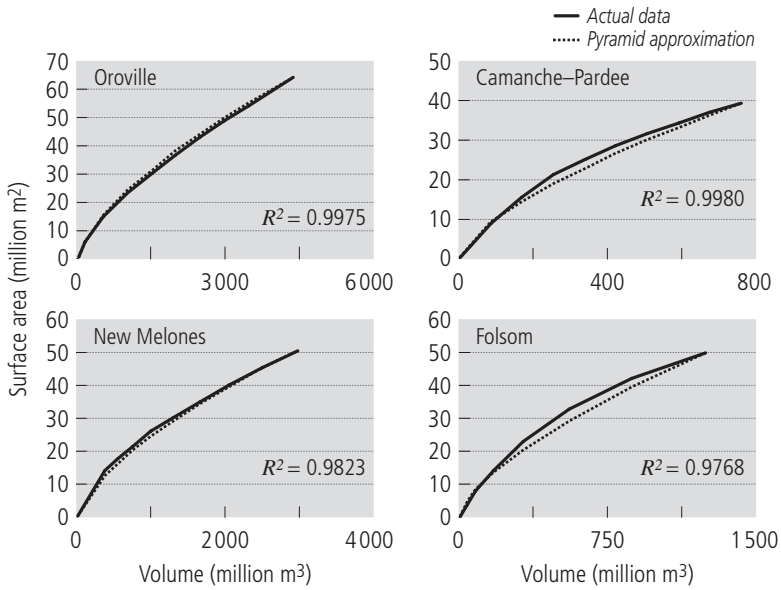

Figure B.1. Comparison between actual data for reservoirs in Sacramento River watershed and pyramid approximation for relationship between area and volume.

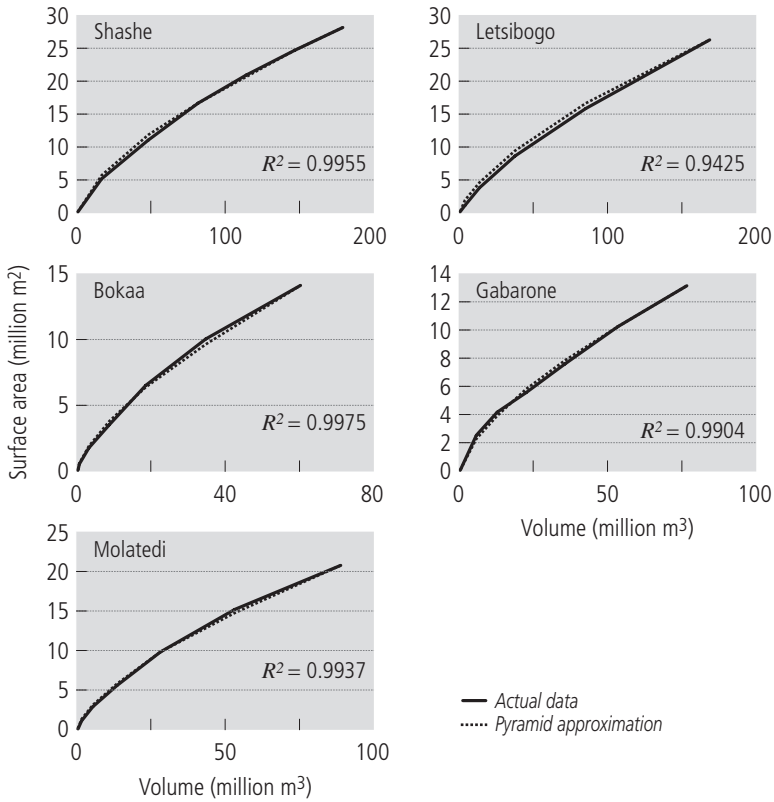

Figure B.2. Comparison between actual data for reservoirs in Limpopo River watershed in Botswana and pyramid approximation for relationship between area and volume.

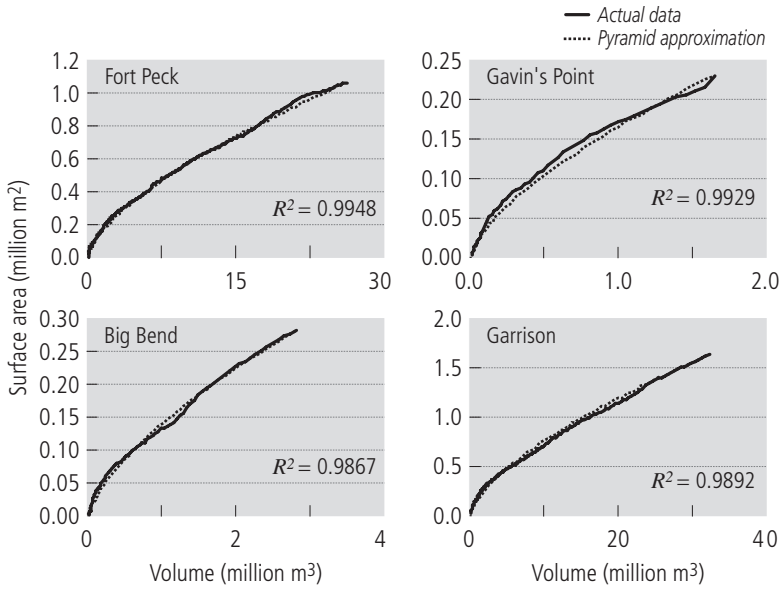

Figure B.3. Comparison between actual data for reservoirs in Missouri River watershed and pyramid approximation for relationship between area and volume. Actual data curves may be smoother than is shown here, since the data source was difficult to read.

References

Allen, R.G., Pereira, L.S., Raes, D., and Smith, M., 1998, Crop evapotranspiration – Guidelines for computing crop water requirements, FAO Irrigation and Drainage Paper 56, Food and Agriculture Organization of the United Nations, Rome, Italy.

Behrens, J.S., 1991, River Basin Operation: An Object-Oriented, Artificial Intelligence Approach, Ph.D. dissertation, University of Colorado, Boulder, CO, USA.

Boer, G.J., Flato, G.M., Reader, M.C., and Ramsden, D., 1998, A transient climate change simulation with historical and projected greenhouse gas and aerosol forcing: Experimental design and comparison with the instrumental record for the 20th century, submitted to *Climate Dynamics*.

Bowling, P., and Strzepek, K., 1997, Examining the Impacts of Land Use Change on Hydrologic Resources, IIASA Interim Report, IR-97-31, International Institute for Applied Systems Analysis, Laxenburg, Austria.

Brown, L., 2001, Chinese water table torture: China's water table levels are dropping fast, *Grist Magazine*, 26 October, http://www.gristmagazine.com/grist/maindish/brown102601.asp.

CHINCOLD, 2001, *The Response to WCD's Report by CHINCOLD*, Dams and Development: A New Framework for Decision-Making – The Report of the World Commission on Dams, World Commission on Dams, http://www.dams.org/report/icold_china.htm.

Chow, V.T., Maidment, D.R., and Mays, L.W., 1988, *Applied Hydrology*, McGraw-Hill, New York, NY, USA.

Cosgrove, W.J., and Rijsberman, F.R., 2000, *World Water Vision: Making Water Everybody's Business*, Earthscan Publications Ltd., London, UK.

Cubasch, U., Hasselmann, K., Hock, H., Maier-Reimer, E., Mikolajewicz, U., Santer, B.D., and Sausen, R., 1992, Time-dependent greenhouse warming computations with a coupled ocean–atmosphere model, *Climate Dynamics*, 8:55–69.

EPA, 1994, *The Hydrologic Evaluation of Landfill Performance (HELP) Model*, Risk Reduction Engineering Laboratory, Office of Research and Development, United States Environmental Protection Agency, Cincinnati, OH, USA.

Falkenmark, M., 1989, The massive water scarcity now threatening Africa: Why isn't it being addressed?, *Ambio*, **18**(2):112–118.

Falkenmark, M., and Lindh, G., 1993, Water and economic development, in P.H. Gleick, ed., *Water in Crisis – A Guide to the World's Fresh Water Resources*, Oxford University Press, New York, NY, USA.

FAO, 1997, Irrigation potential in Africa, *FAO Land and Water Bulletin*, 4, Food and Agriculture Organization of the United Nations, Rome, Italy.

FAO, 2000, Agriculture: Towards 2015/30, Technical Interim Report, Global Perspective Studies Unit, Food and Agriculture Organization of the United Nations, Rome, Italy.

FAO, 2001, *Atlas of Water Resources and Irrigation in Africa*, FAO Land and Water Digital Media Series 13, Food and Agriculture Organization of the United Nations, Rome, Italy.

FAO / IIASA, 2000, *Global Agro-ecological Zoning, Version 1.0*, Land and Water Digital Media Series 11, Food and Agriculture Organization of the United Nations, Rome, Italy.

Fischer, G., and Wiberg D., 2001, Climate change impacts on water-stressed agriculture in Northeast China, in M. Makowski and H. Nakayama, eds., Natural Environment Management and Applied Systems Analysis, IR-01-021, International Institute for Applied Systems Analysis, Laxenburg, Austria.

Fischer, G., Chen, Y., and Sun, L., 1998, The Balance of Cultivated Land in China during 1988–1995, IR-98-047, International Institute for Applied Systems Analysis, Laxenburg, Austria.

Fischer, G., van Velthuizen, H., and Nachtergaele, F.O., 2000, Global Agro-Ecological Zones Assessment: Methodology and Results, IR-00-064, International Institute for Applied Systems Analysis, Laxenburg, Austria.

Flato, G.M., Boer, G.J., Lee, W.G., McFarlane, N.A., Ramsden, D., Reader, M.C., and Weaver, A.J., 1998, The Canadian Centre for Climate Modelling and Analysis Global Coupled Model and its Climate, submitted to *Climate Dynamics*.

Gao, S., Yang, Q., and Lu, Q., 1992, The Changjiang Valley, in Z. Dakang and X. Yan, eds., *The Natural Features of China*, Chinese Academy of Sciences, Institute of Geography, China Pictorial Publishing House, Beijing, China.

Gleick, P.H., 1993, *Water in Crisis: A Guide to the World's Fresh Water Resources*, Oxford University Press, New York, NY, USA.

Gleick, P.H., 1998. *The World's Water 1998–1999: The Biennial Report on Freshwater Resources*, Island Press, Washington, DC, USA.

Heilig, G., 1999, China Food. Can China Feed Itself? International Institute for Applied Systems Analysis, Laxenburg, Austria.

Houghtalen, R.J., and Loftis, J.C., 1988, Irrigation water delivery system operation via aggregate state dynamic programming, *Water Resources Bulletin WARBAQ*, **24**(2): 427–434.

Howe, W., and Henderson-Sellers, A., 1997, *Assessing Climate Change : Results from the Model Evaluation Consortium for Climate Assessment*, Gordon and Breach Science Publishers, Amsterdam, The Netherlands.

ICOLD, 1984, *World Register of Dams*, International Commission on Large Dams, Paris, France.

ICOLD, 1989, *World Register of Dams, 1985 Update* (Régistre mondial des barrages, mise à jour 1988), International Commission on Large Dams (Commission Internationale des Grands Barrages), ICOLD/CIGB, Paris, France.

IIASA, 2001, IIASA-LUC GIS Database. http://www.iiasa.ac.at/Research/LUC/GIS/.

IWMI, 2000, World water supply and demand: 1995 to 2025, International Water Mangement Institute (IWMI), Colombo, Sri Lanka.

Kaczmarek, Z., and Krasuski, D., 1991, Sensitivity of Water Balance to Climate Change and Variability, WP-91-047, International Institute for Applied Systems Analysis, Laxenburg, Austria.

Kaiser, D., Tao, S., Fu, C., Zeng, Z., Zhang, Q., Wang, W.C., and Karl, T., 1996, *Climate Data Bases of the People's Republic of China, 1841–1988*, DOE Technical Report, TR055, Carbon Dioxide Information Analysis Center, Oak Ridge National Laboratory, US Department of Energy, Oak Ridge, TN, USA.

Keller, A., Sakthivadivel. R., and Seckler, D., 2000, Water scarcity and the role of storage in development, in *World Water Scenario Development for the World Water Vision*, http://www.cgiar.org/iwmi/pubs/WWVisn/WWSDChp6.htm (19 July 2004).

Linsley, R.K., Franzini, J.B., Freyberg, D.L., and Tchobanoglous, G., 1992, *Water-Resources Engineering, Fourth Edition*, McGraw-Hill, New York, NY, USA.

Löf, G.O.G., and Hardison, C.H., 1966, Storage requirements for water in the United States, *Water Resources Research*, **2**(3):323–354 (third quarter).

Manabe, S., Stouffer, R.J., Spelman, M.J., and Bryan, K., 1991, Transient responses of a coupled ocean–atmosphere model to gradual changes of atmospheric CO_2. Part 1: Annual mean response, *Journal of Climate*, **4**:785–818.

Manabe, S., Spelman, M.J., and Stouffer, R.J., 1992, Transient responses of a coupled ocean–atmosphere model to gradual changes of atmospheric CO_2. Part 2: Seasonal response, *Journal of Climate*, **5**:105–126.

McCully, P., 1996, *Silenced Rivers – The Ecology and Politics of Large Dams*, Zed Books, London, UK.

Ministry of Water Resources and Electric Power, 1997, *Use of Water Resources in China*, Beijing, China.

Murphy, J. M., 1995a, Transient response of the Hadley Centre coupled ocean–atmosphere model to increasing carbon dioxide. Part I: Control climate and flux adjustment, *Journal of Climate*, **8**:36–56.

Murphy, J.M., 1995b, Transient response of the Hadley Centre coupled model to increasing carbon dioxide. Part III: Analysis of global-mean response using simple models, *Journal of Climate*, **8**:496–514.

Murphy, J.M., and Mitchell, J.F.B., 1995, Transient response of the Hadley Centre coupled ocean–atmosphere model to increasing carbon dioxide. Part II: Spatial and temporal structure of response, *Journal of Climate*, **8**:57–80.

Nanjing Institute of Hydrology and Water Resources, 1996, *Report on the Mid- and Long-term Plans for Water Demand and Supply in China*, Nanjing, China.

New, M., Hulme, M., and Jones, P., 1999, Representing twentieth-century space-time climate variability. Part I: Development of a 1961–90 mean monthly terrestrial climatology, *Journal of Climate*, **12**:829–856.

Oberhuber, J.M., 1993, Simulation of the Atlantic circulation with a coupled sea-ice mixed layer-isopycnal general circulation model. Part I: Model description. *Journal of Physical Oceanography*, **13**:808–829.

Postel, S., 1992, *Last Oasis: Facing Water Scarcity*, W.W. Norton & Company, New York, NY, USA.

Press, W.H., Teukolsky, S.A., Vetterling W.T., and Flannery, B.P., 1992, *Numerical Recipes in C: The Art of Scientific Computing Second Edition*. Cambridge University Press, New York, NY, USA.

Raskin, P., Gleick, P., Kirshen, P., Pontius, G., and Strzepek, K., 1997, Water Rutures: Assessment of Long-range Patterns and Problems, Background Document for the SEI/United Nations Comprehensive Assessment of the Freshwater Resources of the World, Stockholm Environment Institute, Stockholm, Sweden.

Roeckner, E., Arpe, K., Bengtsson, L., Brinkop, S., Dümenil, L., Esch, M., Kirk, E., Lunkeit, F., Ponater, M., Rockel, B., Suasen, R., Schlese, U., Schubert, S., and Windelband, M., 1992, Simulation of the Present-day Climate with the ECHAM 4 Model: Impact of Model Physics and Resolution, Report No. 93, Max Planck Institute for Meteorology, Hamburg, Germany.

Roeckner, E., Arpe, K., Bengtsson, L., Christoph, M., Claussen, M., Dmenil, L., Esch, M., Giorgetta, M., Schlese, U., and Schluzweida, U., 1996, The Atmospheric General Circulation Model ECHAM-4: Model Description and Simulation of Present-day Climate, Report No. 218, Max Planck Institute for Meteorology, Hamburg, Germany.

Rosegrant, M.W., and Ringler, C., 1999, World Water Vision Scenarios: Consequences for Food Supply, Demand, Trade, and Food Security: Results from the IMPACT Implementation of the World Water Vision Scenarios, International Food Policy Research Institute, Washington, DC, USA.

Seckler, D., Amarasinghe, U., Molden, D., De Silva, R., and Barker, R,. 1998, World Water Demand and Supply, 1990 to 2025: Scenarios and Issues. Research Report no. 19, International Water Management Institute, Colombo, Sri Lanka.

Shiklomanov, I.A., 1993, World fresh water resources, in P.H. Gleick, ed., *Water in Crisis – A Guide to the World's Fresh Water Resources*, Oxford University Press, New York, NY, USA.

Shiklomanov, I.A., 1997, *Assessment of Water Resources and Water Availability in the World: Comprehensive Assessment of the Freshwater Resources of the World*, Stockholm Environment Institute, Stockholm, Sweden.

Shiklomanov, I.A., 1998, *World Water Resources: A New Appraisal and Assessment for the 21st Century*, International Hydrological Programme Report, United Nations Educational, Scientific and Cultural Organization, Paris, France.

Shiklomanov, I.A., 1999, *World Water Resources and Water Use: Present Assessment and Outlook for 2025*, State Hydrological Institute, St. Petersburg, Russia.

Shiklomanov, I.A., 2000, World water resources and water use: Present assessment and outlook for 2025, in *World Water Scenarios: Analysis*, World Water Vision, http://www.watervision.org.

Smith, R.A., 1981, Aggregation-Disaggregation Techniques for the Operation of Multi-Reservoir Systems, Ph.D. Dissertation, Colorado State University, Fort Collins, CO, USA.

Smith, M., 1992, CROPWAT, a computer program for irrigation planning and management, *Irrigation and Drainage Paper 46*, Food and Agriculture Organization of the United Nations, Rome, Italy.

SSB 1989–1997, *Statistical Yearbook of China*, State Statistical Bureau, China Statistical Publishing House, Beijing, China.

Thomas, H.A., and Fiering, M.B., 1963, The nature of the storage yield function, in *Operations Research in Water Quality Management*, Harvard University Water Program, Cambridge, MA, USA.

UN, 1997, *Study on Assessment of Water Resources of Member Countries and Demand by User Sectors: China: Water Resources and Their Use*, United Nations, New York, NY, USA.

UN, 1999, *The World at Six Billion*, Population Division, Department of Economic and Social Affairs, United Nations Secretariat, New York, NY, USA.

UN, 2001, Population, Environment and Development, 2001 (wall chart), Population Division, Department of Economic and Social Affairs, United Nations, New York, NY, USA.

US Department of the Interior, 2002, *National Atlas of the United States*, http://www.nationalatlas.gov/index.html.

USACE, 2001, *National Inventory of Dams*, http://crunch.tec.army.mil/nid/webpages/nid.cfm.

USDA, 1985, *National Engineering Handbook, Section 4, Hydrology*, Soil Conservation Service, US Government Printing Office, Washington, DC, USA.

USDA, 1986, *Urban Hydrology for Small Watersheds*, Engineering Division, Soil Conservation Service, Technical Release 55, US Department of Agriculture, Temple, TX, USA.

USDA, 1994, *SWAT Soil and Water Assessment Tool* Agricultural Research Service, Grassland, Soil and Water Research Laboratory, US Department of Agriculture, Temple, TX, USA.

USGS, 2002, *HYDRO1K Elevation Derivative Database*, http://edcdaac.usgs.gov/gtopo30/hydro/.

Viner, D., Hulme, M., and Raper, S.C.B., 1995, Climate Change Scenarios for the IPCC Working Group II Impacts Assessment: Technical Note No. 6, Climatic Research Unit, School of Environmental Sciences, University of East Anglia, Norwich, UK.

Wiberg, D.A., 1998. Climate Change Impacts on Reservoir Operation: The Effect of Changing Mean and Variance of Inflow Time Series, Master's Thesis, Dept. of Civil, Environmental, and Architectural Engineering, University of Colorado at Boulder, CO, USA.

Wollman, N., and Bonem, G.W., 1971, *The Outlook for Water: Quality, Quantity, and National Growth*, John Hopkins Press, Baltimore, MD, USA.

World Bank, 1997, *China 2020 – At China's Table. Food Security Options*, Washington, DC, USA.

Yates, D., 1996, WatBal – An integrated water balance model for climate impact assessment of river basin runoff, *Water Resources Development*, **12**(2):121–139.

International Institute for Applied Systems Analysis
Schlossplatz 1, A-2361 Laxenburg, Austria
Tel: +43 2236 807 Fax: +43 2236 71313
www.iiasa.ac.at

ISBN 3-7045-0143-3